# Immune sensing and effector functions of small intestinal tuft cells

John W. McGinty

A dissertation submitted in partial fulfillment of the
requirements for the degree of
Doctor of Philosophy

University of Washington
2021

Reading Committee:
Jakob von Moltke, Chair
Andrew Oberst
Martin Prlic

Program Authorized to Offer Degree:
Immunology

University of Washington

## Abstract

Immune sensing and effector functions of small intestinal tuft cells

John W. McGinty

Chair of the Supervisory Committee:
Jakob von Moltke
Department of Immunology

Parasitic worm, or helminth, infection represents a significant global health issue, with roughly a quarter of the world's population estimated to be infected at any given time. The branch of the immune system that evolved to defend against helminths is known as "type 2" immunity. While we have a good understanding of how the immune system detects and responds to viruses, bacteria, and fungi, the earliest sensing and signaling events that initiate the anti-helminth immune response remain poorly understood. Recently it was discovered that a rare and largely neglected cell type, called the tuft cell, specifically regulates type 2 immunity in the small intestine. Tuft cells secrete the cytokine IL-25, which activates group 2 innate lymphoid cells (ILC2s) in the underlying lamina propria to amplify the type 2 inflammatory response. Tuft cells were shown to respond to not only helminths, but also certain commensal protists. It remained unclear, however, how tuft cells detect helminths or protists in the intestinal lumen and what tuft cells do besides secrete IL-25.

Looking upstream, we identified succinate as the first activating ligand for small intestinal tuft cells. We first sequenced tuft cells from various tissues, including the small

intestine, to identify tissue-specific gene signatures. Using this data, we identified the succinate receptor, SUCNR1, as a candidate activating receptor that is highly expressed by intestinal tuft cells. Dietary supplementation with succinate activated a feedforward tuft-ILC2 response circuit, thereby inducing a robust type 2 immune response. We further demonstrated that succinate is a secreted metabolite of both helminths and Tritrichomonad protists. Succinate signaling through SUCNR1 was absolutely required for tuft cell sensing of protists, but unexpectedly, was dispensable for mounting an anti-helminth immune response. These findings reveal that innate type 2 immune responses can be activated by monitoring of microbial metabolism. Moreover, these data suggest that tuft cells utilize multiple activation pathways to sense luminal organisms, with the pathway(s) responsible for detecting helminths yet to be discovered.

Upon sensing infection, tuft cells activate ILC2s, which subsequently drive increased tuft cell frequency. This feedforward circuit is essential for intestinal remodeling and helminth clearance. ILC2 activation requires tuft cell-derived IL-25, but whether additional signals regulate the feedforward circuit is unclear. Here, we found that tuft cells secrete cysteinyl leukotrienes (cysLTs) to rapidly activate type 2 immunity following chemosensing of helminth infection. CysLTs cooperated with IL-25 to activate ILC2s, and tuft cell-specific ablation of leukotriene synthesis attenuated type 2 immunity and delayed helminth clearance. Conversely, cysLTs were dispensable for the tuft cell response induced by intestinal protists. These findings identify a novel tuft cell effector function and suggest context-specific regulation of tuft-ILC2 circuits within the small intestine.

Together, these findings advance our understanding of basic tuft cell biology, but more importantly, illuminate an unexpected complexity in how tuft cells discriminate between different environmental encounters. It appears that both the activating input signals and the

resulting effector outputs of tuft cells are specifically tuned to the type of organism sensed. These observations could inform new approaches for the generation of novel, targeted therapies to most effectively help those afflicted by intestinal helminth infection, allergies, or other type 2-associated pathologies.

## TABLE OF CONTENTS

## LIST OF FIGURES

**Chapter 1:**



**Chapter 2:**



**Chapter 3:**

## ACKNOWLEDGMENTS

I thank my mentor, Jakob, for his endless support and encouragement throughout my Ph.D. In the short time the lab has existed Jakob has created an environment in which people come first, and the science thrives as a result. There has not been a day gone by where I woke up and did not want to go into work. His enthusiasm for science is infectious and evident to anyone that has spent any time in the lab. I am deeply appreciative of the freedom Jakob has given me to explore my interests and go after all the half-baked ideas that pop into my mind. Learning and growing in this environment has helped me to realize my potential as a scientist. Above all I value the countless conversations and brainstorming sessions we've shared over the past few years. It was during these informal meetings that I learned to think critically about my work and to understand the broader picture. The confidence I've gained from these talks has only inspired to me to work harder and think bigger and will undoubtedly serve me well down the road.

I have had the great privilege of joining the Moltke Lab as one of the original members. Joining a new lab is sometimes viewed as a risky move, but in my experience, it has been nothing but a positive. I've enjoyed watching the lab grow, seeing new ideas take root, projects develop, papers get published. I owe a great amount to my lab mates, past and present, who have made this a great place to be. They are all talented and hardworking scientists, but more importantly, they are wonderful people to be around. It is easy to go about your work when you find yourself in such a comfortable and welcoming environment.

I thank my committee members for lending their time and expertise to guide me through my graduate career. I have enjoyed discussing my research projects and receiving critical feedback on my work, which was surely improved as a result. I also appreciate the honest

discussions we've had about professional development and career options. It has been extremely helpful to pick the minds of these successful individuals to inform my thinking about my own professional potential.

Finally, I would like to thank all of my classmates in the UW Immunology program. Having such a tight knit group of people to rely on has made all the difference in my graduate school experience. The countless happy hours, MOHAI get togethers, and random hangouts are among my favorite memories of the last few years. I would also like to thank all my Seattle friends outside of the science world for being there for me. While it's nice to have people to commiserate with over the struggles of day to day grad student life, it's equally nice to be able to forget about science completely, if only for a few hours here and there. These friendships surely kept me sane these past four years.

# CHAPTER 1

Introduction

### 1.1 Helminth infection and type 2 immunity

Parasitic worm, or helminth, infection represents a significant global health issue, with roughly a quarter of the world's population estimated to be infected at any given time (1). Helminth infections disproportionately affect individuals of low-income countries and have historically been neglected in research programs of more developed nations (2). By virtue of their parasitic lifestyle, helminths impart significant host morbidity. Intestinal parasites feed on host tissue and compete for key nutrients, resulting in malnutrition, anemia, chronic fatigue, and stunted growth (3). For reasons that are poorly understood, children are particularly susceptible to infection. Childhood infection can result in impaired physical and cognitive development, which has devastating consequences touching on all aspects of life, including the ability to work and support oneself in adulthood. Helminth infection thereby traps the world's poor in a vicious cycle of poverty and disease. Anti-helminthic drugs are an effective tool for clearing infection, however in endemic regions limited access to medication and high exposure rates inevitably lead to rapid reinfection in treated individuals. New approaches to understand, treat, and prevent helminth infection are therefore urgently needed.

The branch of the immune system that evolved to defend against parasitic worms is known as the "type 2" immune response, characterized by production of cytokines such as IL-4, IL-5, and IL-13, polarization of Th2 CD4+ T cells, mucus overproduction, eosinophilia, and generation of IgE-switched antibodies (4). The effectors of the type 2 response act in concert to combat helminths but must strike a delicate balance; the response must be robust enough to restrict parasite colonization and growth, but not so strong that the host suffers collaterally from excessive inflammation.

For most of human history helminth parasitization has been the rule rather than the exception (5). It is only within the last century or so that humans have been able to achieve widespread deworming, largely through improved sanitation and education. An unexpected consequence of this improvement has been a dramatic rise in the incidence of allergic diseases in developed nations (6,7). To explain this phenomenon Rook and colleagues put forward the "old friends" hypothesis, central to which is the appreciation that the human immune system is the result of millions of years of co-evolution between host and various microbial and parasitic partners (8). When these partners were suddenly removed from the equation, the tolerogenic "set point" of the immune system was also thrown into disarray, and the result was a sudden surge in responses directed against otherwise innocuous substances such as pollens, dander, dust mites, and chitin, among many others.

As it turns out, the allergic disorders that have increased so dramatically in recent years are driven by the very same type 2 immune cells that originally evolved to combat helminths, including Th2 CD4+ cells, eosinophils, mast cells, and basophils (9,10). Most commonly prescribed anti-allergy medications, such as antihistamines or leukotriene antagonists, aim to relieve symptoms rather than to address underlying causes of allergic disease. This speaks to a fundamental shortcoming in our understanding of type 2 immunity, more specifically, to the question of how type 2 immune responses are initiated. Why is that such diverse agonists, ranging from inert polysaccharides to pollens to complex, multicellular parasites, all lead to the same type of effector immune response? How is it that the host knows it is infected with a helminth in the first place? Answers to such questions promise to transform our understanding of the rules and rationale underpinning priming of the type 2 axis, and in the process, create

opportunities for the generation of entirely novel therapies with the potential to improve the lives of people all over the world.

### 1.2 Innate immune activation

The fundamental first step in initiating any immune response is a sensing event, in which the host detects the presence of a pathogen. The past few decades have seen intensive research on this topic, and as a result we have an advanced understanding of how it is that the host detects the presence of viruses, bacteria, and fungi. A basic paradigm has emerged in which the host detects pathogens or "non-self" molecules by virtue of specific genetically encoded molecular motifs that are uniquely expressed by a given class of pathogen, so called pathogen-associated molecular patterns (PAMPs) (11). These are typically molecules that are difficult for the pathogen to mutate away from without incurring significant fitness costs, and thus these sensing pathways have been conserved over evolutionary time (12). Example PAMPs include bacterial lipopolysaccharides and peptidoglycans, fungal sugar moieties such as dectin and galectin, and viral RNAs and DNAs. Once detected by host receptors, responding cells initiate a specialized innate immune response, which subsequently directs the development of a highly specific and effective adaptive immune response. Despite significant efforts, no PAMPs have yet been identified that underpin sensing of helminth infection and that specify development of the type 2 immune response.

A major advance in addressing this shortcoming was made in 2010 with the identification of group 2 innate lymphoid cells (ILC2s) as one of the earliest cell types responding to helminth infection (13–15). ILC2s are tissue-resident cells found at various barrier sites including the small intestine, skin, and lung, and as such are well positioned as frontline immune sentinels.

ILC2s are highly similar to adaptive Th2 CD4+ T cells in their gene expression profile, chromatin landscape, and production of effector cytokines that mediate the type 2 immune response (16,17). A key difference between these cells, however, is that ILC2s lack antigen-specific receptors and do not directly recognize pathogens. Instead, they are activated by host-derived signals encountered in the local environment. ILC2 activating signals include the cytokines IL-25, IL-33, and IL-18; the neuropeptides VIP and NMU; and the leukotrienes $LTC_4$ and $LTD_4$ (18). Not all ILC2s are responsive to all signals. Instead, receptor repertoires vary between tissues such that ILC2s are specially tuned to the microenvironment in which they reside (19).

In healthy animals ILC2s typically exist in a basal, inactivated state. During instances of infection or stress, however, activating signals are produced by host cells in the local environment and these drive ILC2s to produce effector cytokines that direct and amplify the developing immune response. ILC2s of the small intestine are particularly responsive to the cytokine IL-25, owing to their high expression of the IL-25 receptor (20). Indeed, IL-25 has long been recognized as a key signal driving the intestinal anti-helminth immune response, however the cellular source of this important cytokine remained enigmatic for many years (21). In 2016, three independent research groups converged to identify a rare and largely neglected epithelial cell type, called the tuft cell, as the source of the critical IL-25 signal (22–24).

### 1.3 Tuft cells

Tuft cells, also known as brush cells or caveolated cells, are a specialized type of epithelial cell found at sites including the small intestine, colon, gall bladder, urethra, trachea, and thymus, among others (25). They were originally identified by microscopy studies in the

1950s but their function was unclear (26). Early work therefore focused on defining morphological characteristics of tuft cells in various tissues. Tuft cells derive their name from a prominent apical cluster of microvilli that extend above neighboring cells. Other notable traits include a bottle shaped cell body, a narrow apical membrane, and the presence of lateral microvilli that project into neighboring cells (27).

Follow up studies began to identify specific tuft cell markers that enabled further characterization, though it has become apparent that makers can vary between tissues. At present, a proposed minimum criteria has been put forward that defines tufts based on the constitutive expression of the lineage-defining transcription factor POU2F3, the cytokine IL-25, the cation channel TRPM5, and the eicosanoid-generating enzymes ALOX5 and COX1/2 (28). In addition, the kinase doublecortin-like kinase 1 (DCLK1) is commonly used to define tuft cells, although this is not expressed by cells in the olfactory epithelium.

The actual function of tuft cells in various tissues has long remained enigmatic, however a renewed focus in recent years has highlighted the potential for a chemosensory function. Most notably, a study in 2008 examined the transcriptome of intestinal tuft cells and revealed a remarkable similarity between tuft cells and type 2 taste cells of the tongue that mediate sensing of bitter, sweet, and umami flavors in food (29).

In taste cell signaling, activation of taste receptors drives an intracellular calcium flux to open the cation channel TRPM5, resulting in cellular depolarization and release of neuromediators that propagate the taste sensation (30). While intestinal tuft cells do not express taste receptors, they do express other components of this chemosensing pathway, including the defining marker TRPM5, and were therefore postulated to serve a sensory function in the intestine (29). This study also highlighted a number of genes with the potential to modulate

immune and neuronal activity, including those for the generation of IL-25, acetylcholine, leukotrienes, and prostaglandins. Tuft cells situated within the intestinal epithelial barrier thus appeared uniquely positioned to sense and respond to luminal encounters, but experimental validation of this idea remained to be demonstrated.

In 2016 three complementary studies were published that unequivocally positioned intestinal tuft cells at the nexus of helminth sensing and initiation of the type 2 immune response (Figure 1). Using an IL-25 fluorescent reporter mouse, von Moltke et al. demonstrated that tuft cells were the sole source of IL-25 in the intestine (24). They further showed that tuft cells engage in a feedforward activation loop, whereby tuft cell-derived IL-25 activates ILC2s to produce IL-13, which then signals on intestinal epithelial stem cells to drive their differentiation towards the tuft cell and goblet cell fates. As the intestinal epithelium turns over every 3-5 days, activation of this tuft-ILC2 circuit led to rapid remodeling of the intestinal epithelium, characterized by tuft cell and goblet cell hyperplasia. This response circuit was restrained in naïve mice and tuft cells were exceedingly rare, comprising less than 0.5% of the epithelium. In the context of helminth infection, tuft cells were activated and the tuft-ILC2 feedforward circuit was engaged to rapidly activate the type 2 immune response and remodel the small intestine to promote parasite expulsion. Genetic deletion of IL-25 in tuft cells, on the other hand, severely impaired the type 2 response and resulted in sustained worm burdens.

In parallel work, Gerbe et al. also observed that intestinal tuft cells undergo significant expansion in number in the context of helminth infection (22). Importantly, they identified POU2F3 as the lineage-defining transcription factor that specifies the tuft cell fate. *Pou2f3*-deficient mice were found to completely lack tuft cells and to have a severe defect in their ability to mount an anti-helminth type 2 immune response. The authors further identified IL-25 as a

unique tuft cell effector molecule, and like von Moltke et al., converged on the model of a tuft cell-ILC2 feedforward response circuit that initiates the type 2 immune response.

Finally, work by Howitt et al. uncovered a TRPM5-dependent chemosensory pathway that is required for tuft cell sensing of not only helminths, but also Tritrichomonad protists (23). These protists are members of the commensal microflora and are common across many research vivariums, but unlike helminths do not obviously impair host fitness. This finding was particularly important as it demonstrated that tuft cells sense both large, multicellular parasites and also much smaller, but innocuous, unicellular protozoans. In both cases tuft cell sensing converged on the TRPM5 pathway and subsequent engagement of the tuft-ILC2 circuit described by von Moltke et al. and Gerbe et al. Accordingly, *Trpm5*-deficient mice exhibited profoundly impaired type 2 immune responses following helminth infection or Tritrichomonad colonization. The work of Howitt et al. thus provided clear experimental evidence of a tuft cell sensory function and highlighted the requirement for this sensing in the initiation of type 2 immunity in the intestine.

### 1.4 Dissertation objective and significance

Helminth infection is a global health concern, overwhelmingly afflicting the world's poorest. New approaches to understand and combat infections are urgently needed. A key gap in our knowledge pertains to the innate immune response that develops immediately following infection. Specifically, the mechanisms that enable the host to detect the presence of helminths in the intestine to trigger a protective immune response remain unknown.

The three studies described above collectively represent a seminal advance in our understanding of innate type 2 immunity. For the first time, we can now pinpoint the cell type

responsible for the earliest sensing of helminths and Tritrichomonad protists. Moreover, these studies provided significant insights into the basic tuft cell biology, generated novel tools to interrogate tuft cell function, and identified mechanisms by which tuft cells sense and respond to environmental encounters. With this foundation established we can now probe the earliest events underlying the initiation of type 2 immunity in the intestine. The aim of this work is thus to identify the specific pathways through which intestinal tuft cells are activated and to explore how this recognition is translated into a productive immune response.

A major question that remains unresolved is how the host first detects the presence of helminths and protists in the small intestine. We now appreciate that tuft cells are the most proximal cell type in this detection cascade. Thus, we can now ask: What are the specific ligands and receptors that tuft cells utilize to detect the presence of helminths and protists in the intestinal lumen? Here we identified succinate as the first known activating ligand of intestinal tuft cells. Succinate, an intermediate of the mammalian TCA cycle, is a secreted metabolite of both helminths and Tritrichomonad protists. We found that succinate sensing by tuft cells was required to induce an anti-protist type 2 immune response, but unexpectedly was dispensable for mounting the anti-helminth immune response. These findings revealed that tuft cells utilize multiple activation pathways to sense luminal organisms and defined a novel paradigm in which type 2 immune responses can be activated by monitoring of microbial metabolism. These findings will be discussed in depth in Chapter 2.

In the second arm of this work, we consider the downstream effector functions of intestinal tuft cells. The role of tuft cells in regulating type 2 immunity was revealed, in part, with the discovery that they are the sole source of the cytokine IL-25 (24). This cytokine has long been appreciated as a key signal driving intestinal ILC2 activation, and thus type 2 immune

responses. Indeed, genetic deletion of IL-25 within tuft cells severely impairs the anti-helminth immune response (24). We hypothesized that in addition to IL-25 production, activated tuft cells might influence the developing immune response in other ways. Here, we identified cysteinyl leukotriene (cysLT) secretion as a novel tuft cell effector function. CysLTs cooperated with IL-25 to rapidly activate the type 2 immune response and, accordingly, genetic ablation of leukotriene synthesis in tuft cells impaired the anti-helminth response. Notably, leukotrienes were not required to mount an anti-protist type 2 response, thereby uncovering a context-dependent regulation of tuft cell effector activity. These findings will be the subject of Chapter 3. Finally, in Chapter 4 we summarize our findings and consider unresolved questions and future directions related to tuft cell biology and their role in regulating intestinal immunity.

## 1.5 Figures

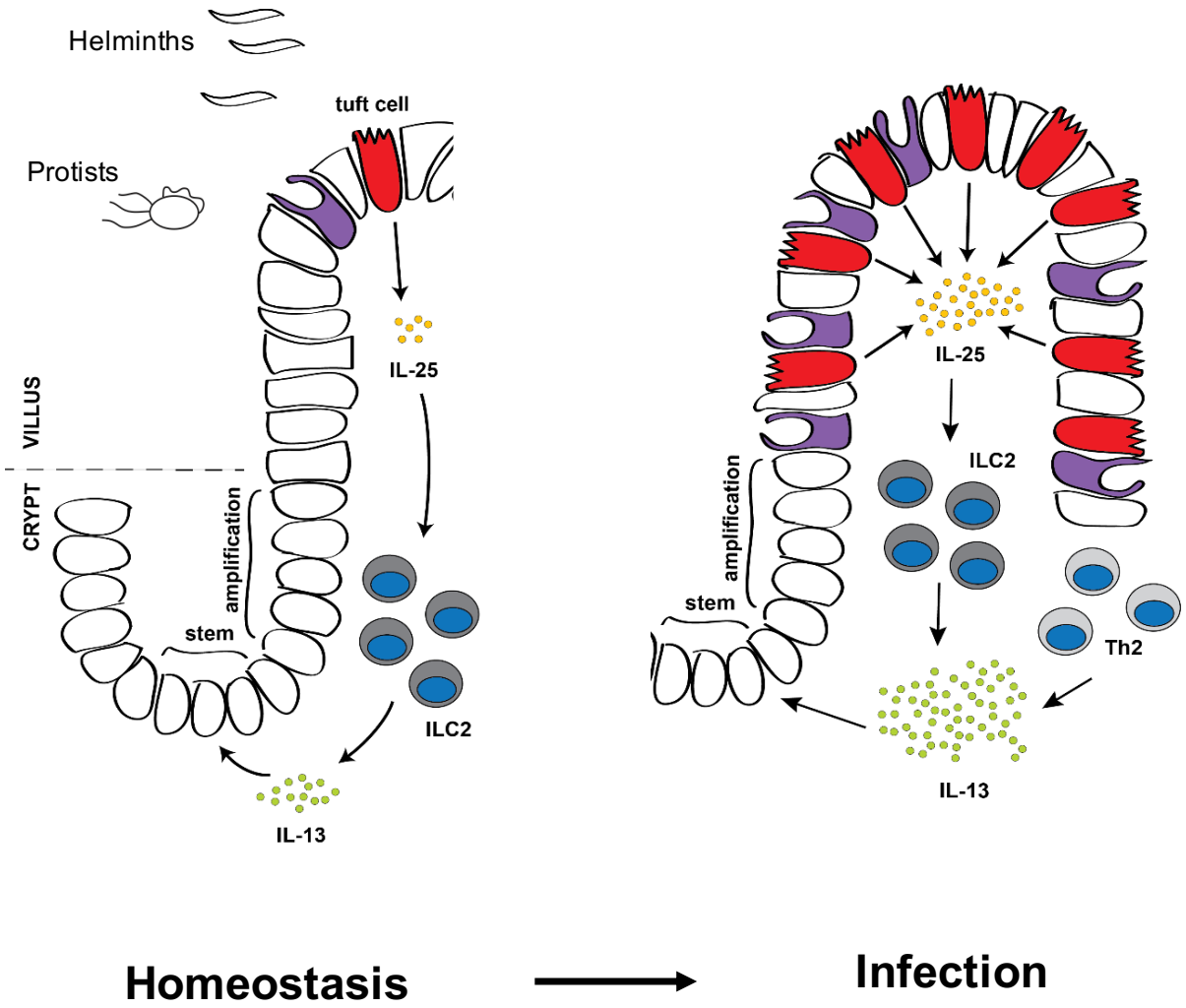


**Figure 1. Model of the tuft-ILC2 response circuit.** Tuft cells are rare type of chemosensory cell positioned within the epithelial barrier of the small intestine. Upon sensing the presence of helminths or Tritrichomonad protists in the intestinal lumen, tuft cells are activated to secrete the cytokine IL-25. This activates ILC2s to secrete IL-13, which then signals back on intestinal stems cells to drive further tuft cell differentiation. This feedforward tuft-ILC2 loop rapidly activates the type 2 immune response and remodels the small intestine to promote helminth expulsion.

# CHAPTER 2

Detection of succinate by intestinal tuft cells triggers a type 2 innate immune circuit

This chapter is adapted from the following publication:

Nadjsombati MS***,** McGinty JW*****, Lyons-Cohen MR, Jaffe JB, DiPeso L, Schneider C, Miller CN, Pollack JL, Nagana Gowda GA, Fontana MF, Erle DJ, Anderson MS, Locksley RM, Raftery D, von Moltke J. Detection of succinate by intestinal tuft cells triggers a type 2 innate immune circuit. Immunity. 2018. 49:33-41.

* Denotes equal contribution

## 2.1 Introduction

Immune responses are initiated upon recognition of foreign organisms, which occurs through detection of specific pathogen-associated molecular patterns. This initial sensing event triggers an innate immune response, which subsequently directs the development of a highly specific adaptive immune response that effectively combats the type of pathogen sensed. Helminths, allergens, and certain protists all induce a type 2 immune response, but the earliest sensing and signaling events that trigger the type 2 response remain unclear. In particular, no ligand/receptor pairs have yet been identified that specifically specify development of an innate type 2 response.

Recently, three groups identified tuft cells as a key population that initiates type 2 immunity in the small intestine (22–24). Upon sensing activating ligands, tuft cells secrete the cytokine IL-25 to activate ILC2s in the underlying lamina propria to initiate inflammation. IL-25 activates ILC2s to produce the hallmark cytokines IL-13, IL-5 and IL-9 that propagate the type 2 response. Among its many cellular targets, IL-13 signals directly on undifferentiated epithelial cells to bias their differentiation towards the tuft and goblet cell fates, resulting in a feed-forward loop of ILC2 activation and tuft and goblet cell hyperplasia, hereafter referred to as the tuft-ILC2 circuit. Given the 3-4 day turnover of intestinal epithelium (31), activation of the tuft-ILC2 circuit rapidly remodels the small intestine (SI) to promote helminth expulsion.

In these initial studies, tuft cells were shown to be activated by the helminths *Nippostrongylus brasiliensis*, *Heligmosomoides polygyrus*, and *Trichinella spiralis*, and by protists of the *Tritrichomonas* genus (22–24). The specific mechanism by which tuft cells sense these organisms to become activated is not known. The work of Howitt et al. demonstrated that tuft cell chemosensing relies on the TRPM5 cation channel to transduce activation signals (23).

Immune responses to helminths and protists are profoundly impaired in mice deficient for this molecule. The cell signaling function of TRPM5 has been extensively studied in type 2 taste cells, which bear striking similarity to tuft cells (29). The lessons learned here provide a useful starting point for considering how tuft cells in the intestine might first be activated.

Type 2 taste cells in the tongue mediate sensing of bitter, sweet, and umami flavors in food. Ligand binding to genetically encoded taste receptors activates taste cells to release neuromediators that propagate the taste sensation (30). Taste receptors are G protein coupled receptors (GPCRs) expressed on the cell surface. Ligand binding triggers activation of the G protein alpha-gustducin, which subsequently activates phospholipase C beta 2 (PLCB2) to generate the secondary messengers $IP_3$ and DAG. $IP_3$ binds to receptors on the endoplasmic reticulum, leading to an intracellular calcium flux that is critical for TRPM5 function. Elevated calcium levels open the TRPM5 channel, resulting in a sodium influx and cellular depolarization that triggers release of neuromediators that propagate the taste sensation (32,33). Thus, the general mode of taste cell activation is ligand binding to a GPCR, followed by an intracellular calcium flux, followed by TRPM5 opening and release of effector molecules.

In 2008 a research group performed microarray analysis of TRPM5+ cells in the intestine, now appreciated to be tuft cells, and found they bore remarkable similarity to type 2 taste cells in the tongue (29). Tuft cells expressed all components of the canonical taste signaling pathway, including alpha-gustducin, PLCB2, and TRPM5, but notably lacked expression of taste receptors. This work thus hinted at a tuft cell chemosensory function similar to that of taste cells. Subsequent investigation of tuft cells at other tissue sites supported this idea. In the airways tuft cells were found to be activated by bitter molecules and bacterial quorum sensing molecules, which altered breathing rate (34,35). Tuft cells in the urethra were similarly found to be activated

by bacterial secretions and bitter molecules, resulting in urethra contraction and urine release (36).

As noted, intestinal tuft cells similarly require signaling through TRPM5 for their function, but the specific ligands and receptors that mediate intestinal tuft cell activation are unknown. We therefore sought to identify the receptors responsible for recognizing helminths and protists in the small intestine.

## 2.2 Results

### mRNA sequencing identifies a transcriptional tuft cell signature

Tuft cells are found at various sites throughout the body, but the general relationship between these different populations is unclear. To better define the shared and unique features of specific tuft cell populations, we sorted tuft cells, identified by expression of the Flare25 reporter, from the small intestine, colon, gall bladder, trachea, and thymus of naïve mice and performed bulk RNA sequencing. We additionally sorted non-tuft epithelial cells from the small intestine as a reference. We then performed principal component analysis, which largely separated tuft cells based on their tissue of origin and demonstrated a close relationship between cells of the intestine as compared to the trachea or thymus (Figure 1A). This was further borne out by hierarchical clustering of differentially expressed genes, where tuft cells from a given tissue clustered together, reflective of tissue-specific gene signatures (Figure 1B). We then analyzed our sequencing data to identify a core tuft cell gene signature that is conserved across all tissues (Figures 1C-F). This list included known tuft cell identifiers such as *Il25*, *Trpm5*, and *Pou2f3*. We also noted conserved expression of several genes of interest previously suggested to be expressed by TRPM5$^{+}$ cells, including *Alox5*, *Chat*, *Ptgs1*, *Gnat3, and Plcb2* (29).

As previously discussed, intestinal tuft cells and type 2 taste cells share a remarkable degree of similarity, including dependence on the lineage-defining transcription factor POU2F3 and expression of the calcium-gated cation channel TRPM5. While taste cell activation is mediated by signaling through genetically encoded taste receptors, we found that intestinal tuft cells lacked expression of any of these canonical taste receptors, suggesting they instead rely on alternative receptors for activation (Figure 1G). Based on our understanding of signaling in TRPM5+ taste cells (30), we predicted that tuft cells would similarly require a calcium flux for

cellular activation and opening of the TRPM5 channel. We thus mined our sequencing data for extracellular receptors that are overrepresented in small intestinal tuft cells as compared to non-tuft cell epithelia and that have previously been shown to induce a calcium flux downstream of ligand binding.

Using these criteria, we identified the GPCRs FFAR3 and SUCNR1 as candidate activating receptors (Figures 1H-I). FFAR3 is a receptor for the short chain fatty acids propionate, butyrate, and acetate, which have been previously implicated in regulating immune function in the intestine (37). SUCNR1 is the receptor for succinate, an intermediate of the mammalian TCA cycle. We confirmed our RNA sequencing data by performing qPCR on sorted tuft and non-tuft epithelial cells, which again demonstrated that *Ffar3* and *Sucnr1* are specifically enriched in small intestinal tuft cells (Figure 1J). Other related short chain fatty acid receptors were either not expressed by tuft cells (*Ffar1, Ffar2*) or were expressed at equivalent levels between tuft and non-tuft epithelial cells (*Ffar4*). We therefore chose to further investigate FFAR3 and SUCNR1 as candidate activating receptors.

**Succinate is sufficient to induce a type 2 immune response in the small intestine**

Tuft cell activation following sensing of helminths or protists triggers the feedforward tuft-ILC2 circuit, characterized by tuft cell and goblet cell hyperplasia (24). To test the requirement for FFAR3 or SUCNR1 in tuft cell activation, we provided short chain fatty acids or succinate in the drinking water *ad libitum* and quantified tuft cell abundance in the distal small intestine 7 days later. Succinate treatment was sufficient to induce robust tuft cell hyperplasia, whereas no response was observed following treatment with propionate, acetate, or butyrate (Figures 2A-B). Succinate-induced tuft cell hyperplasia was evident throughout the small

intestine, however the response appeared to be most robust within the distal section of the tissue (last 10 cm) (Figure 2C). We noted that a concentration of 150mM succinate induced the strongest response, whereas lower or higher concentrations led to reduced hyperplasia (Figure 2D). To better define response kinetics, we performed a treatment time course and found a peak response around 7-8 days (Figure 2E). Thus, for all further studies we chose to treat mice with 150mM succinate for 7 days, unless otherwise noted.

We found that succinate treatment alone was sufficient to reproduce several hallmarks of a type 2 response. In addition to driving tuft cell hyperplasia, succinate treatment drove increased differentiation of goblet cells, identified by PAS staining (Figures 2F-G). These goblet cells were significantly increased in size, reflecting an increase in mucus production (Figure 2H). Examining the draining mesenteric lymph nodes (mLN), we observed increased numbers of ILC2s and eosinophils, both key effectors of the type 2 response (Figures 2I-J). In line with these findings, mice pretreated with succinate were better able to clear *N. brasiliensis* helminth infection relative to controls, providing further evidence that succinate treatment generates a *bona fide* type 2 immune response in the small intestine (Figure 2K).

Because commensal bacteria both produce and consume succinate (38,39), it was possible that dietary succinate supplementation activated type 2 immune responses indirectly by altering the composition of the intestinal microbiome; however, succinate-induced tuft cell hyperplasia was readily detectable in germ-free mice (Figure 2L). Together, our data demonstrate that succinate is an innate immune ligand that is sufficient to induce a multifactorial innate type 2 immune response in the small intestine.

**Succinate signals via the tuft-ILC2 circuit**

We next sought to define the mechanism by which succinate acts to drive the type 2 response. Previously published work identified an innate signaling circuit, in which tuft cells secrete IL-25 to activate ILC2s, which subsequently secrete IL-13 to drive tuft and goblet cell differentiation, as well as to amplify the developing type 2 response (Figure 3A) (24). We similarly found that the response to succinate was entirely dependent on IL-4/13 signaling, as tuft cell hyperplasia was ablated in mice lacking the IL-4Rα chain (Figures 3B-C). The response was largely intact in *Rag1*$^{-/-}$ mice, which lack adaptive lymphocytes, but was lost in *Il2rg*$^{-/-}$ mice that lack both innate and adaptive lymphocytes, strongly suggesting that ILC2s are the relevant source of IL-13 in this model.

The response to succinate was entirely dependent on IL-25, which has previously been shown to be a critical ILC2 activation signaling in the intestine (21,24). Although IL-33 also mediates ILC2 activation, signaling through the IL-33 receptor ST2 was not required for this response. IL-25 is uniquely expressed by intestinal tuft cells, and indeed, these cells were also required as goblet cell hyperplasia and hypertrophy were absent in succinate-treated *Pou2f3*$^{-/-}$ mice that lack tuft cells (Figures 3D-F). The TRPM5 cation channel, a core component of the tuft cell chemonsensory pathway, was similarly required as evidenced by impaired tuft cell hyperplasia and decreased ILC2 and eosinophil numbers in the mLN relative to control mice (Figures 3G-H). Moreover, while ILC2s in wildtype mice rapidly upregulated IL-13 in both the lamina propria and mLN after succinate administration, this response was absent in ILC2s of *Trpm5*$^{-/-}$ mice (Figures 3I-L). As expected, responsiveness to succinate required signaling through the succinate receptor SUCNR1. Thus, all components of the previously described tuft-ILC2 circuit were also required for the succinate-induced type 2 immune response. These data

suggest a model in which tuft cells, via signaling through SUCNR1, sense the presence of succinate in the local environment to become activated and trigger the feedforward tuft-ILC2 circuit that drives intestinal type 2 immunity.

### *N. brasiliensis* and a Tritrichomonad secrete succinate

Given that tuft cells were first described to be activated by intestinal helminths and Tritrichomonad protists, we hypothesized that sensing of succinate might be a mechanism for detection of these luminal organisms. Unlike land vertebrates, which principally generate lactic acid under anaerobic conditions, the anaerobic metabolites of helminths, protists, and bacteria are far more diverse and include hydrogen, ethanol, acetate, propionate, lactate, and others (40). More specifically, organisms that use fumarate as a terminal electron receptor during fermentation are known to secrete succinate as a byproduct (40,41). Indeed, a previous study reported that the helminth *N. brasiliensis* can secrete succinate, but this has not been further investigated (42).

To confirm this finding, we collected *N. brasiliensis* excretory/secretory product (NES) for nuclear magnetic resonance (NMR) analysis. We found that NES contained succinate, as well as additional metabolites including acetate, propionate, and lactate (Figure 4A). We then tested the ability of NES to activate mouse embryonic fibroblasts (MEFs) transduced with *Sucnr1*. Stimulation with either succinate or NES was sufficient to induce an intracellular calcium flux in *Sucnr1*-transduced cells, whereas no response was observed in non-transduced control cells (Figures 4B-C). Thus, *N. brasiliensis* secretes succinate as metabolic byproduct, and this is capable of activating cells expressing SUCNR1.

In the University of Washington vivarium, we also identified a mouse colony that harbored abundant protists with Tritrichomonas-like morphology (Figure S1A). Internal transcribed spacer (ITS) sequencing identified this protist as a previously undescribed Tritrichomonad with >97% and >86% homology to the ITS of *T. musculis* and *T. muris*, respectively (Figure S1B). We designated this new isolate as *T. rainier*. Like *N. brasiliensis*, *T. rainier* secreted succinate upon anaerobic culture (Figure 4D).

**Sensing of *T. rainier*, but not *N. brasiliensis*, requires *Sucnr1***

Sensing of intestinal protists has previously been shown to require GNAT3 and TRPM5, core components of the canonical taste signaling pathway, but these have not been tested in sensing of *N. brasiliensis* (23). We confirmed a requirement for TRPM5 in this response, as evidenced by decreased tuft cell frequencies and a delay in worm clearance in *Trpm5*$^{-/-}$ mice (Figures 4E-F). In contrast, the G protein GNAT3 appeared to be dispensable for mounting the anti-helminth response, hinting at a possible difference in sensing mechanisms for helminths and protists (Figure 4G). Given our observation that both helminths and protists can secrete succinate *in vitro*, we asked whether succinate signaling through SUCNR1 is required for tuft cell sensing of either type of organism *in vivo*. Following *N. brasiliensis* infection, *Sucnr1*$^{-/-}$ mice exhibited comparable tuft cell hyperplasia to wildtype mice. Consequently *Sucnr1*$^{-/-}$ mice were also able to resolve infection in a normal time frame (Figures 4H-I). Thus, succinate sensing is dispensable for tuft cell activation in the context of helminth infection. In stark contrast, we found that tuft cell sensing of *T. rainier* protists was completely dependent on the SUCNR1 signaling pathway. Whereas wildtype mice expanded tuft cells upon *T. rainier* colonization, this response was absent in *Sucnr1*-deficient mice (Figures 4J-K). The requirement for succinate sensing was

further reflected in decreased numbers of ILC2s and eosinophils in the mLN of *Sucnr1*-deficient mice (Figures 4L-M). Altogether, we identify succinate as the first known activating ligand for intestinal tuft cells and demonstrate that tuft cells monitor this metabolite to detect the presence of Tritrichomonad protists colonizing the intestinal lumen.

## 2.3 Discussion

In this study, we identified succinate as the first known activating ligand for intestinal tuft cells. We further demonstrated that succinate sensing mediates detection of Tritrichomonad protists in the intestinal lumen, leading to the generation of a type 2 immune response (Figure 5). Succinate is an intermediate of the mammalian TCA cycle but is typically retained intracellularly in host cells. Microbes and helminths that reside in the intestinal lumen, on the other hand, can secrete succinate as a metabolite, thereby creating the potential for sensing of extracellular succinate (40,41). Indeed, we found that both Tritrichomonad protists and helminths secrete succinate when cultured *in vitro*. Whereas succinate sensing was required for mounting an anti-protist immune response *in vivo*, succinate sensing was dispensable for mounting an anti-helminth response. It thus appears that tuft cells utilize multiple activation pathways for detecting luminal organisms. The ligands and receptors through which tuft cells recognize helminths remains to be determined.

In support of these observations, two other groups recently published studies detailing the requirement for succinate sensing in the initiation of intestinal type 2 immune responses. While studying intestinal ILC2s, Schneider *et al*. identified a mouse line that exhibited unexpectedly high tuft cell numbers (20). This line displayed other characteristics of an ongoing type 2 immune response, including an increase in ILC2 activation and an adaptive lengthening of the small intestine. The authors observed a dramatic expansion in Tritrichomonad protists in the cecum upon weaning, which correlated with a simultaneous increase in tuft cell numbers. They subsequently found that Tritrichomonads secrete succinate as a metabolite and went on to show that providing succinate in the drinking water was sufficient to induce an intestinal type 2 response in a tuft cell-dependent manner.

In a second study, Lei et al. similarly noted that tuft cells express the receptor SUCNR1 and considered what effect succinate might have on tuft cell activation (43). They found that administering succinate in the drinking water induced an intestinal type 2 response, characterized by tuft cell and goblet cell hyperplasia, which required signaling through SUCNR1. They found that sensing of succinate was dispensable for mounting an immune response against *N. brasiliensis*, in agreement with our own findings. Instead, the authors found that disrupting the intestinal microbiome through antibiotic treatment was sufficient to increase tuft cell numbers in a SUCNR1-dependent manner. Although the authors did not identify specific bacterial species that activate tuft cells, they presented the first data implicating a role for tuft cell sensing of bacteria, in addition to the previously described sensing of helminths and protists. Combined, these three studies establish a clear role for tuft cell sensing of protists and bacteria by monitoring the presence of secreted succinate in the local environment.

Our identification of succinate as an innate immune ligand challenges the existing paradigm of innate immune sensing. As an innate immune ligand succinate is unusual. Innate recognition of bacteria, viruses, and fungi relies on sensing of genetically encoded molecules that are typically critical for the organism's survival and normal functioning. Thus, they are difficult to evolve away from and have been conserved over evolutionary time (12). Succinate, on the other hand, is a secreted metabolite. That is, innate type 2 immune responses can be activated by monitoring of microbial metabolism, as opposed to sensing of the organism itself. Moreover, succinate is not unique to microbes but is also expressed by all host cells. An important distinction, however, is that host succinate is sequestered in the mitochondria, whereas microbial succinate is secreted into the extracellular environment. Previous reports have demonstrated that extracellular succinate can activate dendritic cells and macrophages, however this signaling

drives a type 1 immune axis, as opposed to the type 2 axis that is triggered by intestinal succinate sensing (44–46). Whether there are situations in which host succinate can reach the extracellular space to activate intestinal tuft cells is not currently known.

Succinate is also an unusual innate ligand in that it should not be difficult for an organism to evolve away from it. Succinate is secreted as a byproduct in anaerobic metabolic programs where fumarate is used as the terminal electron acceptor, however bacteria and protists employ a myriad of metabolic strategies to survive in the ever-changing environment of the intestinal lumen (40). Thus, if host sensing of this particular metabolic pathway represented a negative pressure on the organism, there would be many ways to quickly move away from succinate secretion. Instead, our data and that of Schneider et al. suggest that Tritrichomonads are unaffected by the type 2 immune response they trigger. Moreover, the presence of these organisms does not seem to negatively impact host fitness in any obvious way.

We are therefore left with the question of why the host should detect these organisms in the first place and why type 2 immune activation is the appropriate host response. One explanation is that there are more pathogenic microbes that tuft cells have evolved to respond to, which aren't present in specific pathogen-free (SPF) vivariums but might be encountered in natural settings. An alternative hypothesis is that these microbes have evolved to manipulate their local environment in a way that is beneficial to them. Perhaps some bacteria and protists thrive in a type 2 inflamed environment, for example taking advantage of the increased mucus production for energy. Finally, sensing of succinate might be a mechanism for monitoring the overall microbial community. In instances of dysbiosis, succinate producing microbes could expand and secrete succinate at high enough levels to be sensed, thereby triggering a

compensatory immune response. Further work will be required to understand the contexts in which succinate sensing is most important.

In sum, we identify succinate as the first known activating ligand for intestinal tuft cells and define a novel paradigm in which innate type 2 immune responses can be activated by monitoring of microbial metabolism.

## 2.4 Material and Methods

### Experimental Animals

Mice aged 6 weeks and older were used for all experiments. Mice were age-matched within each experiment, but pooled results include both male and female mice of varying ages. C57BL/6J mice were bred in house or purchased from Jackson Laboratories. B6.*Rag1*$^{-/-}$ (B6.129S7-Rag1$^{tm1Mom}$/J), B6.Il2rg$^{-/-}$ (B6.129S4-Il12rg$^{tm1Wjhl}$/J), and B6.*Trpm5*$^{-/-}$ (B6.129P2-Trpm5$^{tm1Dgen}$/J) mice were purchased from Jackson Laboratories. B6.*Il25*$^{Flare25/Flare25}$ and B6.*Il13*$^{Smart13/Smart13}$ mice were generated as previously described (47,48). *Il25*$^{-/-}$ mice were generated as previously described (49), generously provided by A. McKenzie, and backcrossed at least 8 generations to C57BL/6J. IL4ra$^{-/-}$ mice were generated as previously described (50), generously provided by F. Brombacher, and backcrossed at least 8 generations to C57BL/6J. B6.*Pou2f3*$^{-/-}$ (Pou2f3 tm1.1(KOMP)Vlcg, Project ID #VG18280) were generously provided by M. Anderson. B6.*Gnat3*$^{-/-}$ mice were generated by pronuclear injection of Cas9 mRNA and two sgRNA (Guide 1: GCTTCAGGAGGATGCTGAGCGGG, Guide 2: CTCCAGTTCTTTGGACCTTCTGG) into fertilized C57BL/6J zygotes at the Gladstone Institutes (San Francisco, CA). B6.*Sucnr1*$^{-/-}$ mice were generated by pronuclear injection of Cas9 mRNA and two sgRNA (Guide 1: CGATTGCATAAAATGCAGAGAGG; Guide 2: AGAGTTATGCCAATGATAAGGGG) into fertilized C57BL/6J zygotes at the Gene Targeting Facility of the Cancer Research Laboratory at UC Berkeley (Berkeley, CA). Founder *Gnat3* and *Sucnr1* mice were genotyped by Sanger sequencing and founders carrying mutations were backcrossed once to C57BL/6J before intercrossing to generate homozygous mutant mice. All mice not purchased from Jackson Laboratories or newly generated were rederived into the University of Washington vivarium. Lewis rats were purchased from Envigo (LEW/SsNHsd).

Except mice noted below, all mice and rats were maintained in specific pathogen-free conditions at the University of Washington and were confirmed to be tritrichomonas-free by qPCR. Germ free mice were housed and treated in the University of Washington Gnotobiotic Animal Core. All experimental procedures (with exceptions noted below) were approved by the Institutional Animal Care and Use Committee at the University of Washington. B6.*Il25*$^{Flare25/Flare25}$ mice used to sort cells for mRNA sequencing and B6.*Gnat3*$^{-/-}$ mice were maintained in specific pathogen-free conditions at the University of California, San Francisco and experimental procedures were approved by the Institutional Animal Care and Use Committee at the University of California, San Francisco. B6.*Il25*$^{Flare25/Flare25}$ were retrospectively found to be colonized with a tritrichomonad of unknown identity.

**Germ Free Mice**

C57BL/6J mice were raised under standard germ free conditions in the University of Washington Gnotobiotic Animal Core. For succinate administration, mice were transferred to hermetically-sealed positive pressure isocages as described (51) and given autoclaved drinking water supplemented with 150 mM sodium succinate hexahydrate ad libitum for 7 days.

**Cell culture and transduction**

Immortalized C57BL/6J mouse embryonic fibroblasts (MEFs; kindly provided by Dr. D. Stetson) and HEK293T were cultured in DMEM supplemented with 10% fetal calf serum (VWR), L-glutamine, penicillin/streptomycin, sodium pyruvate, HEPES and β-mercaptoethanol. For lentiviral transduction, the ORF for mouse *Sucnr1* was obtained directly from prepared cDNA from sorted small intestinal tuft cells (described above). After sequencing verification,

*mSucnr1* was cloned into the pRRL-MND-MCS-2A-Puro lentiviral vector downstream of an MND promoter as previously described (52). VSV-G pseudotyped, self-inactivating lentivirus was prepared by transfecting HEK293T cells with 1.5 μg pVSV-G, 3 μg psPAX-2, and 6 μg pRRL lentiviral vector, and viral supernatant collected and filtered before use. MEFs were incubated with viral supernatant overnight, and media was replaced with fresh culture media. Puromycin (5ug $mL^{-1}$) selection was added 72 hours post transduction and continued for 7 days.

**Short Chain Fatty Acid and Succinate Administration**

Mice were provided with sodium succinate hexahydrate (Alfa Aesar), sodium propionate (Arcos Organics), sodium acetate trihydrate (Fisher Chemical), or sodium butyrate (Alfa Aesar) ad libitum in drinking water. Unless otherwise noted, mice were treated for 7 days with 150 mM agonist, except NaCl, which was given at 300 mM to match sodium molarity with succinate treatment.

**Mouse Infection/Colonization**

Infectious third-stage *N. brasiliensis* larvae (L3) were raised and maintained as described (47). Mice were infected subcutaneously at the base of the tail with 500 *N. brasiliensis* L3 and were euthanized at the indicated time points to collect tissues for staining or to count worm burden. Worm burden was enumerated across the entire small intestine. Wild-type mice naturally colonized with *T. rainier* were used as a source of protists for colonization studies. *T. rainier* colonization status was determined by microscopy and confirmed by qPCR and ITS sequencing. To transfer *T. rainier* to naïve mice, cecal contents of colonized mice were isolated and washed in PBS, filtered through a 70 μm strainer, and spun down. Contents were washed a second time

in PBS and total protists enumerated using a hemocytometer. Mice received a single oral gavage of 20-30 x $10^6$ protists in a volume of 150 μl PBS. After 7 days mice were sacrificed for analysis. Successful colonization was again determined by microscopy and confirmed by qPCR.

**Tissue fixation and staining**

For tuft cell staining, intestinal tissues were flushed with PBS and fixed in 4% paraformaldehyde for 4 h at 4° C. Tissues were washed with PBS and incubated in 30% (w/v) sucrose overnight at 4° C. Small intestine and colon samples were then coiled into "Swiss rolls" and embedded in Optimal Cutting Temperature Compound (Tissue-Tek) and sectioned at 8 μm on a Microm HM550 cryostat (Thermo Scientific). Immunofluorescent staining was performed in Tris/NaCl blocking buffer (0.1 M Tris-HCL, 0.15 M NaCl, 5μg $ml^{-1}$ TSA blocking reagents (Perkin Elmer), pH 7.5) as follows: 1 h 5% goat serum, 1 h primary antibody (αDCLK1, Abcam ab31704), 40 min goat anti-rabbit IgG F(ab')2-AF594 secondary antibody (Life Technologies) and mounted with Vectashield plus DAPI (Vector Laboratories). Tuft cell frequency was calculated using ImageJ software to manually quantify DCLK1+ cells per millimeter of crypt-villus axis. Four 10x images were analyzed for each replicate and at least 30 total villi were counted.

For goblet cell staining, tissues were flushed with PBS, fixed in 10% buffered formalin at 4° C for 3 h, coiled into "Swiss rolls" and returned to formalin. After 24 h tissues were moved to 70% ethanol for storage. Tissue processing, paraffin embedding, sectioning, and staining were performed by the Pathology Research Services Laboratory at the University of Washington. Periodic acid Schiff (PAS) or Alcian blue staining was used to identify goblet cells. Goblet cell frequency was calculated as described above for tuft cells. Hypertrophy was quantified using

ImageJ software to measure the area of at least 80 goblet cells for each biological replicate. Brightfield and fluorescent images were acquired on an Axio Observer.A1 inverted microscope (Zeiss).

**Single-cell tissue preparation**

For single cell epithelial preparations from small intestines, gall bladder, and colon, tissues were flushed with PBS, opened, and rinsed with PBS to remove intestinal contents. Intestinal tissue was cut into 2-5 cm pieces and incubated rocking at 37° C in 15 mL HBSS ($Ca^{+2}$/$Mg^{+2}$-free) supplemented with 5mM dithiothreitol (DTT, Sigma-Aldrich), 5% fetal calf serum (FCS, VWR), and 10mM HEPES (Gibco). Tissues were vortexed vigorously and supernatant was discarded. Tissues were then incubated rocking at 37° C in 15 mL HBSS ($Ca^{+2}$/$Mg^{+2}$-free) supplemented with 5mM EDTA (Invitrogen), 5% FCS, and 10mM HEPES. Tissues were vortexed thoroughly and released epithelial cells were passed through a 70 μm filter. Tissues were then incubated in fresh EDTA/HBSS solution for 15 minutes, vortexed, and filtered. Supernatants were pooled and washed once before staining for flow cytometry.

For lamina propria preparations small intestinal tissue was processed as above to remove the epithelial fraction. Tissues were then rinsed in 20 mL HBSS (with $Ca^{+2}$/$Mg^{+2}$) supplemented with 5% FCS and 10mM HEPES, shaking at 37° C for 20 minutes. Supernatants were discarded and tissues were incubated in 5 mL HBSS (with $Ca^{+2}$/$Mg^{+2}$) supplemented with 3% FCS, 10mM HEPES, 30 μg $mL^{-1}$ DNase I (Sigma Aldrich), and 0.1 Wunsch $mL^{-1}$ Liberase TM (Sigma Aldrich), shaking at 37° C for 30 minutes. Tissues were vortexed and cells were passed through a 70 μm filter and washed. The resulting pellet was resuspended in 40% Percoll (Sigma

Aldrich), centrifuged for 5 minutes at 1500 rpm, and supernatant discarded. Pelleted cells were then washed and stained for flow cytometry.

For mesenteric lymph node preparations, MLN were harvested into RPMI + 5% FBS on ice. Tissues were incubated 30 minutes at 37° C in 5 mL RPMI supplemented with 2 mg $mL^{-1}$ collagenase VIII (Sigma-Aldrich) and 7.5 μg $mL^{-1}$ DNase I (Sigma-Aldrich). Digested MLN were passed through a 70 μM filter and remaining tissue was mashed through filter. Cells were washed once and stained for flow cytometry.

For tracheal epithelium, the trachea was dissected from mice, stored in DMEM + 5% FBS and cleaned of stroma using a dissecting microscope. Tissue was cut into 6 pieces and incubated at room temperature in 16U $mL^{-1}$ Dispase (Corning) in DPBS without $Ca^{2+}$/$Mg^{2+}$. Incubation was monitored carefully and stopped by transfer into DMEM + 5% FBS when epithelium began to lift away from stroma (23-28 minutes). Epithelium was then peeled off under a dissecting microscope and collected in DMEM + 5% FBS on ice. Harvested epithelium was digested in 0.5% Trypsin + EDTA for 20 minutes at 37° C. After digest, cells were vortexed briefly and trypsin was quenched with DMEM + 5% FBS. Cells were washed once and stained for flow cytometry.

For thymic epithelium, thymi were isolated, cleaned of fat and transferred to DMEM + 2% FBS on ice. Thymi were minced with a razor blade and tissue pieces were moved with a glass Pasteur pipette to 15 ml tubes and vortexed briefly in 10 ml of media. Fragments were allowed to settle before removing the media and replacing it with 4 ml of digestion media containing 2% FBS, 100 μg $mL^{-1}$ DNase I (Roche), and 100 μg $mL^{-1}$ Liberase TM (Sigma-Aldrich) in DMEM. Tubes were moved to a 37° C water bath and fragments were triturated through a glass Pasteur pipette at 0 min and 6 min to mechanically aid digestion. At 12 min,

tubes were spun briefly to pellet undigested fragments and the supernatant was moved to 20 ml of 0.5% BSA (Sigma-Aldrich), 2 mM EDTA (TekNova), in PBS (MACS buffer) on ice to stop the enzymatic digestion. This was repeated twice for a total of three 12 min digestion cycles, or until there were no remaining tissue fragments. The single cell suspension was then pelleted and washed once in MACS Buffer. Density-gradient centrifugation using a three-layer Percoll gradient (GE Healthcare) with specific gravities of 1.115, 1.065, and 1.0 was used to enrich for stromal cells. Cells isolated from the Percoll-light fraction, between the 1.065 and 1.0 layers, were then washed and resuspended for staining.

**Flow cytometry and cell sorting**

Single cell suspensions were prepared as described and stained in DPBS + 3% FBS with antibodies to surface markers for 20 min at 4° C, followed by DAPI (Roche) for dead cell exclusion. Samples were FSC-A/SSC-A gated to exclude debris, SSC-H/SSC-W gated to select single cells and gated to exclude $DAPI^+$ dead cells. Samples were run on an LSR II (BD Biosciences) or Aurora (Cytek) and analyzed with FlowJo 10 (Tree Star). For cell sorting, single cell suspensions were prepared and stained as described and sorted into $CD45^{lo}$ $IL25(RFP)^+$ $EpCAM^+$ and $CD45^{lo}$ $IL25(RFP^-)$ $EpCAM^+$ populations using a MoFlo XDP (Beckman Coulter) or an Aria II (BD Biosciences).

**RNA sequencing & analysis**

Single cell suspensions of epithelial cells from gall bladder, small intestine, colon, thymus, and trachea were generated as described above from *Il25*$^{Flare25/Flare25}$ reporter mice. $CD45^{lo}$ $RFP^+$ $EpCAM^+$ tuft cells were sorted from all tissues and $CD45^{lo}RFP^-EpCAM^+$ cells were also sorted

from the small intestine. With the exception of tracheal tuft cells, which were pooled from four mice for each replicate, each biological replicate represents one mouse. Four biological replicates were collected for each sample. Average sorted cells for each sample were as follows: SI_RFP$^{+}$: 35,250; SI_RFP$^{-}$: 55,000; Colon: 14,775; Gall: 2287, Thymus: 1612; Trachea: 255.

Cells were sorted directly into lysis buffer from the Dynabead mRNA Direct Purification Kit (ThermoFisher) and mRNA was isolated according to the manufacturer's protocol. Amplified cDNA was prepared using the NuGen Ovation RNA-Seq system V2 kit, according to the manufacturer's protocol (NuGen Technologies). Sequencing libraries were generated using the Nextera XT library preparation kit with multiplexing primers, according to manufacturer's protocol (Illumina). Library fragment size distributions were assessed using the Bioanalyzer 2100 and the DNA high-sensitivity chip (Agilent Technologies). Library sequence quality was assessed by sequencing single-end 50 base pair reads using the Illumina MiSeq platform and were pooled for high-throughput sequencing on the Illumina HiSeq 4000 by using equal numbers of uniquely mapped reads (Illumina). Twelve samples per lane were multiplexed to ensure adequate depth of coverage. Sequencing yielded a median read depth of 89.2 million reads per sample. The analytic pipeline included de-multiplexing raw sequencing results, trimming adapter sequences, and aligning to the reference genome. Sequence alignment and splice junction estimation was performed using the STAR software program. For differential expression testing, the genomic alignments were restricted to those that map uniquely to the set of known Ensembl IDs (including all protein coding mRNAs and other coding and noncoding RNAs). STAR aggregated mappings on a per-gene basis were used as raw input for normalization by DESeq2 software. Replicates failing quality control at any stage were discarded. Resulting datasets were deposited in the GEO database (GSE114067).

To determine the tuft cell signature, any genes with a mean normalized read count <300 in any tuft cell subset were removed from analysis. Next, genes were ranked based on log2 fold change between the mean expression level in all tuft samples and the mean expression level in all non-tuft samples, with a cutoff of 4. GO Term and KEGG pathway analysis was performed using the Database for Annotation, Visualization, and Integrated Discovery (53,54). Visualization of taste receptor expression was generated using Morpheus (https://software.broadinstitute.org/morpheus/).

**Quantitative RT-PCR**

For tuft cell qPCR, $CD45^{lo}RFP^{+}EpCAM^{+}$ and $CD45^{lo}RFP^{-}EPCAM^{+}$ populations from small intestinal epithelium of *Il25*$^{Flare25/Flare25}$ mice were sorted into Buffer RLT (Qiagen) using an Aria (BD Biosciences). To validate *Gnat3*$^{-/-}$ mice, $CD45^{lo}EpCAM^{+}$ epithelial cells from the small intestine were sorted into Buffer RLT (Qiagen). RNA was isolated using the Micro Plus RNeasy kit (Qiagen) and reverse transcribed using SuperScript Vilo Master Mix (Life Technologies). For tritrichomonas quantification, total DNA was isolated from cecal contents using the QIAmp Fast DNA Stool Mini Kit (Qiagen). Cecal DNA or cDNA were used as template for quantitative PCR with Power SYBR Green reagent on a StepOnePlus cycler (Applied Biosystems). For mouse cells, transcripts were normalized to *Rps17* (40S ribosomal protein S17) expression. For cecal DNA, transcripts were normalized to bacterial 16s rRNA.

**Nuclear Magnetic Resonance Quantification of SCFA and Succinate**

NMR analyses were made using a Bruker AVANCE III 800 MHz equipped with a 5 mm HCN cryoprobe suitable for $^{1}H$ inverse detection with Z-gradients at 298 K. Samples were prepared to

contain 50 μM TSP (3-(trimethylsilyl) propionic-2,2,3,3-$d_4$ acid sodium salt) for quantitative and chemical shift reference. One-dimensional $^1$H NMR spectra were obtained using the CPMG (Carr-Purcell-Meiboom-Gill) pulse sequence that included residual water signal suppression from a pre-saturation pulse during the relaxation delay. For each spectrum, 32k data points were acquired using a spectral width of 9615 Hz. The raw data were processed using a spectral size of 32k points and by multiplying with an exponential window function equivalent to a line broadening of 0.3 Hz. The resulting spectra were phase and baseline corrected and referenced with respect to the internal TSP signal. Bruker Topspin version 3.5pl6 software package was used for NMR data acquisition and processing. Assignment of peaks was made based on $^1$H NMR chemical shifts and spin-spin couplings obtained from the spectra of standard compounds under similar experimental conditions at 800 MHz. Chenomx NMR Suite Professional Software package (version 5.1; Chenomx Inc., Edmonton, Alberta, Canada) was used to quantitate metabolites. This software allows fitting spectral lines using the standard metabolite library for 800 MHz $^1$H NMR spectra and the determination of concentrations. Peak fitting with reference to the internal TSP signal enabled the determination of absolute concentrations for the short chain fatty acids and other organic acids. All NMR experiments were performed in conjunction with the Northwest Metabolomics Research Center at the University of Washington.

**Preparation of *N. brasiliensis* excretory-secretory product (NES)**

Infectious third-stage *N. brasiliensis* larvae (L3) were raised and maintained as described. Lewis rats were infected subcutaneously with 2000 *N. brasiliensis* L3. Mature (L5) worms were collected from the entire small intestine 7 days post infection. Worms were washed 10 times in Wash Solution I (PBS with 200U ml$^{-1}$ Pen-Strep), allowing worms to settle by gravity between

each wash. Worms were allowed to equilibrate in Wash Solution II (RPMI 1640 with 200U $ml^{-1}$ Pen-Strep) for 1 hour at room temperature, before being transferred to a tissue culture flask in NES culturing media (RPMI 1640, with 100U $ml^{-1}$ Pen-Strep, 2mM L-Glutamine and 1% glucose) and cultured at 37° C. Supernatant was collected at 24 and 48 hours and filtered prior to use as NES. For NMR analysis, phosphate buffer prepared in deuterated water (0.1M; pH =7.4) containing TSP (3-(trimethylsilyl) propionic-2,2,3,3-$d_4$ acid sodium salt) was added to NES to achieve a final concentration of 50uM TSP.

**Tritrichomonas culture**

Culture of *T. rainier* was performed as described (Saeki et al., 1983). Briefly, cecums of *T. rainier* colonized mice were flushed with PBS, passed through the 70 um cell strainers and centrifuged at 1000 rpm for 5 min. In order to enrich for tritrichomonads a 40/80% percoll gradient centrifugation step was performed at 1000 g for 15 min with brakes off. Tritrichomonads were collected at the interphase and the tritrichomonad containing fraction was washed with PBS and resuspended in tritrichomonad culture medium. Tritrichomonad culture medium was modified from the method described by (Saeki et al., 1983). To prepare medium, cecums of mice were harvested and homogenized in PBS with 25 volumes of PBS per gram cecum. In order to get homogeneous suspension, the cecal extract was stirred at 4°C for 6 h and then centrifuged at 3500rpm for 10 min and the supernatant was filtered. The filtered cecal extract was used to resuspend the BBL Trichosel™ Broth (BD Biosciences) and titrated to pH 7 with NaOH. The medium was then autoclaved for 10 minutes. After cooling media was supplemented with 10% heat-inactivated horse serum and the following antibiotics; amphotericin B (5ug/mL), ampicillin (100ug/mL), chloramphenicol (100ug/mL),

gentamicin (50ug/mL), kanomycin (100ug/mL), streptomycin (100ug/mL), vanomycin (5ug/mL). The enriched tritrichomonads were resuspended in culture medium at 2 x $10^6$ protists per mL and cultured under anaerobic conditions for 24h. Media was collected and centrifuged 1750 rpm for 10 min. Supernatant was filter (0.22um PVDF filter). For NMR analysis, phosphate buffer prepared in deuterated water (0.1M; pH =7.4) containing TSP (3-(trimethylsilyl) propionic-2,2,3,3-$d_4$ acid sodium salt) was added to tritrichomonad conditioned media to achieve a final concentration of 50uM TSP.

**Tritrichomonas sequencing**

Internal transcribed spacer (ITS) sequencing of the tritrichomonad identified in the University of Washington vivarium was performed as previously described (55). Briefly, DNA was isolated from the cecal contents of colonized mice using the QIAmp Fast DNA Stool Mini Kit (Qiagen) and the ITS region was PCR-amplified using pan-parabasalid primers (Forward: AATACGTCCCCTGCCCTTTGT Reverse: TCCTCCGCTTAATGAGATGC). The resulting PCR product was sequenced by Sanger Sequencing (Genewiz). A BLASTn search identified the sequence as novel but closely related to both murine and human tritrichomonads. Alignment with the ITS sequences of *T. muris* (Accession: AY886843.1) and *T. musculis* (Accession: KX000922.1) showed >97% and >86% sequence identify, respectively. For clarity, we refer to this novel isolate as *Tritrichomonas rainier*, although its precise taxonomic relationship to *T. muris* and *T. musculis* remains to be determined. The ITS sequence for *T. rainier* is available in GenBank (Accession #: MH370486).

**Organoid Culture**

Small intestinal crypt-derived organoids were grown as described (Sato et al., 2013), replacing recombinant R-spondin with supernatants from R-spondin expressing L-cells and replacing recombinant Noggin with supernatants from Noggin expressing cells. Crypts were harvested from the small intestine of naive B6.*Il25*$^{Flare25/Flare25}$ mice and plated on day 0. On day 1 and day 4, media were replaced and organoids were treated with 20 ng ml$^{-1}$ recombinant IL-13 or 10mM sodium succinate. On day 7 organoids were harvested and resuspended in Accutase (Corning). Organoids were sheared with a 28G insulin syringe, incubated for 1 h at room temperature, washed, and then stained for flow cytometry as described above.

**Calcium imaging**

Mouse embryonic fibroblasts were plated 7 x $10^4$ cells/well in 24-well plates coated with poly-D-lysine. After overnight incubation, cells were washed with assay buffer (1X HBSS with $Ca^{2+}$/$Mg^{2+}$, 10mM HEPES, pH 7.4). Cells were incubated for 1 hr at 37°C in assay buffer supplemented with 2.5 mM Fluo-4AM (Invitrogen) and 0.05% pluronic-F127 (Invitrogen). Cells were washed twice with assay buffer and incubated in assay buffer with 1mM probenecid (Biotium) for 30 minutes at 37° C prior to imaging. Cells were maintained at 37° C with 5% $CO_2$ throughout imaging. While imaging, sodium succinate was added to assay buffer at a final concentration of 150uM or 100ul NES or NES culturing media was added to 250ul assay buffer. Following addition of test agonist, ionomycin was added at a final concentration of 1ug mL$^{-1}$. Fluorescence images were collected at 1.44 frames per second with a 40X extra-long working distance objective on a Nikon TiE Inverted Widefield Fluorescence *Nikon microscope* and analyzed with NIS Elements AR 3.2 software. For data presentation, fluorescence/background ($R/R_0$) was quantified over time. More than 50 cells were analyzed per replicate.

**ILC2 Stimulation Assay**

Small intestinal lamina propria ILC2s were isolated from Smart13 reporter mice and sorted as described. Sorted cells were plated at 4000-5000 cells per well in a 96 well plate and incubated overnight in 10 ng/mL IL-7 (R&D Systems) and basal media composed of high glucose DMEM supplemented with non-essential amino acids, 10% FBS, 100 mg/mL streptomycin/penicillin, 10mM HEPES, 1mM sodium pyruvate, 100μM 2-mercaptoethanol, and 2mM L-glutamine. The next morning media was replaced with fresh media and 10 ng/mL IL-7 and cells were stimulated with the indicated agonist. After a six-hour incubation at 37 °C, cells were stained with 1 μl/well of PE-conjugated anti-hCD4 for 20 minutes at 4 °C. Cells were washed, resuspended in DAPI, and analyzed on an LSRII (BD Biosciences).

**Quantification and Statistical Analysis**

All experiments were performed using randomly assigned mice without investigator blinding. Statistical details of experiments can be found in the figure legends. All data points and "n" values reflect biological replicates (i.e. mice), except in 4C where they represent technical replicates. No data were excluded. Statistical analysis was performed as noted in figure legends using Prism 7 (GraphPad) software. Holm-Sidak was used to correct for multiple comparisons. Graphs show mean + SEM.

**Data and Software Availability**

RNA-Seq data are available at the NCBI GEO under accession number GSE114067. The ITS sequence for *T. rainier* is available in GenBank under accession number MH370486.

## 2.5 Acknowledgments

We thank staff at the University of Washington Gnotobiotic Core for assistance with germ free mouse experiments, H.E. Liang for assistance with *Gnat3* CRISPR targeting and validation, Z. Wang for experimental assistance, N. Arpaia for guidance on NMR analysis of intestinal samples, D. Hailey and the Garvey Cell Imaging Lab in the Institute for Stem & Cell Regenerative Medicine for microscopy support, and K. Smith for mice, reagents and advice. JWM is supported by the University of Washington Immunology Training Grant (T32 AI106677). JVM is a Damon Runyon–Dale Frey Breakthrough Scientist and a Searle Scholar. This work was supported by NIH 1DP2 OD024087 (JVM) and the University of Washington. mRNA sequencing was supported by NIH R01 AI26918 (RML) and the SABRE Center at UC San Francisco.

**Author Contributions:** MSN and JWM designed and performed experiments, analyzed data, and wrote the paper with JVM. MRLC, JBJ, and LP assisted with experiments at the University of Washington. CNM and CS assisted with cell isolation for RNA sequencing at UC San Francisco. JLP performed bioinformatics analysis of mRNA sequencing data, with supervision by DJE. GANG performed NMR analysis, with supervision by DR. MFF helped design experiments and write the paper. MSA and RML acquired funding and provided resources for mRNA sequencing. JVM conceived of and supervised the study, performed experiments, analyzed data, and wrote the paper with MSN, JWM, and MFF.

## 2.6 Figures

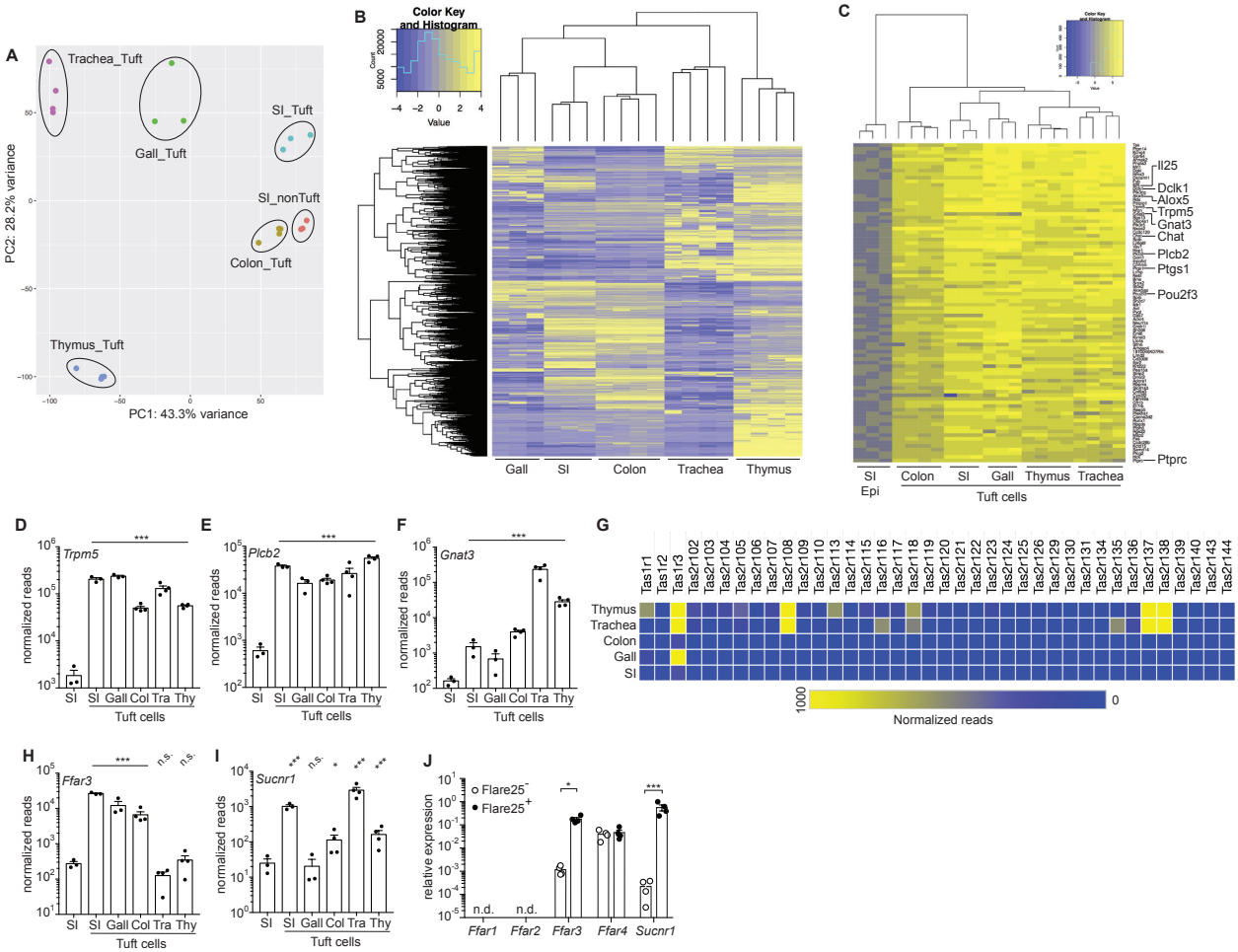


**Figure 1. RNA-Seq identifies a transcriptional tuft cell signature and a tissue-specific chemosensory receptor repertoire**

**(A-I)** Tuft cells (CD45$^{lo}$ EPCAM$^{+}$ Flare25$^{+}$) were sorted from small intestine (SI), gall bladder (Gall), colon (Col), trachea (Tra), and thymus (Thy) of naïve B6.*Il25*$^{Flare25/Flare25}$ mice for mRNA sequencing. Non-tuft epithelial cells of the small intestine (SI Epi; CD45$^{lo}$ EPCAM$^{+}$ Flare25$^{-}$) were sorted as a negative control. **(A)** Principle component analysis of gene expression. **(B)**

Hierarchical clustering of differentially expressed genes (fold change > 8; FDR < 0.01) among tuft cell subsets. **(C)** Ranked list of a tuft cell transcriptional signature ($Log_2$ fold-change >4 in all tuft cells relative to SI Epi). **(D-F)** Normalized read count of indicated genes. **G)** Heat map of normalized read count of all taste receptors. **(H-I)** Normalized read count of indicated genes. **(J)** Indicated genes analyzed by RT-qPCR in small intestinal tuft cells (Flare25$^{+}$) and non-tuft epithelial cells (Flare25$^{-}$). A-I: biological replicates from one mRNA sequencing experiment. J: biological replicates pooled from three experiments. In A-I *, FDR < .05; ***, FDR < .001 by statistical analysis in RNAseq pipeline. In J *, $p < 0.05$; ***, $p < 0.001$ by multiple *t*-tests. n.s., not significant; n.d., not detectable. Graphs show mean + SEM.

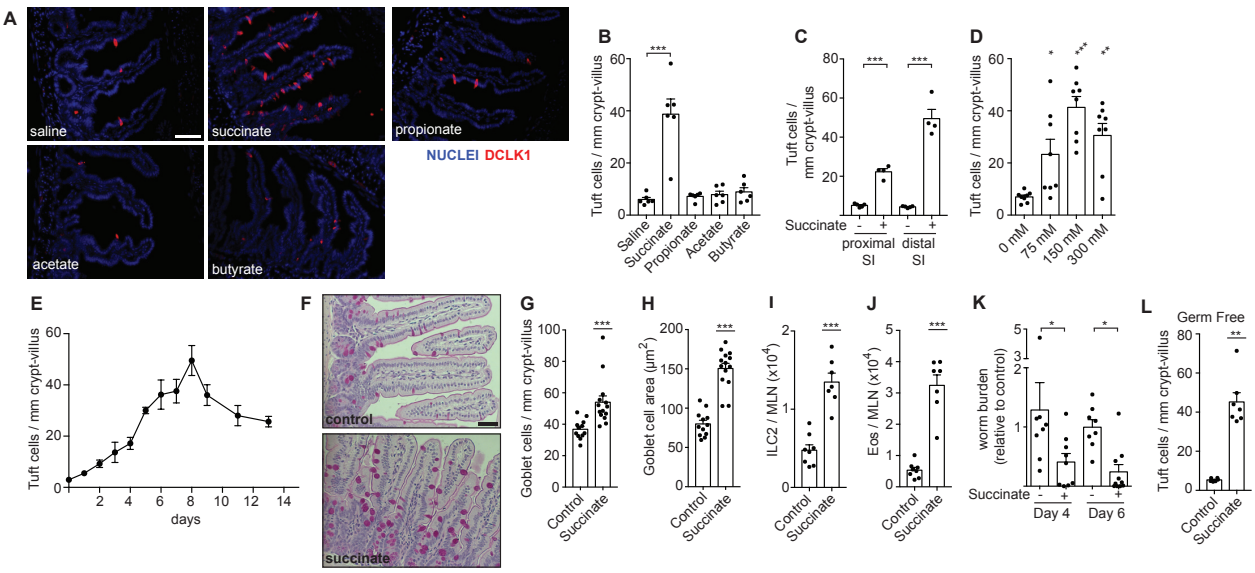


**Figure 2. Succinate is sufficient to induce a type 2 immune response in the small intestine**

**(A-J)** Unless otherwise indicated, wild-type mice were given 150 mM succinate or control water for 7 d. **(A)** Representative images of distal (last 10 cm) small intestine (SI). DCLK1 marks tuft cells. Scale bar = 50 μm **(B)** Quantification of tuft cells in A. **(C)** Tuft cell quantification by microscopy in the proximal (first 10 cm) and distal SI **(D-E)** Tuft cell quantification in the distal SI at indicated **(D)** succinate concetrations and **(E)** timepoints. **(F)** Representative images of middle (10-20 cm from cecum) SI stained with periodic acid-Schiff to visualize goblet cells. Scale bar = 50 μm. **(G-H)** Quantification of goblet cell **(G)** numbers and **(H)** hypertrophy. **(I-J)** Absolute numbers of **(I)** ILC2s and **(J)** eosinophils quantified in MLN by flow cytometry. **(K)** Total worm burden in wild-type mice that received 7 d treatment with 150mM succinate or water control prior to and during infection with *N. brasiliensis*. Worm burden represented as relative to median of control within each experiment. **(L)** Tuft cell quantification in distal SI of germ-free mice treated as in A-J. In B-D, G-L each symbol represents an individual mouse from at least three pooled experiments. In E, each symbol represents the average of 3-9 mice pooled from

three experiments. *, $p < 0.05$; **, $p < 0.01$; ***, $p < 0.001$ by one-way ANOVA with comparison to control (B, D), by Mann-Whitney (G-J, L), or by multiple *t*-test (C, K). Graphs depict mean + SEM.

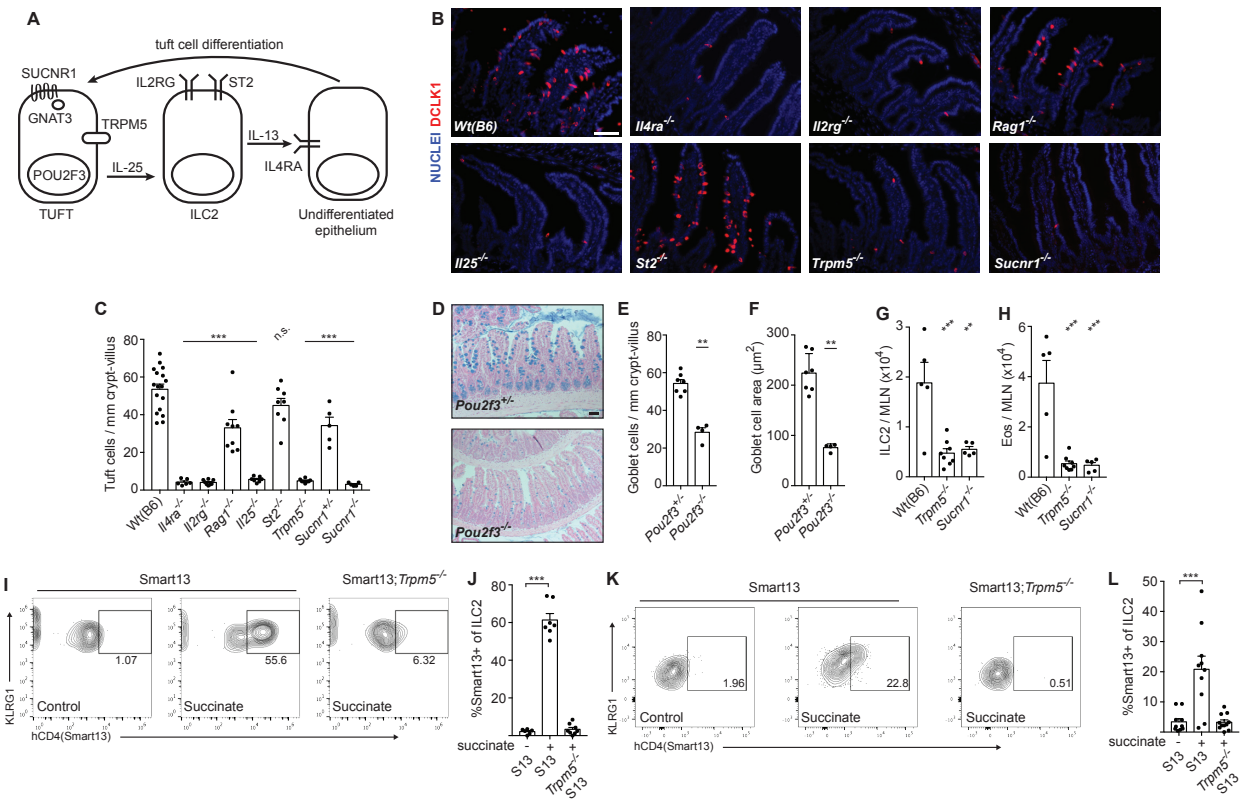


**Figure 3. Succinate signals via the tuft cell-ILC2 circuit in a TRPM5 and SUCNR1-dependent manner**

**(A)** Schematic of cells and proteins in the tuft-ILC2 circuit. **(B-J** Mice of indicated genotypes were given 150 mM succinate for 7 d. **(B)** Representative images of distal (last 10 cm) small intestine (SI). DCLK1 marks tuft cells. Scale bar = 50 µm. **(C)** Quantification of tuft cells in B. **(D)** Representative images of middle (10-20 cm from cecum) SI stained with Alcian blue to visualize goblet cells. Scale bar = 100 µm. **(E-F)** Quantification of goblet cell **(E)** numbers and **(F)** hypertrophy in D. **(G-J)** MLN analyzed by flow cytometry to quantify **(G)** ILC2s, **(H)** eosinophils, and **(I-J)** IL-13 production by ILC2s. Smart13: IL-13 reporter. **(K-L)** Lamina propria cells from mice of indicated genotypes given 150 mM succinate for 36 hours and analyzed as in I-J. In C-H, J-L each symbol represents one mouse from at least two pooled

independent experiments. *, $p < 0.05$; **, $p < 0.01$; ***, $p < 0.001$ by one-way ANOVA (C, G-H, J, L) with comparison to Wt(B6) or untreated Smart13 control, or by Mann-Whitney (E-F). n.s., not significant. Graphs depict mean + SEM.

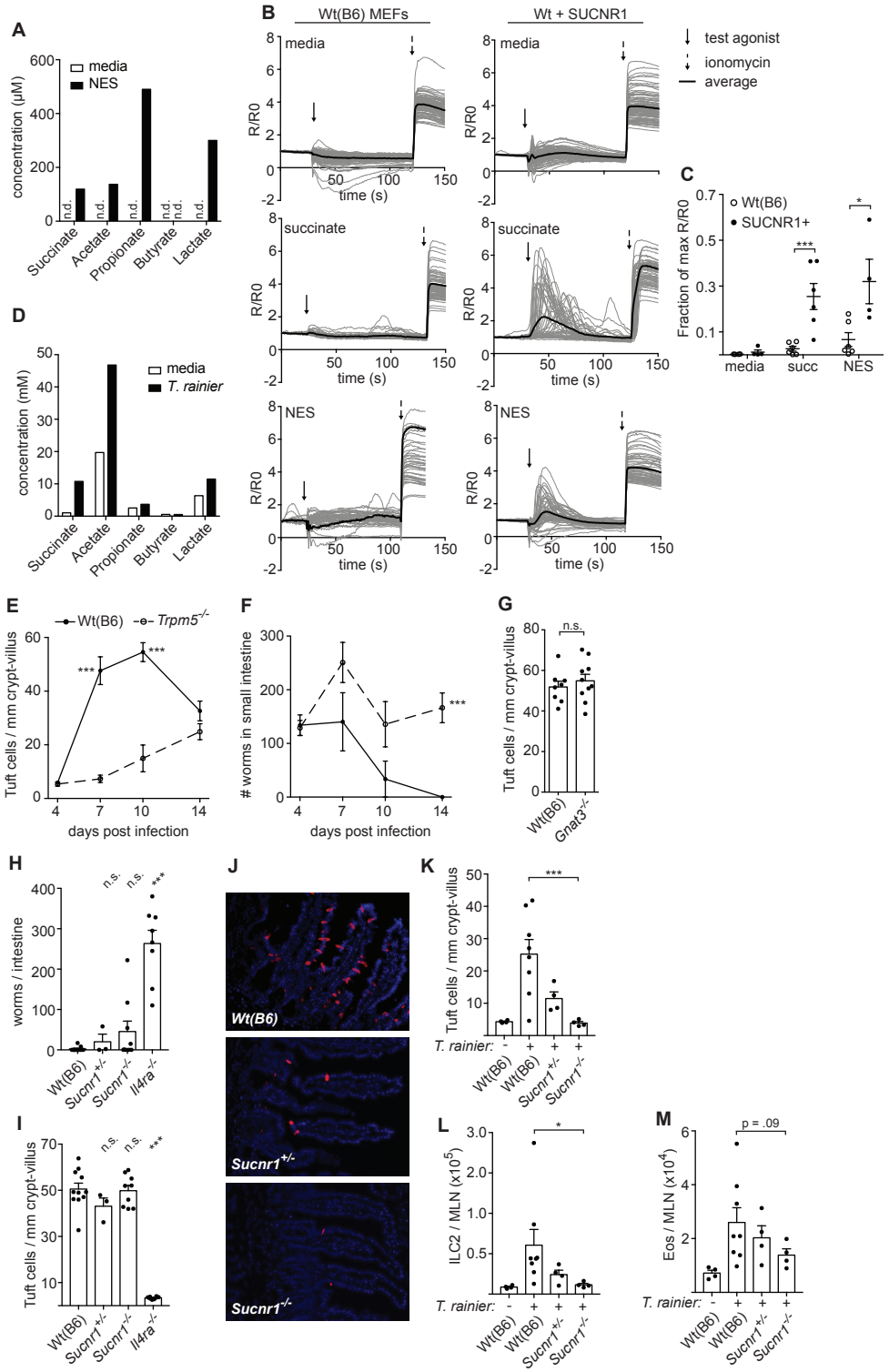


**Figure 4: Immune sensing of *T. rainier* but not *N. brasiliensis* requires SUCNR1**

**(A)** Concentration of indicated molecules measured in *N. brasiliensis* excretory-secretory product (NES) or media control by NMR. **(B)** Representative calcium fluxes in wild-type (B6) or SUCNR1-transduced MEFs treated as indicated. **(C)** Quantification of B. **(D)** Concentrations of indicated molecules measured in *T. rainier* conditioned media or media alone by NMR. **(E-I)** Mice of indicated genotypes were infected with *N. brasiliensis.* **(E)** Tuft cell quantification in the distal (last 10 cm) small intestine (SI), and **(F)** total worm burden at indicated times. **(G)** Tuft cell quantification in the distal SI 7 d post infection. **(H)** Tuft cell quantification in the distal SI and **(I)** total worm burden 8 d post infection. **(J-M)** Mice of indicated genotypes were colonized with *T. rainier* for 7 d or left untreated. **(J)** Representative images of distal SI. DCLK1 marks tuft cells. Scale bar = 50 μm. **(K)** Quantification of tuft cells in J. **(L-M)** MLN analyzed by flow cytometry to quantify **(L)** ILC2s and **(M)** eosinophils. A-B, D show representative data from at least two independent experiments. In C, each symbol represents one technical replicate. In G-I, K-M each symbol represents one mouse from at least two pooled experiments. In E-F each symbol represents the average of 3-10 mice from three pooled experiments. *, $p < 0.05$; **, $p < 0.01$; ***, $p < 0.001$ by one-way ANOVA (H-I, K-M) with comparison to Wt(B6) control, by Mann-Whitney (G), or using multiple *t*-tests (C, E, F). n.s., not significant. Graphs depict mean + SEM.

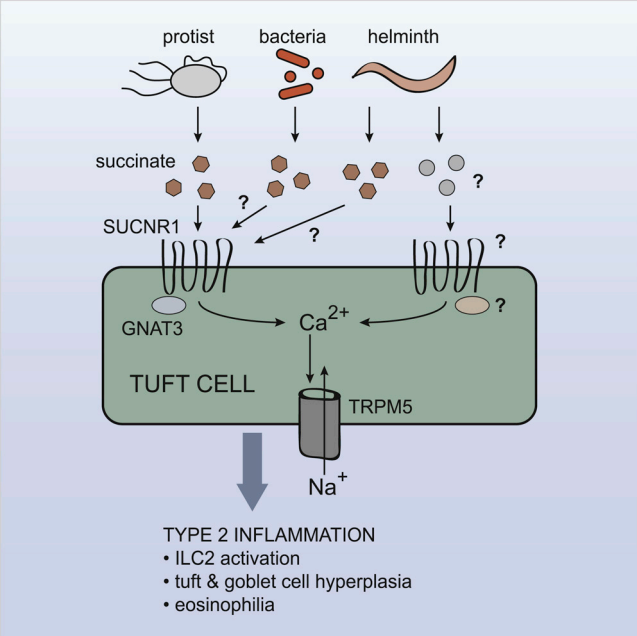


**Figure 5. Proposed model for activation of intestinal tuft cells by succinate.** Tritrichomonad protists that colonize the cecum and distal small intestine secrete succinate as a metabolite. This signals through the receptor SUCNR1, expressed on tuft cells, resulting in an intracellular calcium flux, opening of the TRPM5 cation channel, and release of mediators that initiate a type 2 immune response.

## 2.7 Supplemental Figures

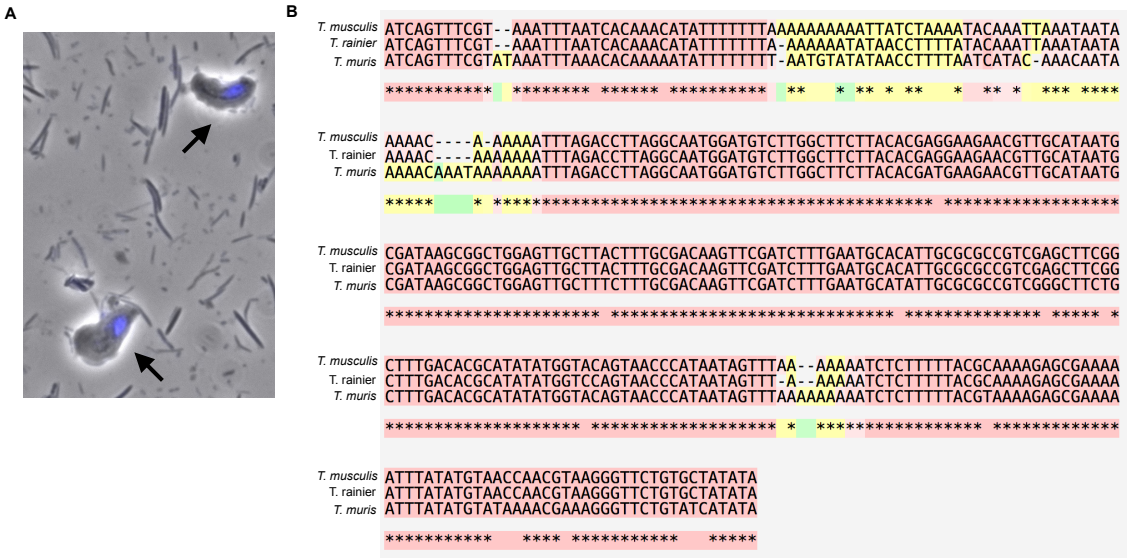


**Figure S1. Related to Figure 4. (A)** Representative images of *T. rainier* (arrows) with DAPI (blue) staining of nuclei. **(B)** Alignment of internal transcribed spacer sequence of *T. rainier* with published sequences for *T. muris* and *T. musculis*.

# CHAPTER 3

## Small intestinal tuft cells secrete cysteinyl leukotrienes to rapidly activate anti-helminth type 2 immunity

This chapter is adapted from the following publication:

McGinty JW, Ting HA, Billipp TE, Nadjsombati MS, Khan DM, Barrett NA, Liang HE, Matsumoto I, von Moltke J. Tuft-cell-derived leukotrienes drive rapid anti-helminth immunity in the small intestine but are dispensable for anti-protist immunity. Immunity. 2020. 52:528-541.

## 3.1 Introduction

While progress has been made in elucidating the specific signals that activate SI tuft cells (20,43,56), less is known about how such signals are converted into an effector response. The chemosensing pathways expressed in tuft cells converge on the calcium-gated membrane cation channel TRPM5, and type 2 immune responses are profoundly delayed or absent in *Trpm5*-deficient mice colonized with helminths or Tritrichomonads (23,56). By analogy to taste receptor cells (30), sodium influx through TRPM5 is presumed to depolarize tuft cell membranes, but the effector functions mobilized downstream of TRPM5 to activate the tuft-ILC2 circuit remain unknown. TRPM5 may regulate the release of IL-25 (57), the only intestinal tuft cell effector molecule identified to date; however based on our understanding of ILC2 activation (discussed below) we predict that physiologic levels of IL-25 are not sufficient to fully activate ILC2 responses.

ILC2s are tissue resident cells widely distributed throughout the body, and they express a specific set of surface receptors that attunes them to signals produced in the local environment (19). ILC2s of the SI are particularly responsive to IL-25 signaling due to their high expression of the IL-25 receptor (20). ILC2s resemble T helper 2 (Th2) $CD4^+$ T cells in their dependence on the lineage-defining transcription factor GATA3 and expression of hallmark cytokines IL-13 and IL-5. Indeed, the chromatin landscapes of ILC2s and effector Th2 cells are nearly identical, suggesting that the same transcription factors are likely to regulate cytokine production in both cell types (16,17). During T cell activation, T cell receptor (TCR) signaling simultaneously induces the AP-1, NF-$\kappa$B, and NFAT transcription factors that cooperatively drive effector gene expression. ILC2s are in part defined by their lack of a TCR, and we and others demonstrated that lung ILC2s must therefore integrate multiple signaling pathways to replicate TCR signaling

and achieve optimal activation (58,59). In the lung, cysteinyl leukotrienes (cysLTs) represent an important signal due to their ability to induce nuclear translocation of NFAT, which synergizes with IL-33-induced AP-1 and NF-$\kappa$B to yield maximal cytokine production. Whether cysLTs are required for immunity to intestinal helminths, and which cells might produce them in this context, has not been investigated.

Leukotrienes are lipid signaling molecules generated by the conversion of arachidonic acid to $LTA_4$ via the enzyme 5-lipoxygenase (5-LO) (60) (Figure 1A). $LTA_4$ is rapidly converted into $LTB_4$ by the enzyme LTA4 hydrolase, or into $LTC_4$ by LTC4 synthase. Following secretion, $LTC_4$ is further converted into $LTD_4$ and $LTE_4$, together comprising the cysLTs. Whereas $LTB_4$ is primarily a chemoattractant, cysLTs are inflammatory mediators, with $LTC_4$ and $LTD_4$ having well-defined roles in promoting allergic pathology in the airways (61). Leukotrienes are not preformed, but rather are synthesized and secreted on demand within minutes. In many cases, leukotriene synthesis is initiated by intracellular calcium flux that activates cytosolic phospholipase A2 (62). Once outside the cell, $LTC_4$ and $LTD_4$ are rapidly converted to the more stable $LTE_4$ (63).

Leukotriene synthesis is canonically thought to be restricted to hematopoietic cells, but tuft cells also express genes required for the synthesis of leukotrienes, including *Pla2g4a, Alox5, and Ltc4s* (29,64). Indeed, expression of these genes is one defining feature of a core tuft cell signature conserved across multiple tissues (56). We therefore hypothesized that tuft cells might generate leukotrienes to amplify type 2 inflammation in the SI.

### 3.2 Results

**Cysteinyl leukotrienes are a non-redundant signal for intestinal ILC2 activation**

Leukotrienes drive ILC2 activation in the lung during allergy and helminth infection (59,65), but less is known about their role in the SI. Given the tissue-specific imprinting of ILC2s (19), we wanted to test if leukotrienes also regulate SI ILC2s. SI ILC2s express both the $LTC_4$ and $LTD_4$ receptors CYSLTR1 and CYSLTR2, similar to lung ILC2s (Figure 1B; gating strategies in Figures S1A-S1B). $LTB_4$ binds to two receptors, the high-affinity LTB4R1 and lower-affinity LTB4R2. SI ILC2s also express *Ltb4r1* (Figure 1B), whereas *Ltb4r2* and the $LTE_4$ receptor *Oxgr1* are low or absent (data not shown). To confirm these findings functionally, we performed an *in vitro* activation assay using SI ILC2s sorted from the *Il13*$^{Smart13}$ (S13) cytokine reporter mouse (66). In these mice, surface expression of non-signaling human CD4 allows for quantification of IL-13 protein expression by flow cytometry. $LTC_4$ and $LTD_4$ robustly activated SI ILC2s in a dose-dependent manner, in accordance with high expression of their receptors, whereas $LTB_4$ and $LTE_4$ had minimal effect in this assay (Figure 1C; gating in Fig S1C). $LTC_4$-induced activation was abolished in the presence of the CYSLTR1-specific inhibitor montelukast (Figure S1D). In contrast, the CYSLTR2 inhibitor HAMI3379 only suppressed ILC2 activation by $LTC_4$ at micromolar doses, likely reflecting inhibition of CYSLTR1 at high concentrations (67). As in the lung, CYSLTR1-mediated sensing of $LTC_4$ and/or $LTD_4$ therefore appears to be the dominant mechanism of leukotriene-driven SI ILC2 activation.

CysLTs are known to cooperate with IL-33 to induce maximal lung ILC2 activation (58,59). Whereas IL-33 is the predominant innate cytokine found in the lung and lung ILC2s express the IL-33 receptor (68), SI ILC2s are highly responsive to the cytokine IL-25, produced exclusively by tuft cells (24). We therefore hypothesized that cysLT signaling might also cooperate with IL-25 to drive ILC2 activation. To test this, we repeated *in vitro* stimulation of SI ILC2s, this time using sub-optimal doses of $LTC_4$, IL-25, or both (Figures 1D-E and S1E). At

these low concentrations, $LTC_4$ or IL-25 alone minimally induced ILC2 activation. When $LTC_4$ and IL-25 were used in combination, however, an additive effect was evident in both the frequency of responding cells and the amount of IL-13 expressed per cell. A similar effect was also observed with the combination of $LTC_4$ and IL-33 (Figures 1F-G).

During lung ILC2 activation, cysLTs are non-redundant due to their ability to induce nuclear translocation of NFAT, which cooperates with IL-33-induced NF-$\kappa$B and AP-1 (59). Specifically, signaling through CYSLTR1 induces a calcium flux that activates calcineurin, resulting in NFAT dephosphorylation and translocation to the nucleus (59,69). IL-25 has also been shown to induce NF-$\kappa$B and AP-1, but a role for NFAT induction has not been reported (70,71). Stimulation of SI ILC2s with $LTC_4$ resulted in NFAT nuclear translocation, which was inhibited by the calcineurin inhibitor cyclosporin A (Figures 1H-I). Conversely, stimulation with IL-25 or IL-33 alone had no effect on NFAT localization. Thus, cysLTs are a non-redundant signal for SI ILC2 activation and cooperate with IL-25 and/or IL-33 to maximize effector cytokine production.

**ILC2 homeostasis in the proximal small intestine is leukotriene-independent and minimally requires IL-25 and IL-33**

We recently identified tuft cells as the sole source of IL-25 in the SI and found they express this cytokine constitutively (24). In that study we also found that ~20% of SI ILC2s from uninfected mice expressed IL-13, which was absent in IL-25-deficient mice. We therefore concluded that IL-25 is constitutively secreted and signals to SI ILC2s homeostatically. Subsequently, tuft cells were shown to be activated by Tritrichomonad protists that are common across vivariums (20,23,56); we determined in retrospect that the mice used in our original study

were likely colonized by these protists as well. This finding prompted us to reevaluate the role of homeostatic IL-25 signaling using naïve, Tritrichomonad-free mice.

We compared IL-13 reporter expression in cells isolated from the proximal SI of naïve wildtype, *Il25*$^{-/-}$, *St2*$^{-/-}$ and *Alox5*$^{-/-}$ mice. *St2* constitutes part of the IL-33 receptor and is required for IL-33 signaling. *Alox5* encodes 5-lipoxygenase, the enzyme that catalyzes the first step in all leukotriene synthesis (Figure 1A). We also included *Trpm5*$^{-/-}$ mice to assess the role of the TRPM5-dependent tuft cell chemosensing pathway during homeostasis. Defining ILC2s in the SI lamina propria as CD45$^{+}$;Lineage(Lin)$^{-}$; KLRG1$^{+}$ cells (gating in Figure S1A), we found that IL-13 expression was generally low, especially when compared to previous measurements made in Tritrichomonad-colonized mice (Figure S2A) (24). IL-13 expression was comparable across genotypes, though some variability between mice was evident. We did note, however, that KLRG1 staining intensity appeared reduced in *Il25*$^{-/-}$ and *Trpm5*$^{-/-}$ mice. We therefore reexamined IL-13 expression in ILC2s identified as CD45$^{+}$;Lin$^{-}$;IL-17RB$^{+}$. Again we found minimal IL-13 expression across all groups, but confirmed that KLRG1 MFI was indeed decreased in *Il25*$^{-/-}$ and *Trpm5*$^{-/-}$ mice (Figures 2A-C; gating in Fig S2B), suggesting some tuft cell-dependent regulation of ILC2s in the absence of any currently known tuft cell agonists.

To get a more complete picture of ILC2 activation states in naïve mice, we sorted CD45$^{+}$;Lin$^{-}$;IL-17RB$^{+}$ cells from the proximal SI lamina propria of wildtype, *Alox5*$^{-/-}$, *Il25*$^{-/-}$, and *St2*$^{-/-}$ Tritrichomonad-free mice and performed bulk RNA sequencing (Table S1). We again found no evidence of a homeostatic role for leukotrienes: wildtype and *Alox5*$^{-/-}$ mice clustered together by PCA and only 24 genes, including *Alox5*, were identified as differentially expressed (FDR <.05, row mean > 10) (Figures 2D-E). We did see more differences in the *Il25*- (142 genes) and *St2*- (88 genes) deficient ILC2s, but here too the homeostatic role of these cytokines

was limited (Tables S2-4). In particular, the fold-change in gene expression was generally small, although we cannot rule out more significant post-transcriptional changes (Figure 2F). *Klrg1* mRNA, for example, was downregulated only 0.8 fold in *Il25*$^{-/-}$ ILC2s, but clearly decreased at the protein level (Fig 2C). Also notable was the lack of effector cytokines on the list, with the exception of *Areg*, which was downregulated only in *St2*$^{-/-}$ ILC2s. Among the genes that were differentially expressed, we were surprised to see very little overlap between *Il25*- and *St2*-deficient ILC2s, despite related signaling pathways downstream of ST2 and the IL-25 receptor. Several NF-κB and AP-1 related genes were uniquely downregulated in the absence of *St2*, suggesting homeostatic and/or developmental defects that would be interesting to explore further. Overall, however, these results demonstrate that at homeostasis, leukotrienes do not modulate ILC2 gene expression in the proximal SI whereas IL-25 contributes minimally, but detectably.

**Cysteinyl leukotrienes drive rapid ILC2 activation following helminth infection**

ILC2s are tissue-resident cells that rapidly respond to local cues to initiate type 2 inflammation. To probe the earliest signaling events driving SI ILC2 activation we used helminth infection. *H. polygyrus* naturally infects mice through the oral route and transits directly to the proximal SI to establish infection, allowing us to deliver activating signals to the SI in a precisely timed manner. Sixteen hours after oral gavage with *H. polygyrus* L3 larvae, ILC2s in the proximal SI exhibited upregulated IL-13 expression (Figures 3A-B). This response was abolished in TRPM5-deficient and IL-25-deficient mice, placing tuft cell sensing of *H. polygyrus* upstream of ILC2 activation, as previously described (23,24). Infection did not alter tuft cell *Il25* expression at this time (Figure 3C; gating in Figure S3A). While IL-33 elicited in response to

parasite damage has previously been shown to drive type 2 immunity in the SI (72), IL-33 signaling was not required for this initial tuft cell-dependent anti-helminth response (Figure 3B).

We found that *Alox5*$^{-/-}$ mice also had impaired ILC2 activation at this early time point, indicating that leukotrienes are required for ILC2 activation *in vivo* (Figure 3B). Consistent with *in vitro* findings, administration of the CYSLTR1 antagonist montelukast resulted in a similar defect in ILC2 activation, demonstrating that $LTC_4$ and/or $LTD_4$ serve a non-redundant function (Figure 3D). While there was no difference in the number of lamina propria ILC2s between wildtype and *Alox5*$^{-/-}$ mice at steady state (Figure S3B), we observed reduced proliferation of ILC2s early during *H. polygyrus* infection in *Alox5*$^{-/-}$ mice (Figure 3E). We were unable to isolate viable cells from infected tissue at later time points, so we examined mesenteric lymph nodes as a proxy. After four days of *H. polygyrus* infection, ILC2 number and activation were marginally increased compared to uninfected mice, whereas the response during *N. brasiliensis* infection was much more pronounced (Figures S3C-F). In both cases, ILC2 number and activation were decreased in *Alox5*$^{-/-}$ mice. Collectively, these results demonstrate that cysLTs are rapidly induced in the SI following helminth sensing by tuft cells and are required for optimal ILC2 activation.

**Tuft-ILC2 circuit activation and worm clearance are delayed in the absence of cysteinyl leukotrienes**

ILC2 activation following helminth infection is regulated by tuft cells through the feed-forward tuft-ILC2 circuit (24). As ILC2 activation was impaired in the initial response to *H. polygyrus* infection in *Alox5*$^{-/-}$ mice, we predicted that induction of the tuft-ILC2 circuit itself would also be disrupted. At homeostasis there was no difference in the number of tuft cells

between wildtype and *Alox5*$^{-/-}$ mice, consistent with similar basal ILC2 activity (Figures 4A-B). Four days after *H. polygyrus* infection, however, wildtype mice developed tuft cell hyperplasia in the proximal SI, a response that was absent in *Alox5*$^{-/-}$ mice. Impaired tuft cell hyperplasia was also evident later during infection (Figure 4C). This response required signaling through CYSLTR1, further implicating $LTC_4$ and $LTD_4$ as the relevant mediators; however, we cannot rule out non-redundant contributions of other 5-LO-dependent leukotrienes (e.g. $LTB_4$ from tuft cells or other lipids generated by transcellular biosynthesis) (Figure 4D). IL-25, but not IL-33, signaling was required for the early tuft cell response (Figure 4E).

*H. polygyrus* establishes chronic infection in mice, making it a poor model for assessing the role of type 2 responses in worm clearance. To gauge whether leukotriene signaling contributes to restriction of helminths, we turned to *N. brasiliensis*, a rat-adapted helminth that causes a self-limiting infection in mice. In this model *N. brasiliensis* L3 larvae are injected subcutaneously, briefly transit through the lung, and reach the proximal SI around day 2-3 post-infection where they mature into adult worms. Accordingly, we first detected tuft cell hyperplasia in the proximal SI, with the distal SI displaying delayed kinetics in comparison (Figure 4F). At day 5 post-infection tuft cell numbers were noticeably increased in the proximal SI of *N. brasiliensis*-infected wildtype mice. As with *H. polygyrus*, *Alox5*$^{-/-}$ mice failed to induce tuft cell hyperplasia both at this early time point in the proximal SI (Figures 4G-H) and in the distal SI 7 days after infection (Fig 4I). Results were replicated in littermate controls, indicating that microbiome differences do not mediate observed differences (Figure S4A).

Intestinal organoids are three-dimensional cultures that contain all intestinal epithelial cell types and are commonly used to study epithelial biology *in vitro* (73). Using this system, we found that *Alox5*$^{-/-}$ intestinal stem cells have no intrinsic defect in their ability to differentiate into

tuft cells following IL-13 stimulation (Figure S4B) and that cysLTs do not induce tuft cell expansion directly (Figure S4C). Further, the infection-induced increase in intestinal epithelial turnover, as assessed by *in vivo* BrdU pulse-chase, was marginally increased in *Alox5*$^{-/-}$ mice, confirming that the defect in tuft cell hyperplasia is not caused by a general delay in epithelial differentiation (Figure S4D). Arachidonic acid metabolism generates leukotrienes but can also produce prostaglandins, which have previously been implicated in anti-helminth immunity (74). To rule out a contribution of arachidonic acid being shunted into the prostaglandin pathway in the absence of 5-LO (Figure 1A), we treated leukotriene-deficient mice with ibuprofen to inhibit the cyclooxygenase enzymes that mediate prostaglandin synthesis; however, this had no effect on tuft cell numbers (Figure S4E).

Intestinal remodeling and increased goblet cell mucus secretion constitute part of the "weep and sweep" response that develops to promote worm expulsion. After 7 days of *N. brasiliensis* infection, *Alox5*$^{-/-}$ mice had fewer goblet cells than wildtype mice and these were smaller in size, indicating reduced mucus production (Figures 4J-L). The failure of *Alox5*$^{-/-}$ mice to efficiently induce the tuft-ILC2 circuit also resulted in sustained worm burdens at day 7, a time when wildtype mice begin to clear infection (Figure 4M). Despite this defect, both wildtype and *Alox5*$^{-/-}$ mice cleared infection by day 14, indicating that additional leukotriene-independent mechanisms of control exist. Nonetheless, these data collectively suggest a model in which cysLTs are rapidly induced in the SI following tuft cell sensing of helminths, and that this signal, along with IL-25, drives ILC2 activation to kickstart the tuft-ILC2 feed-forward circuit.

**Tuft cells synthesize cysteinyl leukotrienes**

ILC2 activation following helminth infection requires IL-25, produced exclusively by tuft cells in the SI (24). Accordingly, IL-25 deficiency impairs worm clearance following helminth infection (21). When compared head-to-head, we found the clearance defect is more severe in tuft cell-deficient *Pou2f3*$^{-/-}$ mice than *Il25*$^{-/-}$ mice (Figure 5A), suggesting the existence of additional tuft cell effector functions. As published tuft cell transcriptomes include enzymes required for the synthesis of cysLTs (29,56,64), we hypothesized that tuft cells themselves might secrete leukotrienes.

To confirm previous transcriptomic data, we sorted tuft cells and non-tuft epithelium from the SI using the Flare25 reporter mouse and performed qPCR (Figure 5B; gating in Figure S5A). Tuft cells highly and specifically expressed *Alox5* and *Alox5ap*, encoding 5-lipoxygenase (5-LO) and 5-lipoxygenase activating protein (FLAP), respectively, core components of the leukotriene synthesis pathway. Tuft cells additionally expressed *Pla2g4a,* a calcium-dependent phospholipase that liberates arachidonic acid from cell membranes; *Ltc4s*, required for the synthesis of all cysLTs; and *Lta4h*, the enzyme that generates $LTB_4$. We confirmed expression of 5-LO at the protein level by microscopy (Figure 5C). 5-LO signal colocalized with the tuft cell marker DCLK1 and was not detected in non-tuft epithelial cells. Virtually all tuft cells had detectable 5-LO, regardless of infection status (Figures S5B). Consistent with previous studies of 5-LO (60), we found the protein localized to both the nucleus and the cytosol in naïve mice. We also observed instances of 5-LO translocating to the nuclear membrane in tuft cells of infected mice (Figure 5D), indicative of active leukotriene synthesis (75,76). Additional 5-LO-expressing cells, likely of myeloid origin, were found in the lamina propria, but staining intensity was consistently highest in tuft cells. Human duodenal tuft cells, identified by pEGFR staining (77), also consistently expressed 5-LO protein (Figures 5E and S5C).

To assess the capacity of tuft cells to generate cysLTs, we made two-dimensional monolayers from primary epithelial cells (78,79). Because the ligand that mediates helminth sensing is not yet known, we used ionomycin to simulate the intracellular $Ca^{2+}$ flux that occurs downstream of chemosensing in tuft cells and activates TRPM5 (80–82). This was sufficient to induce cysLT production and secretion into the supernatant (Figure 5F). The response was entirely dependent on tuft cells, as cysLT production was absent in monolayers from *Pou2f3*-deficient mice that lack tuft cells but maintain all other epithelial lineages. Our ability to detect cysLTs was also partially TRPM5-dependent, demonstrating regulation of tuft-cell-derived leukotrienes by the chemosensing pathway. Wildtype and TRPM5-deficient cultures contained equivalent tuft cell numbers (data not shown). We further found that stimulation with *N. brasiliensis* excretory/secretory product (NES) induced cysLT secretion in a tuft cell-dependent manner (Figure 5G). Together these results confirm that tuft cells secrete cysLTs downstream of chemosensing.

Helminth infection results in cellular damage and release of endogenous ligands that can drive innate immune responses. For example, ATP was recently shown to be released from intestinal tissue isolated from *H. polygyrus*-infected mice (83) and to activate airway tuft cells (84). We therefore considered whether danger-associated molecular pattern (DAMP) signaling might induce cysLT production. Using previously published tuft cell transcriptomic data (56) we identified ATP (*P2rx1* and *P2rx4*) and adenosine (*Adora1*) receptors expressed by intestinal tuft cells. Unlike airway tuft cells, intestinal tuft cells do not express *P2ry2*. Stimulation of epithelial monolayers with either ATP or adenosine, however, failed to induce cysLT secretion (Figure S5D). We additionally tried to measure IL-25 protein secretion by ELISA following stimulation of monolayers with ionomycin or helminth products, but could not detect a signal in any

condition. Thus, the specific helminth ligand(s) that elicit cysLT and perhaps IL-25 secretion by tuft cells remains to be determined.

**Tuft cells are the physiologic source of leukotrienes for induction of anti-helminth immunity in the small intestine**

Our data demonstrate that TRPM5-dependent sensing of helminths and cysLT signaling are both required for ILC2 activation and intestinal remodeling, and that tuft cells synthesize cysLTs. These findings suggest a model in which tuft cells respond to infection by synthesizing and secreting cysLTs that signal to ILC2s in the underlying lamina propria to initiate the feed-forward tuft-ILC2 circuit. Canonically, however, the hematopoietic compartment is thought to be the dominant source of leukotrienes, with mast cells, eosinophils, basophils, and macrophages being among the chief producers (85).

To identify the relevant source of leukotrienes *in vivo*, we generated reciprocal bone marrow chimeras using wildtype and *Alox5*$^{-/-}$ mice and infected these with *N. brasiliensis* for 7 days. Wildtype mice reconstituted with *Alox5*-deficient bone marrow retained their ability to mount a type 2 response following infection, as measured by tuft cell expansion in the SI, whereas leukotriene-deficient hosts reconstituted with wildtype bone marrow failed to mount a response (Figure 6A). This defect was also observed in wildtype hosts reconstituted with bone marrow from *Cysltr1*$^{-/-}$*Cysltr2*$^{-/-}$ mice (Figure 6B). These experiments identify a radio-resistant cell population as the relevant intestinal source of leukotrienes during helminth infection and implicate $LTC_4$ and/or $LTD_4$ as the primary mediators acting on bone marrow-derived cells.

To test the contribution of tuft cell-derived leukotrienes to the anti-helminth response, we generated *Alox5*-floxed mice to allow for cell-specific abrogation of leukotriene production

(Figure S6A). We crossed these mice to the *Villin1*-cre strain to delete 5-LO expression in the intestinal epithelium, which we confirmed by immunofluorescence (Figure S6B). Epithelium-specific 5-LO deletion impaired the development of tuft cell hyperplasia in the proximal SI 5 days after infection with *N. brasiliensis*, indicating a defect in IL-13 signaling in these mice (Figures 6C-D). Similar results were observed in the distal SI after 7 days of *N. brasiliensis* infection (Figure 6E) and in the proximal SI 4 days following infection with *H. polygyrus* (Figure 6F). Within the intestinal epithelium, 5-LO expression is restricted to tuft cells. Nevertheless, to target tuft cells more specifically we generated and validated *Pou2f3*-cre$^{Ert2}$-eGFP mice (Figures S6C-E). Tamoxifen-treated *Alox5*$^{fl/fl}$*;Pou2f3*-cre$^{Ert2}$ mice also showed impaired tuft cell expansion 5 days after *N. brasiliensis* infection. Both the *Vil*-cre$^{+}$ and *Pou2f3*-cre$^{Ert2+}$ strains phenocopied globally-deficient *Alox5*$^{-/-}$ mice, despite expression of 5-LO in many non-epithelial cells (Figures 6C-E). Consistent with these results and the bone marrow chimera experiments, deletion of 5-LO in mucosal mast cells using *Cpa3*-cre or macrophages and granulocytes using *LysM*-cre had no effect on the development of tuft cell hyperplasia.

While leukotrienes are required for airway type 2 responses, including ILC2 activation, deletion of tuft cells or 5-LO expression within tuft cells had no impact on the lung response following *N. brasiliensis* infection (Figures S6F-H), further underscoring the tissue-specific regulation of ILC2 activation and downstream inflammation. This finding also suggests that defects in SI type 2 responses following *N. brasiliensis* infection are tissue-intrinsic and not due to changes in the immune response during the lung phase of infection.

Returning to the SI, we further noted impaired goblet cell hyperplasia and hypertrophy in *Alox5*$^{fl/fl}$*; Vil*-cre$^{+}$ and *Pou2f3*-cre$^{Ert2+}$ mice, which again phenocopied the defect found in *Alox5*$^{-/-}$ mice (Figures 6G-I). Consequently, mice lacking synthesis of leukotrienes in tuft cells failed to

resolve helminth infection by 7 days-post infection (Figure 6J). Collectively, we identify tuft cells as the physiologically relevant source of cysLTs induced in the SI immediately following helminth infection and implicate cysLTs as a key effector that, in combination with IL-25, triggers the tuft-ILC2 circuit. We note that tuft cell-deficient *Pou2f3*$^{-/-}$ mice clear *N. brasiliensis* infection even more slowly than *Alox5*$^{-/-}$*Il25*$^{-/-}$ double-deficient mice, suggesting that additional tuft cell effector functions remain to be discovered (Figure 6K).

**Cysteinyl leukotrienes are dispensable for protist-induced type 2 immunity**

In addition to sensing helminth infection, tuft cells in the SI are activated by the microbial metabolite succinate, secreted by certain Tritrichomonad protists and unidentified bacterial species that colonize the distal ileum and cecum (20,43). We previously demonstrated that succinate administered in drinking water is sufficient to induce a type 2 immune response via the tuft-ILC2 circuit in the distal SI (56). Here we found that ILC2s isolated from the distal SI of wildtype and *Alox5*$^{-/-}$ mice had equivalent IL-13 expression following short-term succinate treatment (Figures 7A-B). Accordingly, we found no differences in distal tuft cell hyperplasia after seven days of succinate treatment in *Alox5*$^{-/-}$ or *Alox5*$^{fl/fl}$*;Vil*-cre$^{+}$ mice (Figures 7C-E).

We considered whether the neuropeptide neuromedin U (NMU), recently shown to activate ILC2s in an NFAT-dependent manner (86–88), might contribute to ILC2 activation in this context; however the response towards succinate was also independent of NMU receptor (NMUR1) signaling (Figure 7F).

Given that tuft cells in the distal SI have higher *Sucnr1* expression and are more responsive to succinate than tuft cells in the proximal SI (20,56), we hypothesized that the capacity to generate cysLTs might also vary between these sites. We found no difference in

expression of genes related to leukotriene synthesis in tuft cells sorted from the proximal and distal SI, nor did we find changes in expression of 5-LO protein (Figures 7G-H). While epithelial monolayers derived from the distal SI were capable of generating cysLTs *in vitro*, succinate stimulation was insufficient to drive this response (Figure 7I). Colonization of *Alox5*$^{fl/fl}$ and *Alox5*$^{fl/fl}$*;Vil*-cre$^{+}$ mice with the succinate-producing protist *Tritrichomonas musculis* resulted in equivalent tuft cell hyperplasia seven days later (Figures 7J-K). Tuft cell-derived cysLTs therefore appear to be dispensable for the innate response directed against succinate-producing protists yet required for the response directed against helminths. These data suggest that tuft-ILC2 circuits in the SI are regulated in a context-dependent manner and that innate type 2 immune responses are qualitatively different for distinct classes of organisms, even within the same tissue.

### 3.3 Discussion

Tuft cells have recently emerged as key initiators of type 2 immunity in the SI. Expression of a conserved chemosensing pathway enables tuft cells to sense luminal contents and activate the tuft-ILC2 circuit, leading to a protective immune response. Although production of IL-25 has been identified as a critical effector function, the greater delay in helminth clearance in tuft cell-deficient mice versus those lacking only IL-25 suggests additional mechanisms of immune regulation by tuft cells. In this study we demonstrate that tuft cells inducibly produce cysLTs following helminth infection and show that these leukotrienes cooperate with IL-25 to drive ILC2 activation (Figure 8). These findings are consistent with the recent report of cysLT production by airway tuft cells, although the receptor(s) and ligand(s) driving the response in these two tissues are distinct (84).

CysLTs are inflammatory lipids to which SI ILC2s appear particularly responsive. Indeed, we observed cysLT-dependent ILC2 activation just 16 hours after helminth infection. Our finding that cysLTs and IL-25 cooperate to drive ILC2 activation is consistent with the emerging model that ILC2s must integrate multiple transcriptional pathways for activation, analogous to those engaged during T cell TCR signaling (18,58,59). CysLTs are non-redundant due to their ability to induce NFAT nuclear translocation, which cooperates with IL-25-induced NF-$\kappa$B and AP-1. We had hoped to test if exogenous cysLTs are sufficient to activate intestinal ILC2s *in vivo,* as they are *in vitro* and in the lung (59), but we did not detect ILC2 activation at low doses and higher doses were toxic due to pleiotropic effects. Therefore, we cannot make any definitive conclusions.

In addition to cysLTs, recent work also demonstrated that the neuropeptide NMU can activate ILC2s in an NFAT-dependent manner (86–88). We consider it likely that cysLTs and NMU serve both redundant and non-overlapping roles in the SI, as is often the case in type 2 immunity (14,89). Leukotriene deficiency delays helminth clearance, but infection is still eventually resolved, indicating that redundant mechanisms indeed exist. Additional studies are required to disentangle the contexts in which individual signals are most relevant. Given the central role tuft cells play in sensing helminth infection and initiating immune responses, however, we consider tuft cell-derived cysLTs as the likely earliest source for an NFAT-inducing signal driving ILC2 activation. Other sources of cysLTs may contribute later during the response.

In some respects, it is counterintuitive that a single cell type produces two ILC2 activating ligands. The selective mobilization of NF-$\kappa$B and NFAT by IL-25 and cysLTs, respectively, can enable unique states of ILC2 activation. For example, cysLTs, but not IL-25 or

IL-33, can drive IL-4 production by ILC2s (65,90). We suspect there are also important temporal aspects to the regulation of ILC2s by leukotrienes and IL-25. Specifically, we found little evidence of leukotriene signaling at homeostasis, while deletion of *Il25* led to homeostatic changes in ILC2s, even in Tritrichomonad-free mice. The homeostatic status of tuft cells and ILC2s in wild mice and in humans remains uncertain, but to the extent that succinate sensing is involved, our findings suggest this would lead to IL-25 but not cysLT signaling. Once released, IL-25 has a much longer half-life than $LTC_4$ and $LTD_4$, further distinguishing the kinetic functions of these two signals. In sum, while IL-25 may provide both homeostatic and induced activation, cysLTs are well suited for rapid "on/off" regulation of the tuft-ILC2 circuit.

We have focused here on regulation of the tuft-ILC2 circuit, but many other leukotriene receptor-expressing cells populate the small intestine and may also respond to tuft cell-derived cysLTs (91). Given the rapid extracellular degradation of $LTC_4$ and $LTD_4$, any responding cells would need to reside near or migrate in close proximity to tuft cells. Neurons, Th2 effector cells, intraepithelial lymphocytes, endothelial cells, and the smooth muscle surrounding lacteals are all candidates that warrant further investigation. IL-25 might also have additional targets aside from ILC2s. Most notably, tuft cells themselves express the IL-25 receptor and may therefore engage in autocrine signaling (29).

How IL-25 and cysLTs are secreted from tuft cells remains to be determined. TRPM5 is required for transduction of all tuft cell-activating signals identified to date, but its exact role remains elusive. In type 2 taste cells TRPM5 activation results in cellular depolarization and release of neuromediators that propagate the taste sensation (30). TRPM5 may therefore regulate release of pre-formed IL-25 stored in tuft cells, as was suggested by one recent study (57) and by our finding that the MFI of KLRG1 on ILC2s was similarly decreased in naïve *Il25*$^{-/-}$ and *Trpm5*$^{-}$

$^{/-}$ mice. An alternative, but not mutually exclusive, model is that some IL-25 is secreted constitutively. Tuft cells constitutively express *Il25* (24,29) and we found no evidence of transcriptional induction on a per cell basis following helminth infection. Given the canonical signal peptide encoded by *Il25* mRNA, IL-25 protein should be delivered into the endoplasmic reticulum during translation, but how it is further trafficked remains uncertain. We had hoped to explore mechanisms of IL-25 secretion using our monolayer system or the scraped villi technique reported by Luo *et al.* but could not detect IL-25 under any conditions using commercially available IL-25 ELISAs. Clarification of the timing and mechanism of IL-25 secretion must therefore await development of improved *in vitro* tuft cell culture conditions and enhanced reagents for detection of IL-25 protein.

Similarly, it remains unclear how the TRPM5-dependent chemosensing pathway interacts with leukotriene production. Our *in vitro* data demonstrate a requirement for TRPM5 in the generation of cysLTs in response to calcium flux, but we were not able to distinguish between defects in synthesis versus secretion, or perhaps both. Further experiments will be required to dissect the precise interplay between chemosensing, TRPM5, and leukotriene generation.

Perhaps the most unexpected finding of this study was the differential requirement for cysLTs in the response to helminths versus succinate-producing protists. Tuft cell ligands may vary, but effector output has generally been considered stereotyped, at least within the SI. Indeed, all tuft cell-dependent immune responses identified in the SI to date also require IL-25. We find that tuft cell-derived cysLTs, on the other hand, are required to drive the innate anti-helminth response but are dispensable for the response directed against succinate-producing protozoans. The nature of innate type 2 responses in the SI therefore appears to be qualitatively different for distinct organisms. Succinate-producing protists like *T. musculis* colonize the distal

SI and cecum and are common across vivariums. While such protists modulate immunological tone, they do not seem to impair host fitness nor do they themselves seem to be affected by a strong type 2 response (20,23,56,92,93). Generating inflammatory leukotrienes could therefore be considered a disproportionate response to a harmless commensal. Parasitic helminths, on the other hand, inflict significant damage, compete for nutrients, and generally decrease host fitness. A more robust inflammatory response might be appropriate in this context.

How this differential regulation is achieved at the cellular level remains to be determined since all tuft cells express the enzymes required for cysLT synthesis. Is succinate signaling alone insufficient to drive cysLT generation within tuft cells, as we observed *in vitro*? Or are cysLTs actually produced in response to succinate *in vivo* but are redundant for ILC2 activation in this context? Does tuft cell sensing of helminths rely on the recognition of one ligand that drives simultaneous production of IL-25 and cysLTs, or are there multiple signals that independently drive production of each effector? We favor the hypothesis that tuft cell effector output is in part stimulus-specific. Differential regulation of effectors would enable nuanced control over the immunological tone of the SI and consequently physiologic adaption appropriate to the type of organism sensed (e.g. parasite vs. commensal). Testing such hypotheses will likely require identification of additional tuft cell activating ligands and the receptors through which they signal, as well as additional effector molecules through which tuft cells orchestrate the innate type 2 response.

Lastly, how well murine tuft cell biology reflects that of humans remains to be determined. We found that human tuft cells in healthy duodenal tissue consistently expressed 5-LO protein, and others recently demonstrated that human intestinal tuft cells express the accessory protein FLAP (94), together suggesting that these cells are primed to synthesize

leukotrienes. In this regard it is notable that the commonly prescribed asthma and allergy medication montelukast, a CYSLTR1 inhibitor, is administered as an ingestible tablet. What effect, if any, this drug has on intestinal physiology or immunity is not clear but may prove relevant when considering type 2-associated pathologies in the intestine.

### 3.4 Materials and Methods

#### Experimental Animals

Mice aged 6 weeks and older were used for all experiments. Mice were age-matched within each experiment, but pooled results include both male and female mice of varying ages. C57BL/6J mice were bred in house or purchased from Jackson Laboratories. B6.*Alox5*$^{-/-}$ (B6.129S2-Alox5$^{tm1Fun}$/J), B6.*Trpm5*$^{-/-}$ (B6.129P2-Trpm5$^{tm1Dgen}$/J), B6.*Cysltr1*$^{-/-}$ (C57BL/6N-Cysltr1$^{tm1Ykn}$/J), B6.*Villin1*-cre (B6.Cg-Tg(Vil1-cre)1000Gum/J), and B6.LysM-cre (B6.129P2-Lyz2$^{tm1(cre)Ifo}$/J) mice were purchased from Jackson Laboratories. B6.*Pou2f3*$^{-/-}$ (Pou2f3 tm1.1(KOMP)Vlcg, Project ID #VG18280) were rederived from sperm stored in the Canadian Mouse Mutant Repository. B6.*Il25*$^{Flare25/Flare25}$ and B6.*Il13*$^{Smart13/Smart13}$ mice were generated as previously described (24,66). B6.*Il25*$^{-/-}$ mice were generously provided by A. McKenzie via R. Locksley. B6.*Il1rl1*$^{-/-}$ (*St2*$^{-/-}$) mice were generously provided by S. Akira via R. Locksley. B6.Cpa3-cre (B6.Tg(Cpa3-cre)3Glli) mice were generously provided by A. Piliponsky. *Nmur1*$^{tm1.1(KOMP)Vlcg}$ mice were generously provided by V. Kuchroo. *Alox5*$^{-/-}$, *Il25*$^{-/-}$, *St2*$^{-/-}$, and *Trpm5*$^{-/-}$ mice were crossed to the B6.*Il13*$^{Smart13/Smart13}$ line. *Il25*$^{-/-}$ and *St2*$^{-/-}$ mice were further crossed to the B6.*Arg1*$^{YARG}$ reporter line (95). *Cysltr1*$^{-/-}$ (96) and *Cysltr2*$^{-/-}$ (97) mice were crossed to generate a double knockout line and bone marrow was generously provided by N. Barrett. All mice were maintained in specific pathogen-free conditions at the University of Washington and were confirmed to be free of *T. musculis* and *T. rainier* by microscopy and qPCR, except those specifically colonized with *T. musculis* as noted.

#### Alox5-flox Mice

B6.*Alox5*$^{fl/fl}$ mice with loxP sites flanking the 6$^{th}$ exon of *Alox5* were generated by homologous gene targeting in C57BL/6 embryonic stem cells. Exon 6, which contains critical iron-binding residues, was selected for deletion to replicate the targeting strategy used for B6.129S2-Alox5$^{tm1Fun}$/J global knockout mice. A 2.0 kb 5' homology arm containing the 5' loxP site and spanning exon 6 of *Alox5* was assembled using overlap extension PCR and cloned into pKO915-DT (Lexicon Genetics) using EcoRI and XhoI. Next, a 2.0 kb 3' homology arm was amplified and inserted into the pK0915-DT vector containing the 5' homology arm using SacII and SmaI. Lastly, a pre-assembled selection cassette containing frt-flanked neomycin and a 3' loxP site was sub-cloned into the homology arm-containing pKO915-DT vector using AscI. The selection cassette was screened for insertion in the proper orientation and the final construct was linearized with NotI and transfected by electroporation into C57BL/6 embryonic stem cells (PRXB6T). Cells were grown on irradiated feeders with the aminoglycoside G418 in the media, and neomycin-resistant clones were screened for 5' and 3' homologous recombination by PCR. Two positive clones were selected for injection (Gladstone Institutes, San Francisco) into albino C57BL/6 blastocysts to generate chimaeras. Male pups with highest ratios of black-to-white coat color from a single clone were selected to breed with homozygous Gt(Rosa26)$^{FLP1/FLP1}$ females (Jackson Laboratories catalog # 009086) to excise the neomycin resistance cassette. Deletion of neomycin was confirmed by PCR. *Alox5*$^{fl/fl}$ genotyping primers were as follows: A5FL_F: TGTTTGGCTACCAGTTCCTGAATGG; A5FL_R: AGCAGATGACAGTTGGGTGACTATG (460 bp wildtype band; 577 bp knock-in band; no band after CRE-mediated excision)

**Pou2f3-Cre$^{ERT2}$-ires-EGFP Mice**

A CreERT2-ires-EGFP followed by FRT-flanked PGK-Neo cassette was inserted by a homologous recombination in place of the initial ATG codon of *Pou2f3* gene of C57BL/6J-derived ES cells. Chimeric mice were mated with an FLP strain to remove the PGK-Neo cassette. After excluding the FLP allele by mating with C57BL/6J, heterozygous *Pou2f3*-CreERT2-ires-EGFP mice were obtained.

**Mouse Infection and Treatment**

*H. polygyrus* and *N. brasiliensis* larvae were raised and maintained as previously described (66,98). Mice were infected by oral gavage with 200 *H. polygyrus* L3 or subcutaneously with 500 *N. brasiliensis* L3 and euthanized at the indicated time points to collect tissues for staining or to count worm burden. In experiments using *Pou2f3*-CreErt2-eGFP mice, animals were administered 2.5mg tamoxifen by oral gavage at days 0, 2, and 5 post-infection. Worm burden was enumerated across the entire small intestine. For *in vivo* CYSLTR1-inhibition experiments, mice were injected intraperitoneally with 10mg/kg montelukast (Cayman Chemical) one hour prior to oral gavage with *H. polygyrus*. For ibuprofen experiments mice were given 1mg/ml ibuprofen ad libitum in drinking water starting one day prior to infection and continuing through the course of the experiment. For BrdU incorporation experiments mice were injected intraperitoneally with 1mg BrdU at the indicated time point and tissue harvested 24 hours later.

**Succinate Treatment and Protist Colonization**

For succinate experiments mice were given 150mM sodium succinate hexahydrate (Alfa Aesar) ad libitum in drinking water for the indicated amount of time. For protist colonization experiments, wildtype mice vertically colonized with *Tritrichomonas musculis* were used as a

source of protists. Colonization of naïve mice was performed as previously described (56). Briefly, cecal contents were collected, washed in PBS, filtered through a 70μm strainer, and washed again. Total protist numbers were estimated using a hemocytometer. Naïve mice were colonized by oral gavage with 40-50 $x10^6$ protists. Intestinal tissue was collected seven days later for analysis.

**Tissue Fixation and Staining**

For tuft cell staining, intestinal tissues were flushed with PBS and fixed in 4% paraformaldehyde for 4 hours at 4° C. Tissues were washed with PBS and incubated in 30% (w/v) sucrose overnight at 4° C. Samples were then coiled into "Swiss rolls" and embedded in Optimal Cutting Temperature Compound (Tissue-Tek) and sectioned at 8 μm on a Microm HM550 cryostat (Thermo Scientific). Immunofluorescent staining was performed in Tris/NaCl blocking buffer (0.1 M Tris-HCL, 0.15 M NaCl, 5μg $ml^{-1}$ TSA blocking reagents (Perkin Elmer), pH 7.5) as follows: 1 h 5% goat serum, 1 h primary antibody (αDCLK1, Abcam ab31704), 40 min goat anti-rabbit IgG F(ab')2-AF594 secondary antibody (Invitrogen) and mounted with Vectashield plus DAPI (Vector Laboratories). Tuft cell frequency was calculated using ImageJ software to manually quantify DCLK1+ cells per millimeter of crypt-villus axis. Four 10x images of the swiss roll were analyzed for each replicate and at least 30 total villi were counted. Mouse 5-LO staining was performed as for DCLK1 above, with following modifications: 1 h 10% goat serum at room temperature (RT), overnight rabbit anti-5-LO (Sigma Aldrich, SAB1410449) at 4° C, 40 min goat anti-rabbit IgG F(ab')2-AF594, 1 h 10% rabbit serum at RT, 2 h αDCLK1-AF488 (custom conjugation of ab31704) at RT. Human 5-LO staining was performed as above,

replacing αDCLK1-AF488 with anti-pEGFR-AF488 (Abcam ab205827). Human duodenal tissue samples were collected during either Roux-en-Y or whipple procedures on three different deidentified patients and obtained through Northwest BioSpecimen. The University of Washington Institutional Review Board has determined that the deidentified tissue specimens used in this study do not meet the federal regulatory definition of research on human subjects.

For BrdU staining slides were rehydrated in PBS, incubated in 2 M HCl for 1 hr, and then neutralized in 0.1 M sodium borate for 10 min. Staining was performed as follows: 1 h Fc Block at RT, overnight rabbit-anti-BrdU-AF594 (Abcam ab220076) and Fc Block at 4° C, 1 min wash in PBS, 10 min fix in 0.2% paraformaldehyde at RT. BrdU incorporation was determined as the distance from the crypt to most distal $BrdU^+$ cell per villus, counting at least 25 villi per sample.

For goblet cell staining, tissues were flushed with PBS, fixed in 10% buffered formalin at 4° C for 3 hours, coiled into "Swiss rolls" and returned to formalin. After 24 hours tissues were moved to 70% ethanol for storage. Tissue processing, paraffin embedding, sectioning, and staining were performed by the Pathology Research Services Laboratory at the University of Washington. Alcian blue staining was used to identify goblet cells. Goblet cell frequency was calculated as described above for tuft cells. Hypertrophy was quantified using ImageJ software to measure the area of at least 80 goblet cells for each biological replicate. Brightfield and fluorescent images were acquired on an Axio Observer A1 inverted microscope (Zeiss) and on an AR1 confocal microscope (Nikon).

**Single-cell Tissue Preparation**

For single cell epithelial preparations from small intestines, tissues were flushed with PBS, opened, and rinsed with PBS to remove intestinal contents. Intestinal tissue was cut into 2-5 cm pieces and incubated rocking at 37° C in 15ml HBSS ($Ca^{+2}$/$Mg^{+2}$-free) supplemented with 5mM dithiothreitol (DTT, Sigma-Aldrich), 5% fetal calf serum (FCS, VWR), and 10mM HEPES (Gibco). Tissues were vortexed vigorously and supernatant was discarded. Tissues were then incubated rocking at 37° C in 15ml HBSS ($Ca^{+2}$/$Mg^{+2}$-free) supplemented with 5mM EDTA (Invitrogen), 5% FCS, and 10mM HEPES. Tissues were vortexed thoroughly and released epithelial cells were passed through a 70 μm filter. Tissues were then incubated in fresh EDTA/HBSS solution for 15 minutes, vortexed, and filtered. Supernatants were pooled and washed once before staining for flow cytometry.

For lamina propria preparations small intestinal tissue was processed as above to remove the epithelial fraction. Tissues were then rinsed in 20ml HBSS (with $Ca^{+2}$/$Mg^{+2}$) supplemented with 5% FCS and 10mM HEPES, shaking at 37° C for 20 minutes. Supernatants were discarded and tissues were incubated in 5ml HBSS (with $Ca^{+2}$/$Mg^{+2}$) supplemented with 3% FCS, 10mM HEPES, 30 μg/ml DNase I (Sigma Aldrich), and 0.1 Wunsch/ml Liberase TM (Sigma Aldrich), shaking at 37° C for 30 minutes. Tissues were vortexed and cells were passed through a 70 μm filter and washed. The resulting pellet was resuspended in 40% Percoll (Sigma Aldrich), centrifuged for 5 minutes at 1500 rpm, and supernatant discarded. Pelleted cells were then washed and stained for flow cytometry. Note: to preserve IL-17RB staining, a modified protocol

was used to isolate lamina propria cells for data in Figures 2 and S2. See "RNA Sequencing and Analysis" below for details.

For lung preparation tissue was dissociated by gentleMACS (Miltenyi Biotec) using program lung_01. Tissue was then incubated in HBSS (with $Ca^{+2}$ and $Mg^{+2}$) supplemented with 0.2mg/ml LiberaseTM (Roche) and 25 μg/ml Dnase I (Sigma) for 35 minutes shaking at 37° C, and subsequently run on gentleMACS using program lung_02. Cells were then filtered through a 70 μm strainer, washed, and stained for flow cytometry.

**Flow cytometry and cell sorting**

Single cell suspensions were prepared as described and stained in DPBS + 3% FBS with antibodies to surface markers for 20 min at 4° C, followed by DAPI (Roche) for dead cell exclusion. For intracellular cytokine staining cells were first washed in DPBS and stained with Zombie Violet fixable viability dye (BioLegend) for 20 min at 4° C and subsequently stained with antibodies to surface markers for 20 min at 4° C. Cells were then fixed and permeabilized using the FoxP3 Transcription Factor Staining Buffer kit (eBioscience) following manufacturer's instructions. Cells were further stained with antibodies to intracellular proteins for 30 minutes at room temperature. Samples were FSC-A/SSC-A gated to exclude debris, SSC-H/SSC-W gated to select single cells and gated to exclude dead cells. Samples were run on an LSR II (BD Biosciences) or Aurora (Cytek) and analyzed with FlowJo 10 (Tree Star). For cell sorting, single cell suspensions were prepared and stained as described and sorted on an Aria II (BD Biosciences).

**Quantitative RT-PCR**

For ILC2 qPCR, 10,000 small intestinal $CD45^+Lin^-KLRG1^+$ cells and 10,000 lung $CD45^+Lin^-Thy1.2^+ST2^+$ cells from C57BL/6J mice were sorted into Buffer RLT (Qiagen) using an Aria II (BD Biosciences). Lineage dump included the markers CD3, CD4, CD5, CD8, CD11b, CD19, FcER1, and NK1.1. 10,000 tuft cells were sorted as $CD45^-EpCAM^+$ $RFP^+$ from small intestinal epithelium of *Il25*$^{Flare25/Flare25}$ mice or as $CD45^-EpCAM^+CD24^+SiglecF^+$ from small intestinal epithelium of C57BL/6J mice. Previous RNA sequencing confirmed that these two gating strategies yield identical tuft cell transcriptional profiles. RNA was isolated using the Micro Plus RNeasy kit (Qiagen) and reverse transcribed using SuperScript Vilo Master Mix (Life Technologies). cDNA was used as template for quantitative PCR with Power SYBR Green reagent on a StepOnePlus cycler (Applied Biosystems). Transcripts were normalized to *Rps17* (40S ribosomal protein S17) expression.

**RNA Sequencing and Analysis**

In order to maintain IL-17RB staining that was lost with extended lamina propria tissue processing described above, single cell suspensions were prepared from the proximal small intestine of naïve mice using a modified protocol. All data in Figure 2 and Figure S2 were generated using this modified digestion protocol. Before tissue collection, mice were anesthetized with ketamine/xylazine. Next, the small intestine was nicked at the stomach and transected at the cecum and flushed with 20 mL 37˚C HBSS (no $Ca^{+2}/Mg^{+2}$) + 10 mM HEPES. The mice were then perfused through the heart with 40 mL of 30 mM EDTA + 10 MM HEPES in HBSS (no $Ca^{+2}/Mg^{+2}$). Five minutes after initiating perfusion, the first 5 cm of the proximal SI

were harvested, fileted open, transferred to 35 mL ice cold HBSS (no $Ca^{+2}/Mg^{+2}$) + 10 MM HEPES and shaken vigorously for 30 seconds to release epithelial cells. Intestinal pieces were stored in HBSS + 5% FCS on ice and then transferred into pre-warmed digest buffer composed of 5ml HBSS (with $Ca^{+2}/Mg^{+2}$) supplemented with 3% FCS, 10mM HEPES, 30 μg/ml DNase I (Sigma Aldrich), and 0.1 Wunsch/ml Liberase TM (Sigma Aldrich), shaking at 37° C for 30 minutes. Tissues were vortexed and cells were passed through a 70 μm filter and washed. The resulting pellet was resuspended in 40% Percoll (Sigma Aldrich), centrifuged for 5 minutes at 1500 rpm, and supernatant discarded. Pelleted cells were then washed and stained for flow cytometry and sorting.

500 ILC2s were sorted as $CD45^{+}Lin^{-}IL\text{-}17RB^{+}$ directly into lysis buffer from the SMART-Seq v4 Ultra Low Input RNA Kit (Takara) and cDNA was generated following manufacturer's instructions. Four biological replicates were collected for each genotype. Each biological replicate represents one mouse. Next-generation sequencing and analysis was performed by the Benaroya Research Institute Genomics Core. Sequencing libraries were generated using the Nextera XT library preparation kit with multiplexing primers, according to manufacturer's protocol (Illumina), and library quality was assessed using the Tapestation (Agilent). High throughput sequencing was on HiSeq 2500 (Illumina), sequencing dual-indexed and single-end 58 base pair reads. All samples were in the same run with target depth of 5 million reads to reach adequate depth of coverage.

Sequencing was inspected by FASTQC (v0.11.3) and yielded a median read depth of 8.7 million reads per sample. The following analytic pipeline was managed on the Galaxy platform (99). Reads were trimmed by 1 base at the 3' end, and then trimmed from both ends until base calls had a minimum quality score of at least 30 (Galaxy FASTQ Trimmer tool v1.0.0). Sequence alignment was performed using STAR aligner (v2.4.2a) with the GRCm38 reference genome and gene annotations from Ensembl release 91. Gene counts were generated using HTSeq-count (v0.4.1). Quality metrics were compiled from PICARD (v1.134), FASTQC (v0.11.3), and HTSeq-count. Raw input from HTseq-count was normalized in DESeq2. Uniquely mapped Ensembl IDs (genes and non-coding RNAs) with a mean normalized read count <10 were excluded. The gene *Arg1* was not included in the analysis as the *Arg1*$^{Yarg}$ reporter allele appeared to interfere with sequencing reads in the *Il25*$^{-/-}$ and *St2*$^{-/-}$ strains. The resulting datasets were deposited in the Gene Expression Omnibus (GEO:GSE144956).

**ILC2 Stimulation Assay**

Small intestinal lamina propria ILC2s were isolated from Smart13 reporter mice and sorted as described. Sorted cells were plated at 4000-5000 cells per well in a 96 well plate and incubated overnight in 10 ng/ml IL-7 (R&D Systems) and basal media composed of high glucose DMEM supplemented with non-essential amino acids, 10% FBS, 100 U/mL penicillin, 100mg/mL streptomycin, 10mM HEPES, 1mM sodium pyruvate, 100μM 2-mercaptoethanol, and 2mM L-glutamine. The next morning media was replaced with fresh media and 10 ng/ml IL-7 and cells were stimulated with the indicated agonist. After a six-hour incubation at 37 °C, cells were

stained with 1 μl/well of PE-conjugated anti-human CD4 for 20 minutes at 4 °C. Cells were washed, resuspended in DAPI, and analyzed on an LSRII (BD Biosciences).

**NFAT Imaging**

ILC2s were sorted from the small intestine lamina propria and cultured overnight in 10 ng/ml IL-7 (R&D Systems), as described above. The next morning cells were treated for 30 min with 1μM cyclosporin A (CSA) where indicated, followed by 90 min treatment with 100nM $LTC_4$, 100ng/ml IL-25, 100ng/ml IL-33, or 30ng/ml PMA and 500ng/ml ionomycin. Cells were then affixed to slides by Cytospin and treated for 5 min with ice-cold methanol. Slides were stained as follows: 30 min block with 10% goat serum, 1 h rabbit-anti-NFATC2 (NFAT1: clone D43B1, Cell Signaling Technology), 40 min goat anti-rabbit IgG F(ab')2-AF594 secondary antibody (Invitrogen). Cells were counterstained with DAPI and imaged on an Axio Observer A1 inverted microscope (Zeiss).

**Bone Marrow Chimeras**

Congenically-marked donor bone marrow cells were isolated from leg bones from mice of the indicated genotype. Bones were rinsed in 70% ethanol, rinsed three times in PBS, and then ground using a pestle. Extracted cells were washed in PBS and filtered through a 70 μm strainer. Cells were spun down and resuspended in ACK lysing buffer for five minutes to remove red blood cells. Cells were then washed in PBS and resuspended in RPMI. Recipient mice were irradiated (1000 rads) and retro-orbitally injected with $5x10^6$ cells. Mice were placed on Baytril-medicated water for two weeks post-transfer and rested for at least six weeks to allow for

hematopoietic reconstitution. Chimeric mice were infected with *N. brasiliensis* as described and intestinal tissue harvested on day 7 post-infection for enumeration of tuft cells. Chimerism was confirmed at time of harvest by staining splenocytes with congenic markers CD45.1 and CD45.2.

**Organoid Culture**

Small intestinal crypt-derived organoids were grown as described with modifications described below (100). Briefly, proximal small intestine was isolated and villi manually scraped off with a glass coverslip. Tissue was then washed three times in cold PBS with vigorous shaking before 30 minute 4° C incubation in 2mM EDTA to release epithelial crypts, which were washed in PBS and filtered through a 70 μm strainer. Pelleted crypts were resuspended in Matrigel and plated at 400-500 crypts per well in a prewarmed plate, incubated at 37 °C for 5 minutes to allow for Matrigel solidification, and complete organoid media added. Organoid media was composed of DMEM/F12 supplemented with 2mM glutamine, 100 U/mL penicillin, 100mg/mL streptomycin, 10mM HEPES, 1X N2 supplement (Life Technologies), 1X B27 supplement (Life Technologies), 500mM N-acetylcysteine, 50μg/ml mEGF, and replacing recombinant R-spondin with supernatants from R-spondin expressing L-cells and replacing recombinant Noggin with supernatants from Noggin expressing cells. Crypts were harvested from the proximal (first 10cm) small intestine of naïve C57BL/6J mice and plated on day 0. On day 1 and day 4, media was replaced and organoids were treated with 20 ng/ml recombinant IL-13 or 10nM of the indicated leukotriene. On day 7 organoids were harvested and resuspended in Accutase (Corning). Organoids were sheared with a 28G insulin

syringe, incubated for 1h at room temperature, washed, and then stained for flow cytometry as described above. Tuft cells were identified as $CD45^{-}EpCAM^{+}SiglecF^{+}CD24^{+}$.

**Cysteinyl Leukotriene ELISA**

Intestinal monolayer cultures were generated for ELISA experiments. Intact epithelial crypts were isolated from the small intestine following the protocol described for organoid culture. After crypts were isolated, however, they were resuspended in complete organoid media supplemented with 10μM Y27632 (Stemcell Technologies) and 10μM SB431542 (Stemcell Technologies) and plated in warm plates pre-coated with Matrigel. Plates were coated with Matrigel by adding 100 μl of 2% Matrigel in cold DMEM to each well in 48-well plates and incubating at least 30 minutes at 37 °C. Matrigel media was aspirated before plating crypts in organoid media. After plating, cells were incubated overnight at 37 °C to allow adherence and media containing unattached cells was replaced the next day, followed by an additional hour of incubation. Media was then aspirated, test stimuli added, and cells incubated for 30 minutes at 37 °C. Supernatants were collected and used to perform ELISA using the Cysteinyl Leukotriene Express ELISA kit (Cayman Chemical) following manufacturer's instructions.

***N. brasiliensis* Excretory-Secretory Product (NES) Preparation**

To generate NES, Lewis rats were infected subcutaneously with 5000 *N. brasiliensis* L3. Mature (L5) worms were collected from the entire small intestine 7 days post infection. Worms were washed 10 times in Wash Solution I (PBS with 200 U $mL^{-1}$ Pen-Strep), followed by a 40 minute incubation in Wash Solution 1 at room temperature. Worms were allowed to equilibrate in Wash

Solution II (RPMI 1640 with 200 U $mL^{-1}$ Pen-Strep) for 1 hr at 37°C, before being transferred to a tissue culture flask in NES culturing media (RPMI 1640, with 100 U $mL^{-1}$ Pen-Strep, 2mM L-Glutamine and 1% glucose) and cultured at 37°C. Supernatant was collected at 24, 48, and 72 hr and filtered prior to use as NES.

**Quantification and Statistical Analysis**

All experiments were performed using randomly assigned mice without investigator blinding. All data points reflect biological replicates (i.e. mice), except in Figures 1I, S4B-C, 5F-G, S5D, and 7I where they represent technical replicates. No data were excluded. Statistical analysis was performed as noted in figure legends using Prism 7 (GraphPad) software. Graphs show mean + SEM.

**Data and Code Availability**

RNA-seq data are available at the NCBI Gene Expression Omnibus under accession number GEO: GSE144956.

### 3.5 Acknowledgments

We thank D. Hailey and the Garvey Cell Imaging Lab in the Institute for Stem Cell & Regenerative Medicine for microscopy support, M. Black and the UW Cell Analysis Facility for flow cytometry support, the mouse husbandry staff in the UW SLU vivarium, Northwest BioSpecimen for human tissue samples, V. Gersuk, M. Rosasco, and the Benaroya Research Institute Genomics Core for help with RNA sequencing, V. Kuchroo at Brigham and Women's Hospital for mice, and M. Fontana for helpful comments on the manuscript. JWM was supported by the University of Washington Immunology Training Grant (T32 AI106677). MSN was supported by the UW Immunology Department's Titus Fellowship. JVM is a Searle Scholar. This work was supported by NIH 1DP2 OD024087 (JVM) and the University of Washington. The *Alox5*-flox mouse was generated at the University of California, San Francisco with generous funding support from R. Locksley (NIH RO1 AI026918, UCSF Diabetes Research Center, and Sandler Asthma Basic Research Center at UCSF for support of H-EL, targeting, and mouse costs).

**Author contributions:** JWM conceived of and performed experiments, analyzed data, and wrote the paper with JVM. H-AT, TEB, MSN, and DMK assisted with additional experiments. H-AT analyzed RNA sequencing data. NAB provided *Cysltr1*$^{-/-}$*Cysltr2*$^{-/-}$ bone marrow for chimera experiments. H-EL generated the *Alox5*-flox mouse line. IM generated the *Pou2f3*-cre$^{Ert2}$-eGFP mouse line. JVM conceived of and supervised the study and wrote the paper with JWM.

## 3.6 Figures

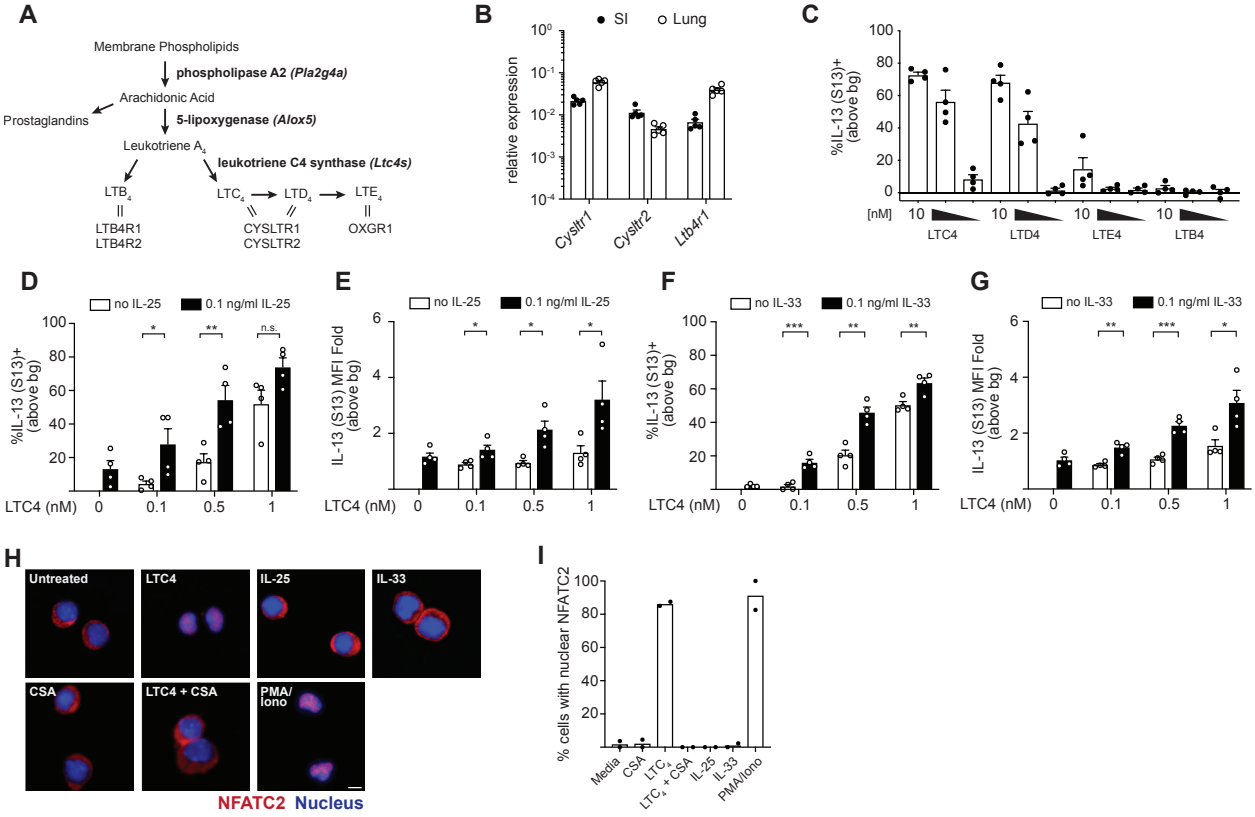


**Figure 1. Cysteinyl leukotrienes are a non-redundant signal for intestinal ILC2 activation**

**(A)** Schematic of leukotriene synthesis. Enzymes are listed in bold. Double lines represent ligand/receptor interactions. **(B)** Gene expression in ILC2s sorted from the small intestine (SI) lamina propria and lung. **(C)** Frequency of Smart13$^{+}$ SI ILC2s following 6 hour *in vitro* culture with the indicated leukotriene. Three 10-fold dilutions from 10-0.1 nM are shown. **(D,F)** Frequency and **(E,G)** mean fluorescence intensity (MFI) of Smart13$^{+}$ SI ILC2s following 6 hour *in vitro* culture with the indicated combinations of $LTC_4$ and IL-25 (D,E) or IL-33 (F,G). **(H)** SI ILC2s were treated for 30 min with 1μM cyclosporin A (CSA) where indicated, followed by 90

min treatment with 100nM $LTC_4$, 100ng/ml IL-25, 100ng/ml IL-33, or 30ng/ml PMA and 500ng/ml ionomycin. Cells were stained with anti-NFATC2 (red) and DAPI (blue). Scale bar: 20μm. **(I)** Quantification of cells with nuclear NFATC2. At least 30 cells were counted for each condition. In (B)-(G) each symbol represents an individual mouse pooled from two or more experiments. In (I) symbols are technical replicates representative of three independent experiments. bg, background. *$p < 0.05$, **$p < 0.01$, ***$p < 0.001$ by multiple t tests (D-G). n.s., not significant. Graphs depict mean + SEM.

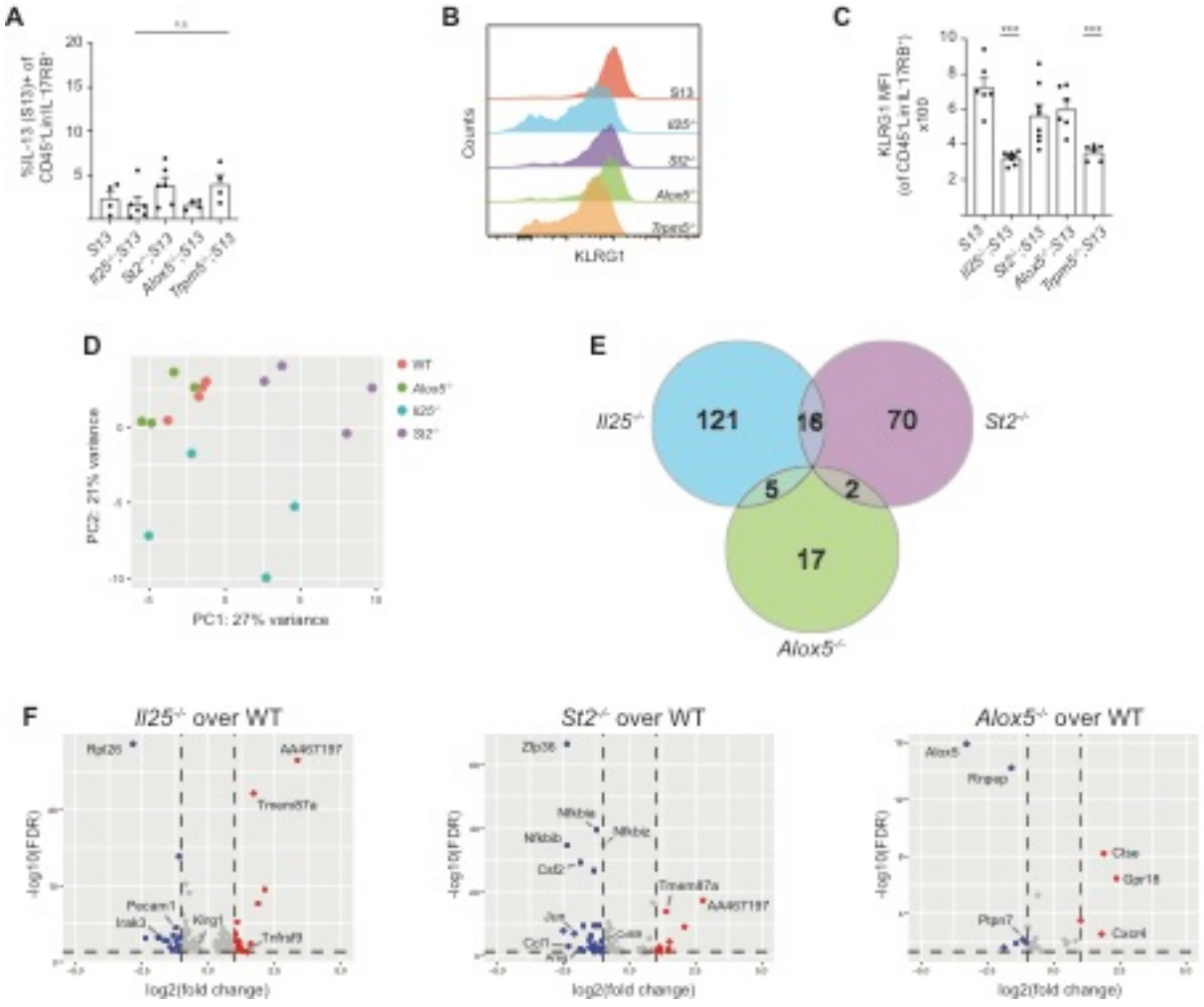


**Figure 2. ILC2 homeostasis in the proximal small intestine is leukotriene-independent and minimally requires IL-25 and IL-33**

**(A)** Quantification of Smart13 expression by ILC2s ($CD45^+$;$Lineage^-$;$IL\text{-}17RB^+$) in the proximal (first 5cm) small intestine (SI) of naïve mice. **(B)** Mean fluorescence intensity (MFI) of KLRG1 expression by ILC2s. **(C)** Quantification of MFI in (B). **(D-F)** ILC2s of the indicated genotype were sorted from the proximal SI of naïve mice for mRNA sequencing. **(D)** PCA of top 500 differentially expressed genes (DEG). **(E)** Venn diagram depicting number of DEGs for each genotype as compared to wildtype (FDR <.05, row mean >10). **(F)** Volcano plots depicting

DEGs as compared to wildtype (FDR <.05, row mean >10). Red = log2 fold change > 1, blue = log2 fold change < 1. In (A) and (C) each symbol represents an individual mouse pooled from two or more experiments. *p < 0.05, **p < 0.01, ***p < 0.001 by one way ANOVA (A, C) with comparison to Smart13. n.s., not significant. Graphs depict mean + SEM.

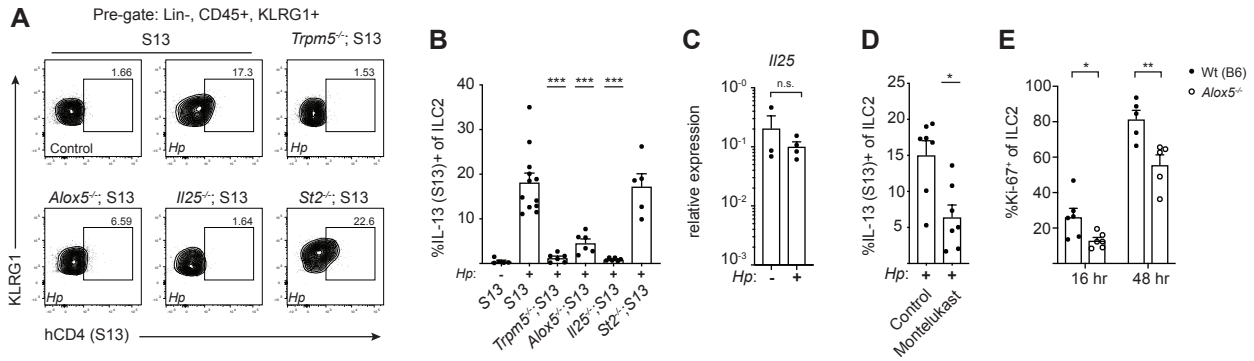


**Figure 3. Cysteinyl leukotrienes drive rapid ILC2 activation following helminth infection**

**(A)** Flow cytometry for Smart13 expression by ILC2s in the proximal (first 10cm) small intestine (SI) 16 hours after infection with *H. polygyrus*. **(B)** Quantification of Smart13 expression in (A). **(C)** *Il25* mRNA expression in tuft cells sorted from the proximal SI of naïve Wt(B6) mice and mice infected with *H. polygyrus* for 16 hours. **(D-E)** Analysis of ILC2s from the proximal SI. **(D)** Smart13+ ILC2s in mice treated with montelukast (10mg/kg) 60 min prior to 16 hours infection with *H. polygyrus*. **(E)** ILC2 Ki-67 expression at the indicated time points following infection with *H. polygyrus*. In (B)-(E) each symbol represents an individual mouse pooled from two or more experiments. S13, Smart13. *Hp*, *H. polygyrus*. *p < 0.05, **p < 0.01, ***p < 0.001 by one way ANOVA (B) with comparison to infected S13, by Mann-Whitney (C-D), or by multiple t tests (E). n.s., not significant. Graphs depict mean + SEM.

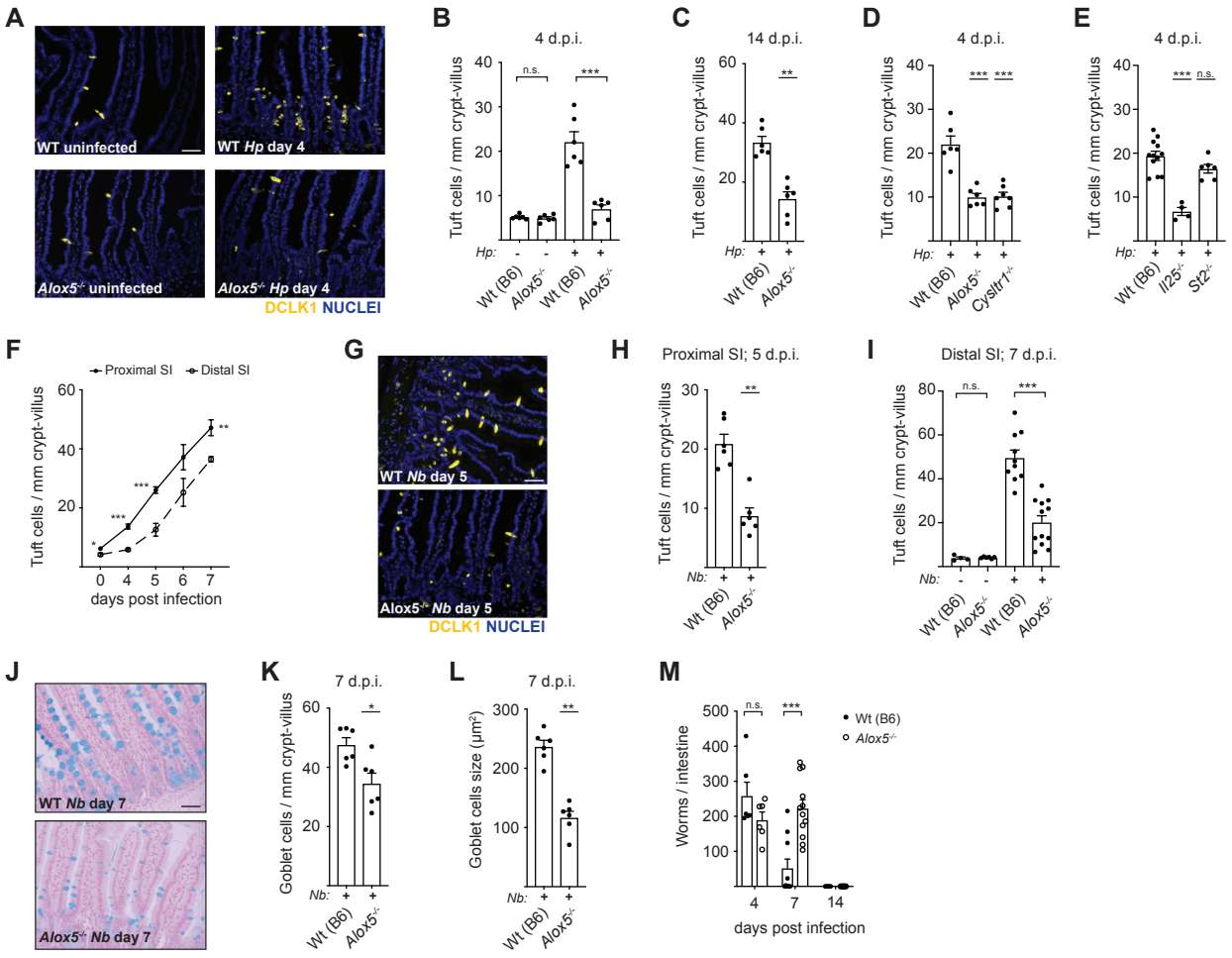


**Figure 4. Tuft-ILC2 circuit activation and helminth clearance are delayed in the absence of cysteinyl leukotrienes**

**(A)** Mice were infected with *H. polygyrus* for 4 days. Tuft cell frequency in the proximal (first 10cm) small intestine (SI) was determined. DCLK1 (yellow) marks tuft cells. DAPI (blue) marks nuclei. Scale bar: 50µm. **(B)** Quantification of tuft cells in (A). **(C)** Tuft cell frequency in the proximal SI after 14 days of *H. polygyrus* infection. **(D-E)** Tuft cell frequency in the proximal SI of the indicated genotypes after 4 days of *H. polygyrus* infection. **(F)** Tuft cells were quantified in the proximal and distal (last 10cm) SI of wildtype mice at the indicated time points post-*N.*

*brasiliensis* infection. **(G)** Representative images of proximal SI on day 5 post-*N. brasiliensis* infection. Scale bar: 50μm. **(H)** Quantification of tuft cells in (G). **(I)** Tuft cell frequency in the distal SI after 7 days of *N. brasiliensis* infection. **(J)** Goblet cells identified in the jejunum (10-20cm from stomach) by alcian blue staining 7 days after infection with *N. brasiliensis*. Representative images are shown. Scale bar: 50μm. **(K-L)** Quantification of goblet cell (K) number and (L) size in (J). **(M)** Worm burden across the entire SI at the indicated time points post-*N. brasiliensis* infection. In (B)-(E), (H)-(I), and (K)-(M) each symbol represents an individual mouse pooled from two or more experiments. In (F) each symbol represents the average of five mice pooled from two experiments. *Hp, H. polygyrus. Nb, N. brasiliensis.* S13, Smart13. d.p.i., days post infection. *$p < 0.05$, **$p < 0.01$, ***$p < 0.001$ by Mann-Whitney (C, H, K-L), by multiple t tests (B, F, I, M), or by one way ANOVA (D-E) with comparison to Wt(B6). n.s., not significant. Graphs depict mean + SEM.

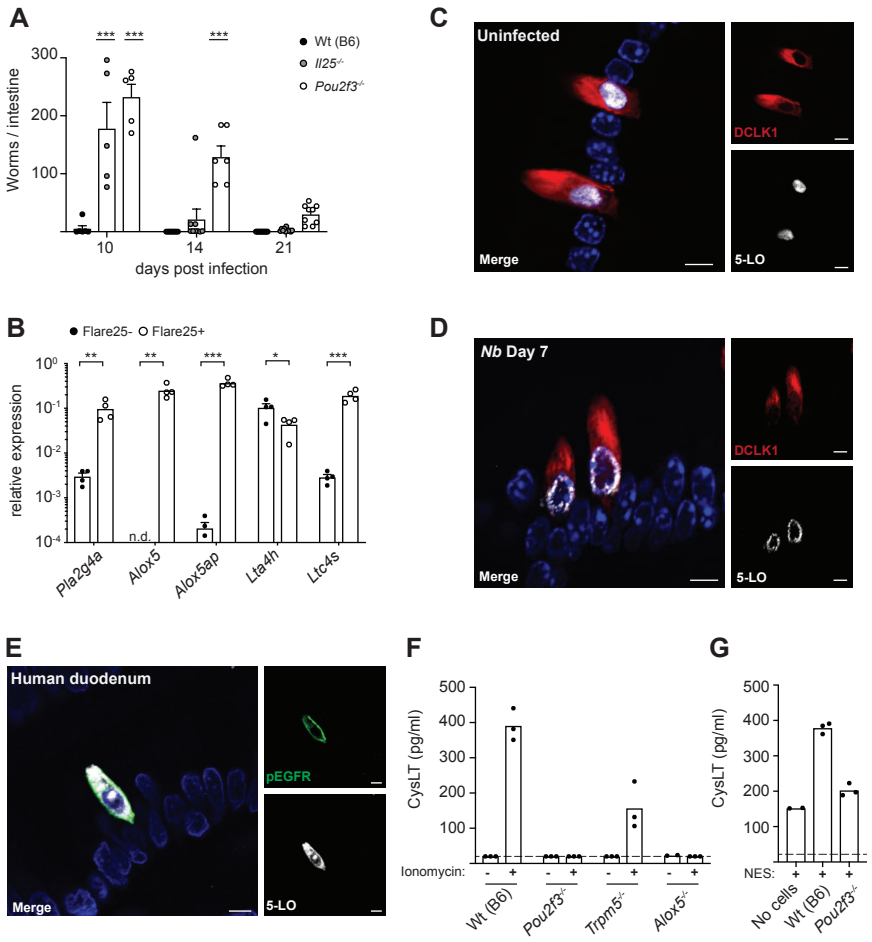


**Figure 5. Tuft cells synthesize cysteinyl leukotrienes**

**(A)** Mice were infected with *N. brasiliensis* and worm burden determined across the entire small intestine (SI) at the indicated time points. **(B)** Gene expression in tuft cells (Flare25$^{+}$) and non-tuft epithelial cells (Flare25$^{-}$) sorted from the entire SI. **(C)** Colocalization of 5-LO (white) and DCLK1 (red) in the proximal (first 10cm) SI of a naïve mouse. DAPI (blue) marks nuclei. Representative images are shown. Scale bars: 5μm. **(D)** Example of 5-LO localizing to the nuclear membrane in tuft cells from the proximal SI of a mouse infected with *N. brasiliensis* for 7 days. Scale bars: 5μm. **(E)** Colocalization of 5-LO (white) and pEGFR (green) in a human

duodenal tissue section. Images are representative of three different patient samples. Scale bars: 5μm. **(F-G)** Cysteinyl leukotriene (cysLT) production in supernatants of intestinal monolayer cultures derived from mice of the indicated genotype following stimulation with 1μg/ml ionomycin (F) or 100μl NES (G) for 30 minutes. Dashed line represents limit of detection. In (A)-(B) each symbol represents an individual mouse from two or more pooled experiments. In (F)-(G) each symbol is a technical replicate and representative of three or more experiments. *Nb, N. brasiliensis*. n.d., not detected. *$p < 0.05$, **$p < 0.01$, ***$p < 0.001$ by two way ANOVA (A) with comparison to Wt(B6) or by multiple t tests (B). n.s., not significant. Graphs depict mean + SEM.

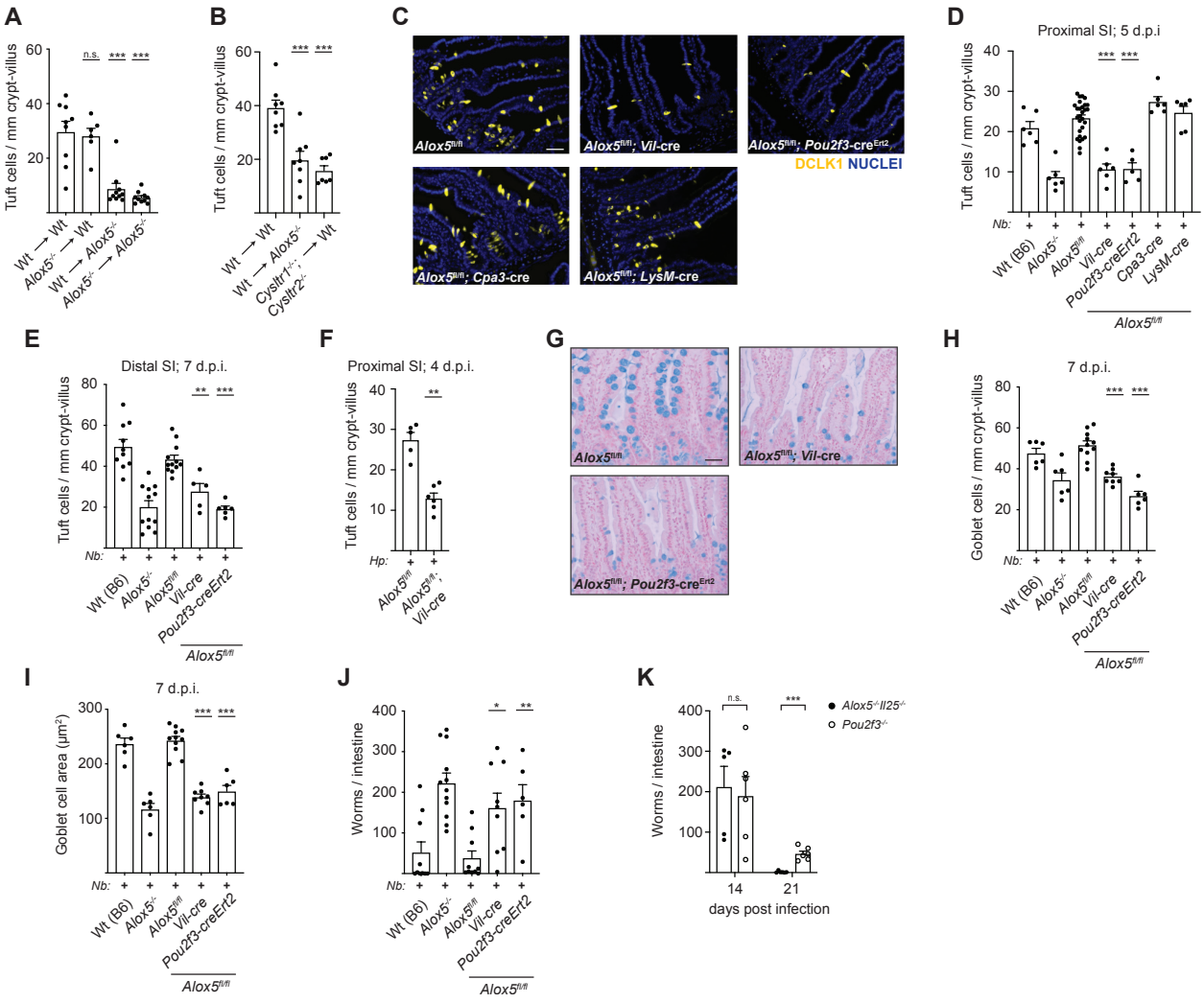


**Figure 6. Tuft cells are the physiologic source of leukotrienes for induction of type 2 immunity in the small intestine**

**(A-B)** Quantification of tuft cells in the distal (last 10cm) small intestine (SI) of chimeric mice of the indicated genotypes 7 days after *N. brasiliensis* infection. **(C)** Representative images of the proximal (first 10cm) SI 5 days post-*N. brasiliensis* infection. DCLK1 (yellow) marks tuft cells. DAPI (blue) marks nuclei. Scale bar: 50µm. **(D)** Quantification of tuft cells in (C). **(E)** Tuft cell frequency in the distal SI after 7 days of *N. brasiliensis* infection. **(F)** Tuft cell frequency in the

proximal SI after 4 days of *H. polygyrus* infection. **(G)** Mice were infected with *N. brasiliensis* for 7 days and goblet cells identified in the jejunum (10-20cm from stomach) by alcian blue staining. Representative images are shown. Scale bar: 50μm. **(H-I)** Quantification of goblet cell (H) number and (I) size in (G). **(J-K)** Worm burden across the entire SI of *N. brasiliensis* infected mice at (J) day 7 or at (K) the indicated time points post-infection. In (A)-(B), (D)-(F), and (H)-(K) each symbol represents an individual mouse from two or more pooled experiments. In (D-E) and (H-J) Wt(B6) and *Alox5*$^{-/-}$ are the same as in Figure 4, shown for comparison. *Hp, H. polygyrus. Nb, N. brasiliensis.* S13, Smart13. d.p.i., days post infection. *$p < 0.05$, **$p < 0.01$, ***$p < 0.001$ by one way ANOVA (A-B, D-E, H-J) with comparison to WT->WT or *Alox5*$^{fl/fl}$, by Mann-Whitney (F), or by multiple t tests (K). n.s., not significant. Graphs depict mean + SEM.

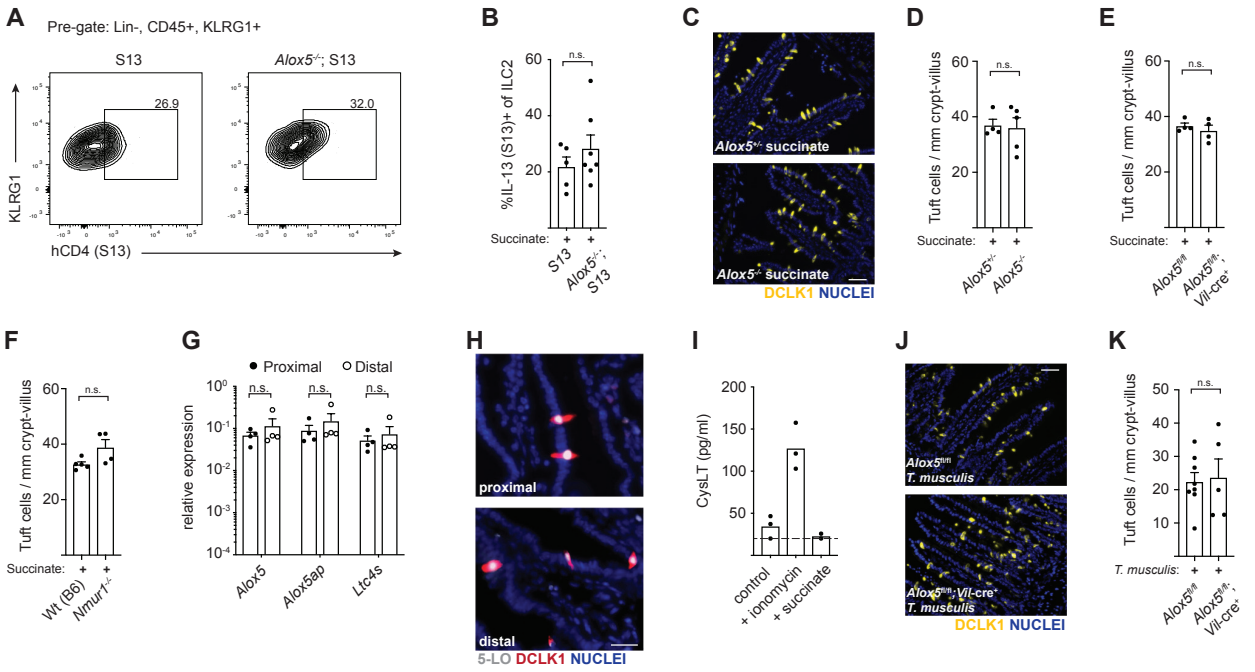


**Figure 7. Cysteinyl leukotrienes are dispensable for protist-induced type 2 immunity**

**(A)** Flow cytometry for Smart13 expression by ILC2s in the distal (last 10cm) small intestine (SI) after 36 hours of succinate treatment (150mM in drinking water). **(B)** Quantification of Smart13 expression in (A). **(C)** Tuft cells in the distal SI after 7 days of succinate treatment. DCLK1 (yellow) marks tuft cells. DAPI (blue) marks nuclei. Scale bar: 50µm. **(D)** Quantification of tuft cells in (C). **(E-F)** Quantification of tuft cells in the distal SI of mice treated with succinate for 7 days. **(G)** Gene expression in tuft cells sorted from the proximal (first 10cm) or distal SI of naïve Wt(B6) mice. **(H)** Colocalization of 5-LO (white) and DCLK1 (red) in the proximal and distal SI of naïve mice. DAPI (blue) marks nuclei. Scale bar: 25µm. **(I)** Cysteinyl leukotriene (cysLT) production in supernatants of distal SI epithelial monolayer cultures following 30 minute stimulation with 500ng/ml ionomycin or 10mM succinate. Dashed line represents limit of detection. **(J)** Tuft cells in the distal SI 7 days post-colonization with *T.*

*musculis*. Scale bar: 50μm. **(K)** Quantification of tuft cells in (J). In (B), (D-G) and (K) each symbol represents an individual mouse from two or more pooled experiments. In (I) symbols are technical replicates representative of two independent experiments. S13, Smart13. *T. musculis*, *Tritrichomonas musculis*. *p < 0.05, **p < 0.01, ***p < 0.001 by Mann-Whitney (B, D-F, K) or by multiple t tests (G). n.s., not significant. Graphs depict mean + SEM.

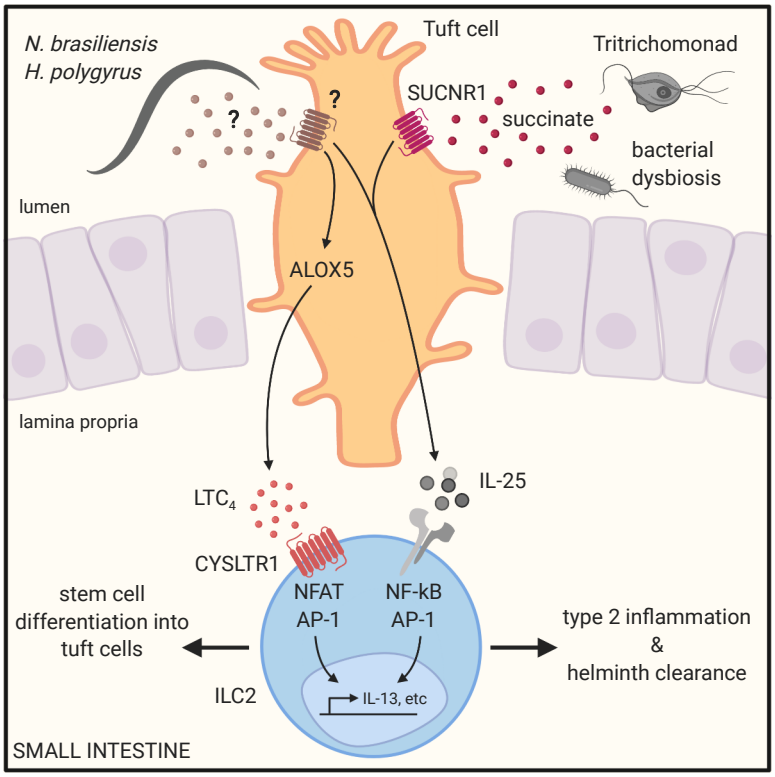


**Figure 8. Proposed model by which helminths initiate anti-helminth type 2 immune response in the small intestine.** Upon sensing helminths, intestinal tuft cells are activated to secrete cysteinyl leukotrienes and IL-25. These two mediators cooperate to drive ILC2 activation and IL-13 production, thereby triggering the feedforward tuft-ILC2 circuit that promotes helminth expulsion.

## 3.7 Supplemental Figures

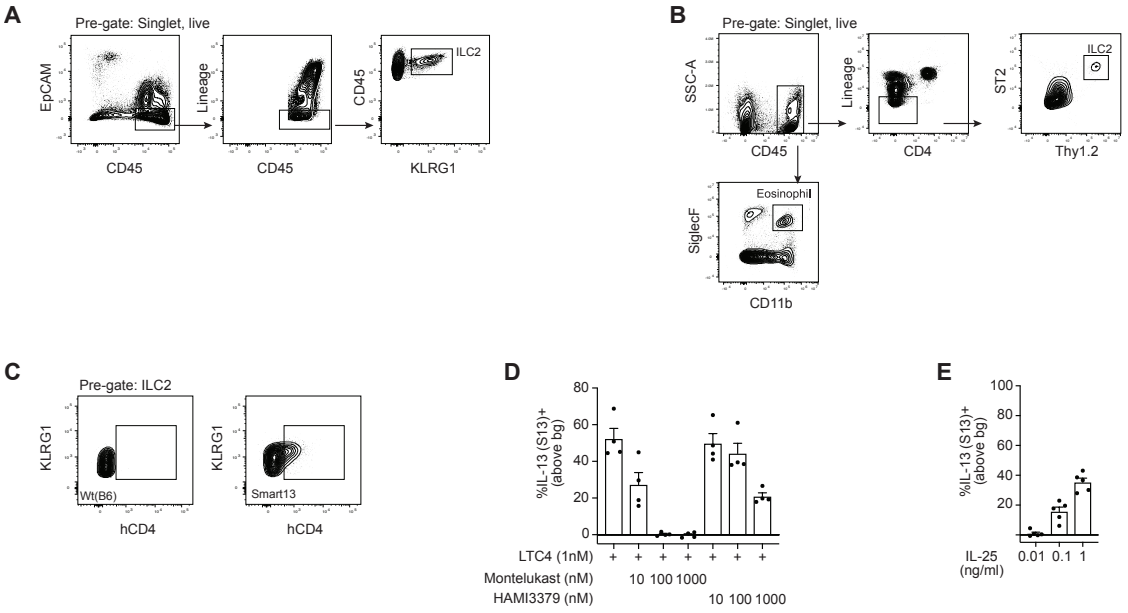


**Figure S1. Related to Figure 1**

**(A)** Gating strategy for identification of ILC2s by KLRG1 expression in the small intestine (SI) lamina propria. **(B)** Gating strategy for identification of ILC2s and eosinophils in the lung. **(C)** Example gating strategy for quantification of Smart13 reporter expression. **(D)** Sorted SI ILC2s were treated *in vitro* with the indicated inhibitor for 30 minutes prior to stimulation with $LTC_4$ for 6 hours. Smart13 expression was subsequently determined by flow cytometry. **(E)** IL-25 dose response for SI ILC2 Smart13 induction. In (D)-(E) each symbol represents an individual mouse from two or more pooled experiments.

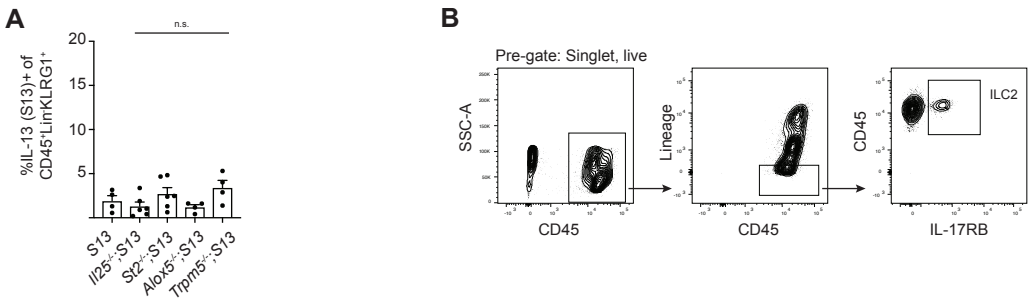


**Figure S2. Related to Figure 2**

**(A)** Quantification of Smart13 expression by ILC2s in the proximal (first 5cm) small intestine (SI) of naïve mice. ILC2s were identified as $CD45^{+}$;$Lineage^{-}$;$KLRG1^{+}$. **(B)** Gating strategy for identification of ILC2s by IL-17RB expression in the SI lamina propria. In (A) each symbol represents an individual mouse pooled from three experiments. *$p < 0.05$, **$p < 0.01$, ***$p < 0.001$ by one way ANOVA (A) with comparison to Smart13. n.s., not significant. Graphs depict mean + SEM.

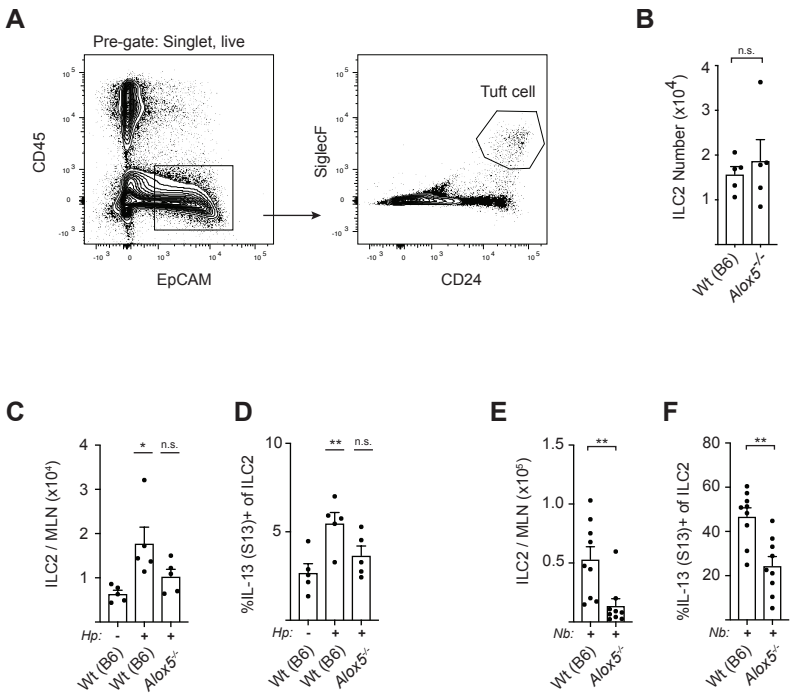


**Figure S3. Related to Figure 3**

**(A)** Gating strategy for identification of tuft cells in Wt(B6) mice. **(B)** ILC2 number in the proximal (first 10cm) small intestine (SI) lamina propria of naïve mice. **(C)** ILC2 number and **(D)** Smart13 expression in mesenteric lymph nodes four days after *H. polygyrus* infection. **(E)** ILC2 number and **(F)** Smart13 expression in mesenteric lymph nodes five days after *N. brasiliensis* infection. In (B)-(F) each symbol represents an individual mouse from two or more pooled experiments. *Hp, H. polygyrus. Nb*, *N. brasiliensis*. MLN, mesenteric lymph node. *p < 0.05, **p < 0.01, ***p < 0.001 by Mann-Whitney (B, E, F) or by one way ANOVA (C, D) with comparison to Wt(B6). n.s., not significant. Graphs depict mean + SEM.

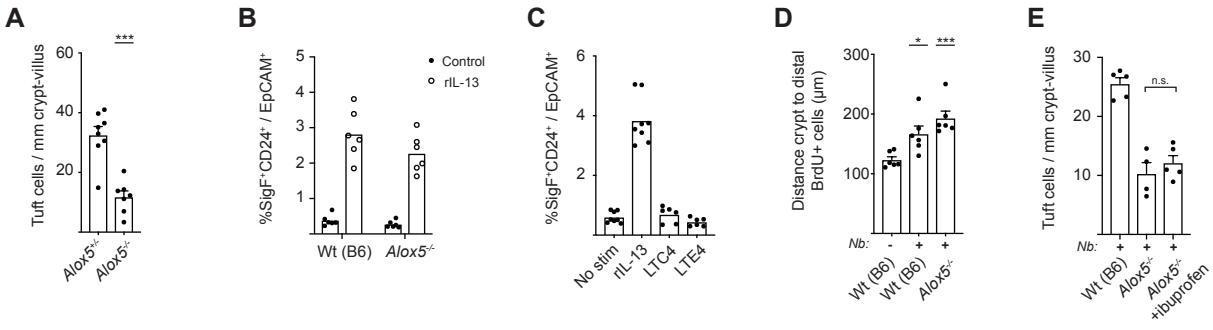


**Figure S4. Related to Figure 4**

**(A)** Frequency of tuft cells in the distal (last 10cm) small intestine (SI) of littermates after 7 days of *N. brasiliensis* infection. **(B)** Frequency of tuft cells in organoid cultures derived from mice of the indicated genotype left untreated or stimulated with 20ng/ml recombinant IL-13 for one week. **(C)** Frequency of tuft cells in organoid cultures stimulated with 20ng/ml recombinant IL-13, 10nM $LTC_4$, or 10nM $LTE_4$ for one week. **(D)** Mice of the indicated genotype were infected with *N. brasiliensis* and injected with 1mg BrdU on day 5 post-infection. After 24 hours the proximal (first 10cm) SI was harvested and BrdU incorporation determined as the distance from the crypt to most distal $BrdU^+$ cell per villus. **(E)** Mice were provided ibuprofen-medicated (1mg/ml) or control drinking water ad libitum starting one day prior to infection and then infected with *N. brasiliensis* for 5 days. Tuft cell frequency in the proximal SI was determined. In (A) and (D)-(E) each symbol represents an individual mouse from two or more pooled experiments. In (B)-(C) symbols represent technical replicates combined from two experiments. *Nb, N. brasiliensis.* $*p < 0.05$, $**p < 0.01$, $***p < 0.001$ by Mann-Whitney (A) or by one way ANOVA (D-E) with comparison to Wt(B6). n.s., not significant. Graphs depict mean + SEM.

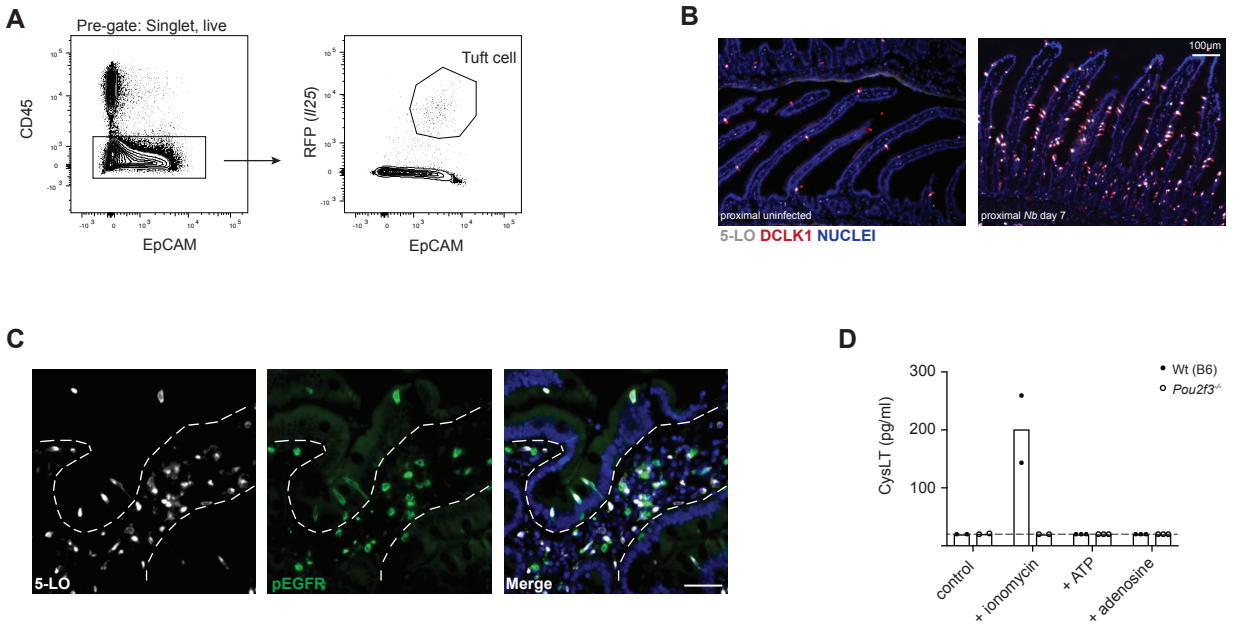


**Figure S5. Related to Figure 5**

**(A)** Gating strategy for identification of tuft cells in Flare25 mice. **(B)** Colocalization of 5-LO (white) and DCLK1 (red) in the proximal (first 10cm) small intestine (SI) of a naïve mouse and after 7 days of *N. brasiliensis* infection. Scale bar is as shown. **(C)** Colocalization of 5-LO (white) and pEGFR (green) in a human duodenal tissue section. Dashed line outlines the basolateral membrane of the epithelial layer. Scale bar: 50µm. **(D)** Cysteinyl leukotriene (cysLT) production in supernatants of intestinal monolayer cultures derived from wildtype mice following 30 minute stimulation with 1µg/ml ionomycin, 100µM ATP, or 100µM adenosine. Dashed line represents limit of detection. In (D) symbols are technical replicates representative of two independent experiments. In (B)-(C) images are representative of two or more independent experiments. *Nb, N. brasiliensis*.

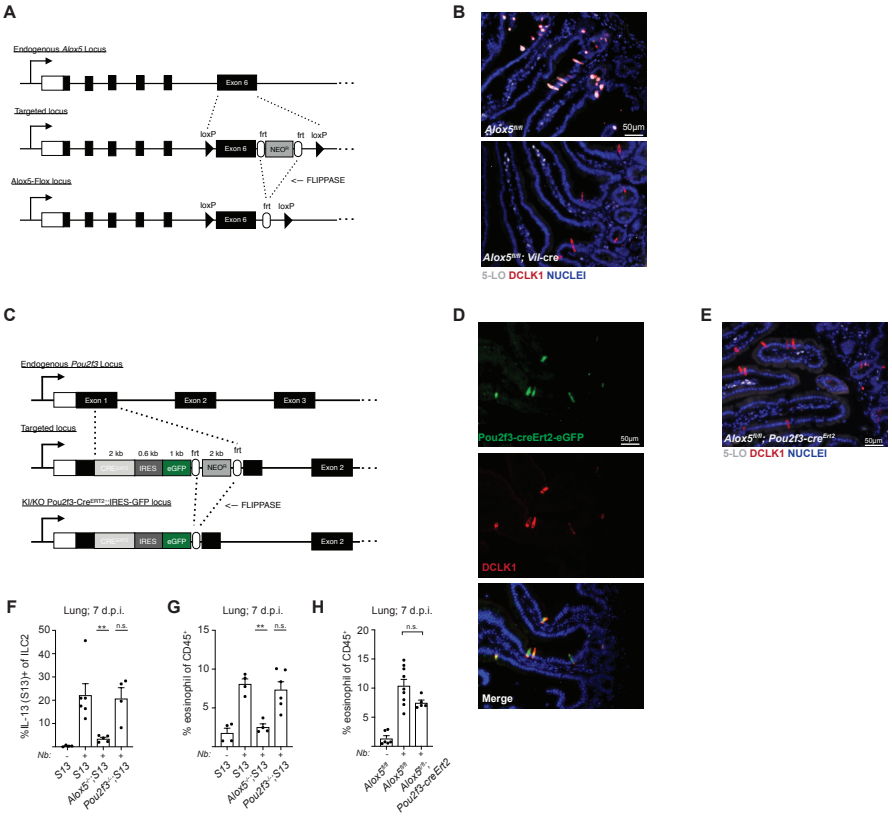


**Figure S6. Related to Figure 6**

**(A)** Gene targeting strategy for the *Alox5-flox* mouse. **(B)** 5-LO abrogation in cre-expressing mice was confirmed by staining for 5-LO (white) and DCLK1 (red) in the proximal (first 10cm) small intestine (SI) of *Alox5*$^{fl/fl}$ or *Alox5*$^{fl/fl}$;*Vil*-cre$^{+}$ mice infected with *N. brasiliensis* for 5 days. 5-LO expression was maintained in the lamina propria of both strains. **(C)** Gene targeting strategy for the *Pou2f3*-cre$^{Ert2}$-eGFP mouse. **(D)** Colocalization of *Pou2f3*-cre$^{Ert2}$-eGFP (green) and DCLK1 (red) in the proximal SI of naïve mice. **(E)** 5-LO deletion within tuft cells was confirmed by staining for 5-LO (white) and DCLK1 (red) in the proximal SI of tamoxifen treated *Alox5*$^{fl/fl}$;*Pou2f3*-cre$^{Ert2+}$ mice infected with *N. brasiliensis* for 5 days. 5-LO expression was

absent in tuft cells but maintained in the lamina propria. **(F)** Frequency of Smart13$^{+}$ ILC2s in the lung after 7 days of *N. brasiliensis* infection. **(G-H)** Eosinophil frequency in the lung after 7 days of *N. brasiliensis* infection. In (F)-(H) each symbol represents an individual mouse from two or more pooled experiments. *Nb, N. brasiliensis.* *p < 0.05, **p < 0.01, ***p < 0.001 by one way ANOVA (F-H) with comparison to infected Smart13 or *Alox5*$^{fl/fl}$. n.s., not significant. Graphs depict mean + SEM.

# CHAPTER 4

Summary and future directions

## 4.1 Summary

### Succinate is an activating ligand for intestinal tuft cells

In Chapter 2 we identify succinate as an activating ligand for intestinal tuft cells. We find that administration of succinate is sufficient to induce a multifaceted type 2 immune response in the small intestine, which required signaling through the receptor SUCNR1 expressed on tuft cells. This response was characterized by rapid activation of tissue resident ILC2s. Activated ILC2s generated IL-13, which signaled on epithelial stem cells to drive tuft cell and goblet cell differentiation and hyperplasia. Activation of this feedforward circuit was accompanied by eosinophilia, which is classically associated with type 2 responses. Accordingly, mice pre-treated with succinate were better able to resolve helminth infection as compared to control mice, owing to their enhanced type 2 immune response.

We found that succinate is produced as a metabolic byproduct by both helminths and Tritrichomonads when cultured *in vitro*. Whereas succinate sensing was dispensable for mounting an anti-helminth immune response, SUCNR1 signaling was absolutely required to mount an anti-protist response. We thereby demonstrate that type 2 immune responses can be initiated by monitoring microbial metabolism. The mechanisms by which tuft cells detect the presence of helminths in the intestinal lumen remain to be elucidated.

### Intestinal tuft cells secrete cysteinyl leukotrienes to drive type 2 immunity

In Chapter 3 we show that tuft cells produce cysLTs to initiate type 2 immune responses following detection of helminths, but not Tritrichomonad protists. CysLTs are inflammatory lipids that have long been associated with asthma in the airways, however little was known about their involvement in intestinal type 2 immune responses. We found that intestinal ILC2s are

highly responsive to cysLT stimulation. We demonstrated that cysLTs specifically engage NFAT transcriptional pathways in ILC2s, which cooperate with IL-25 induced pathways to promote optimal ILC2 activation. We found that cysLTs drive ILC2 activation *in vivo* in the context of helminth infection; mice lacking the ability to generate cysLT failed to properly activate intestinal ILC2 responses. CysLT-induced ILC2 activation was observed within hours of infection, suggesting that these are one of the earliest mediators induced following sensing of helminths.

As a result of defective ILC2 activation, mice lacking cysLTs failed to engage the feed-forward tuft-ILC2 circuit in a timely manner. This was reflected in impaired tuft cell and goblet cell hyperplasia, reduced mucus production, and ultimately a delay in worm clearance. We then went on to demonstrate that tuft cells are the physiologic source of cysLTs during helminth infection. Using genetic models, we found that deleting cysLT synthesis specifically within tuft cells recapitulated the defective type 2 responses observed in globally-deficient mice. We thereby identified cysLT secretion as a novel tuft cell effector function.

In addition to helminths, tuft cells also sense and respond to succinate-producing Tritrichomonad protists. We unexpectedly found that cysLTs were entirely dispensable for the tuft cell response elicited by these protists. Mice lacking cysLTs were able to activate ILC2s, engage the tuft-ILC2 circuit, and generate a robust type 2 immune response following treatment with succinate or colonization with Tritrichomonads. Our findings uncover a context-dependent regulation of tuft cell effector responses, wherein tuft cells tailor effector output to modulate type 2 responses depending on the type of luminal organism encountered.

### 4.2 Conclusions and future directions

Combined, these data expand our understanding of basic tuft cell biology, but more importantly, reveal an unexpected complexity in how intestinal tuft cells discriminate between different microbial encounters. It appears that both the activating input signals and resulting effector outputs are specifically tuned to the type of organism sensed. Tuft cells detect helminths through a mechanism that remains to be determined, but that does not require sensing of succinate. Sensing of helminths results in secretion of both IL-25 and cysLTs, which then act together to drive type 2 immunity. Tuft cells additionally detect Tritrichomonad protists and bacteria by sensing the metabolite succinate. Responses induced by succinate require IL-25, but not cysLTs. Tuft cell responses therefore appear to be context-dependent.

Why might such complexity exist? Succinate-producing protists and bacteria colonize the distal ileum and cecum at high numbers. While these organisms can modulate the immunological tone of the intestine during states of dysbiosis, they do not seem to negatively affect the health status of the host. In stark contrast, helminth parasites compete for host resources, impart significant morbidity, and generally decrease host fitness. In this situation a more robust inflammatory response might be required to resolve infection, whereas a strong response against commensal protists would be unwarranted. We speculate that tuft cells have evolved to regulate host immune responses such that the magnitude and quality of the response is proportional to the type of organism sensed. A deeper understanding of contextual tuft cell responses promises to enable development of targeted therapies that maximally benefit patients suffering from helminth infection, allergies, and other type 2-associated pathologies.

An interesting observation that emerged from these studies is that tuft cells appear to be adapted to their local environment. Indeed, we found that tuft cells from different tissue sites can be identified by distinct gene expression profiles. We suspect that tuft cells at different sites are

imbued with distinct effector activities, but this idea requires experimental validation. We also found that tuft cells can adapt to microenvironments within the same tissue. This is best evidenced by expression levels of the succinate receptor; tuft cell expression of the receptor SUCNR1 increases along the length of the small intestine, with ileal tuft cells bearing the highest expression. Consequently, these distal tuft cells are the most sensitive to succinate stimulation. Given that the protists and bacteria that secrete succinate as a metabolite are also found in the highest abundance at these distal sites, one might posit that tuft cells can become adapted to the signals likely to be encountered in their immediate environment. Of note, many, but not all, helminth parasites localize to the duodenal region of the proximal small intestine. The mechanism of helminth sensing by tuft cells remains unknown, but we hypothesize that tuft cells in the proximal small intestine might similarly be specially adapted at this site to maximize their ability to detect the presence of helminths. A deeper understanding of tissue- and region-specific tuft cell adaptions might shed further light on how tuft cells function to shape the immune state of their local environment.

Another concept that warrants further investigation is the nature of tuft cell activating signals. We identified the metabolite succinate as the first activating ligand for intestinal tuft cells. Tuft cell detection of Tritrichomonad protists and certain bacteria completely depends on their ability to sense succinate via the receptor SUCNR1. This finding established the precedent that innate type 2 immune responses can be activated by monitoring microbial metabolism. Whether other metabolites can also trigger a type 2 immune response remains unknown. Notably, the mechanism by which tuft cells detect helminths is not currently known. Given our recent findings, it is worth considering that tuft cells might similarly detect helminths by virtue of the metabolites they secrete. In support of this idea, we found that we could activate tuft cells

*in vitro* by stimulating them with helminth secretory products, though the identity of the activating signal within this mixture remains an open area of investigation. On the other hand, our data demonstrate that sensing of helminths does not rely on signaling through SUCNR1 or GNAT3, as is the case for sensing of protists. Thus, it remains possible that tuft cell sensing of helminth infection relies on an entirely different mechanism of detection.

Further research efforts should also consider the specific organisms that tuft cells have evolved to detect. Currently the only organisms that have been experimentally demonstrated to activate tuft cells are the helminths *N. brasiliensis*, *H. polygyrus*, *T. spiralis*, and the protists *T. musculis* and *T. rainier* (22–24,56). There is also evidence that tuft cells can be activated by succinate-producing bacteria, but the identity of these species remains unclear (43). Expanding the list of activating organisms will undoubtedly deepen our understanding of tuft cell biology by providing new tools for probing tuft cell responses and opening inroads for identifying specific activating signals. A broader understanding of the contexts in which tuft cells operate also promises to uncover the logic underlying tuft cell responses. Why is it that tuft cells are triggered by both helminths *and* protists, two organisms that differ dramatically in size, complexity, life cycle, abundance, localization, and interaction with the host? What are the evolutionary pressures that have led to this situation?

Finally, a question remains of how well murine tuft cell biology reflects that of humans. Current research relies heavily on mouse models. These offer the advantage of genetic knockouts to test the requirement of specific cells and signaling pathways in tuft cell responses, as well as to probe tuft cell activation in a controlled fashion. As a result, most of our understanding of tuft cell biology stems from murine studies. The ultimate goal, however, is to transform these observations into novel therapies to improve the lives of people suffering from helminths,

allergies, and other type 2-associated disorders. Human studies come with intrinsic challenges. Intestinal biopsies are invasive and samples are difficult to obtain. Moreover, helminths disproportionately affect the world's poor and are prevalent in regions lacking healthcare infrastructure, creating additional barriers for sample access for researchers in developed countries. Human genetic diversity often complicates experimental conclusions, and prior and ongoing infections undoubtedly influence the immune status of a given individual. For these reasons no study as yet examined the tuft cell response in helminth infected people. The data that do exist from healthy human samples indicate that tuft cells are found in the small intestine and express many of the same identifying markers, including CHAT, COX1, HPGDS, ALOX5, and FLAP (94,101). Thus, there is reason to believe that human and murine tuft cells might behave in a similar manner, but additional studies are needed to fully demonstrate this.

## References


1. Pullan RL, Smith JL, Jasrasaria R, Brooker SJ. Global numbers of infection and disease burden of soil transmitted helminth infections in 2010. Parasites Vectors. 2014 Jan 21;7(1):37.

2. Hotez PJ, Brindley PJ, Bethony JM, King CH, Pearce EJ, Jacobson J. Helminth infections: the great neglected tropical diseases. J Clin Invest. 2008 Apr 1;118(4):1311–21.

3. Crompton DWT, Nesheim MC. Nutritional impact of intestinal helminthiasis during the human life cycle. Annu Rev Nutr. 2002 Jul 1;22(1):35–59.

4. Grencis RK. Immunity to helminths: resistance, regulation, and susceptibility to gastrointestinal nematodes. Annu Rev Immunol. 2015;33:201–25.

5. Cox FEG. History of Human Parasitology. Clinical Microbiology Reviews. 2002 Oct 1;15(4):595–612.

6. Bach J-F. The effect of infections on susceptibility to autoimmune and allergic diseases. N Engl J Med. 2002 Sep 19;347(12):911–20.

7. Yazdanbakhsh M, Matricardi PM. Parasites and the hygiene hypothesis: regulating the immune system? Clin Rev Allergy Immunol. 2004 Feb;26(1):15–24.

8. Rook GAW, Brunet LR. Microbes, immunoregulation, and the gut. Gut. 2005 Mar;54(3):317–20.

9. Broide DH. Molecular and cellular mechanisms of allergic disease. Journal of Allergy and Clinical Immunology. 2001 Aug 1;108(2, Supplement):S65–71.

10. Rothenberg ME, Saito H, Peebles RS. Advances in mechanisms of allergic disease in 2016. Journal of Allergy and Clinical Immunology. 2017 Dec 1;140(6):1622–31.

11. Janeway CA, Medzhitov R. Innate Immune Recognition. Annu Rev Immunol. 2002 Apr 1;20(1):197–216.

12. Buchmann K. Evolution of Innate Immunity: Clues from Invertebrates via Fish to Mammals. Front Immunol [Internet]. 2014 [cited 2021 Jan 8];5. Available from: https://www.frontiersin.org/articles/10.3389/fimmu.2014.00459/full

13. Moro K, Yamada T, Tanabe M, Takeuchi T, Ikawa T, Kawamoto H, et al. Innate production of T(H)2 cytokines by adipose tissue-associated c-Kit(+)Sca-1(+) lymphoid cells. Nature. 2010 Jan 28;463(7280):540–4.

14. Neill DR, Wong SH, Bellosi A, Flynn RJ, Daly M, Langford TKA, et al. Nuocytes represent a new innate effector leukocyte that mediates type-2 immunity. Nature. 2010 Apr 29;464(7293):1367–70.

15. Price AE, Liang H-E, Sullivan BM, Reinhardt RL, Eisley CJ, Erle DJ, et al. Systemically dispersed innate IL-13–expressing cells in type 2 immunity. Proc Natl Acad Sci U S A. 2010 Jun 22;107(25):11489–94.

16. Van Dyken SJ, Nussbaum JC, Lee J, Molofsky AB, Liang H-E, Pollack JL, et al. A tissue checkpoint regulates type 2 immunity. Nature Immunology. 2016 Dec;17(12):1381–7.

17. Shih H-Y, Sciumè G, Mikami Y, Guo L, Sun H-W, Brooks SR, et al. Developmental Acquisition of Regulomes Underlies Innate Lymphoid Cell Functionality. Cell. 2016 May 19;165(5):1120–33.

18. McGinty JW, von Moltke J. A three course menu for ILC and bystander T cell activation. Current Opinion in Immunology. 2020 Feb 1;62:15–21.

19. Ricardo-Gonzalez RR, Van Dyken SJ, Schneider C, Lee J, Nussbaum JC, Liang H-E, et al. Tissue signals imprint ILC2 identity with anticipatory function. Nat Immunol. 2018;19(10):1093–9.

20. Schneider C, O'Leary CE, von Moltke J, Liang H-E, Ang QY, Turnbaugh PJ, et al. A Metabolite-Triggered Tuft Cell-ILC2 Circuit Drives Small Intestinal Remodeling. Cell. 2018 12;174(2):271-284.e14.

21. Fallon PG, Ballantyne SJ, Mangan NE, Barlow JL, Dasvarma A, Hewett DR, et al. Identification of an interleukin (IL)-25–dependent cell population that provides IL-4, IL-5, and IL-13 at the onset of helminth expulsion. J Exp Med. 2006 Apr 17;203(4):1105–16.

22. Gerbe F, Sidot E, Smyth DJ, Ohmoto M, Matsumoto I, Dardalhon V, et al. Intestinal epithelial tuft cells initiate type 2 mucosal immunity to helminth parasites. Nature. 2016 Jan 14;529(7585):226–30.

23. Howitt MR, Lavoie S, Michaud M, Blum AM, Tran SV, Weinstock JV, et al. Tuft cells, taste-chemosensory cells, orchestrate parasite type 2 immunity in the gut. Science. 2016 Mar 18;351(6279):1329–33.

24. von Moltke J, Ji M, Liang H-E, Locksley RM. Tuft-cell-derived IL-25 regulates an intestinal ILC2-epithelial response circuit. Nature. 2016 Jan 14;529(7585):221–5.

25. Ting H-A, Moltke J von. The Immune Function of Tuft Cells at Gut Mucosal Surfaces and Beyond. The Journal of Immunology. 2019 Mar 1;202(5):1321–9.

26. Rhodin J, Dalhamn T. Electron microscopy of the tracheal ciliated mucosa in rat. Zeitschrift für Zellforschung. 1956 Jul 1;44(4):345–412.

27. von Moltke J. Chapter 31 - Intestinal Tuft Cells. In: Said HM, editor. Physiology of the Gastrointestinal Tract (Sixth Edition) [Internet]. Academic Press; 2018 [cited 2021 Jan 13].

p. 721–33. Available from: http://www.sciencedirect.com/science/article/pii/B9780128099544000311

28. O'Leary CE, Schneider C, Locksley RM. Tuft Cells—Systemically Dispersed Sensory Epithelia Integrating Immune and Neural Circuitry. Annual Review of Immunology. 2019;37(1):47–72.

29. Bezençon C, Fürholz A, Raymond F, Mansourian R, Métairon S, Le Coutre J, et al. Murine intestinal cells expressing Trpm5 are mostly brush cells and express markers of neuronal and inflammatory cells. J Comp Neurol. 2008 Aug 10;509(5):514–25.

30. Chaudhari N, Roper SD. The cell biology of taste. J Cell Biol. 2010 Aug 9;190(3):285–96.

31. Barker N. Adult intestinal stem cells: critical drivers of epithelial homeostasis and regeneration. Nature Reviews Molecular Cell Biology. 2013 Dec 11;15:19.

32. Finger TE, Danilova V, Barrows J, Bartel DL, Vigers AJ, Stone L, et al. ATP signaling is crucial for communication from taste buds to gustatory nerves. Science. 2005 Dec 2;310(5753):1495–9.

33. Huang YA, Roper SD. Intracellular Ca2+ and TRPM5-mediated membrane depolarization produce ATP secretion from taste receptor cells. J Physiol. 2010 Jul 1;588(Pt 13):2343–50.

34. Krasteva G, Canning BJ, Hartmann P, Veres TZ, Papadakis T, Mühlfeld C, et al. Cholinergic chemosensory cells in the trachea regulate breathing. Proc Natl Acad Sci U S A. 2011 Jun 7;108(23):9478–83.

35. Tizzano M, Gulbransen BD, Vandenbeuch A, Clapp TR, Herman JP, Sibhatu HM, et al. Nasal chemosensory cells use bitter taste signaling to detect irritants and bacterial signals. Proc Natl Acad Sci U S A. 2010 Feb 16;107(7):3210–5.

36. Deckmann K, Filipski K, Krasteva-Christ G, Fronius M, Althaus M, Rafiq A, et al. Bitter triggers acetylcholine release from polymodal urethral chemosensory cells and bladder reflexes. Proc Natl Acad Sci U S A. 2014 Jun 3;111(22):8287–92.

37. Parada Venegas D, De la Fuente MK, Landskron G, González MJ, Quera R, Dijkstra G, et al. Short Chain Fatty Acids (SCFAs)-Mediated Gut Epithelial and Immune Regulation and Its Relevance for Inflammatory Bowel Diseases. Front Immunol [Internet]. 2019 [cited 2021 Jan 7];10. Available from: https://www.frontiersin.org/articles/10.3389/fimmu.2019.00277/full

38. Ferreyra JA, Wu KJ, Hryckowian AJ, Bouley DM, Weimer BC, Sonnenburg JL. Gut microbiota-produced succinate promotes C. difficile infection after antibiotic treatment or motility disturbance. Cell Host Microbe. 2014 Dec 10;16(6):770–7.

39. De Vadder F, Kovatcheva-Datchary P, Zitoun C, Duchampt A, Bäckhed F, Mithieux G. Microbiota-Produced Succinate Improves Glucose Homeostasis via Intestinal Gluconeogenesis. Cell Metab. 2016 Jul 12;24(1):151–7.

40. Müller M, Mentel M, van Hellemond JJ, Henze K, Woehle C, Gould SB, et al. Biochemistry and Evolution of Anaerobic Energy Metabolism in Eukaryotes. Microbiol Mol Biol Rev. 2012 Jun;76(2):444–95.

41. Tielens AG. Energy generation in parasitic helminths. Parasitol Today. 1994 Sep;10(9):346–52.

42. Saz DK, Bonner TP, Karlin M, Saz HJ. Biochemical observations on adult Nippostrongylus brasiliensis. J Parasitol. 1971 Dec;57(6):1159–62.

43. Lei W, Ren W, Ohmoto M, Urban JF, Matsumoto I, Margolskee RF, et al. Activation of intestinal tuft cell-expressed Sucnr1 triggers type 2 immunity in the mouse small intestine. Proc Natl Acad Sci USA. 2018 22;115(21):5552–7.

44. Littlewood-Evans A, Sarret S, Apfel V, Loesle P, Dawson J, Zhang J, et al. GPR91 senses extracellular succinate released from inflammatory macrophages and exacerbates rheumatoid arthritis. Journal of Experimental Medicine. 2016 Aug 1;213(9):1655–62.

45. Rubic T, Lametschwandtner G, Jost S, Hinteregger S, Kund J, Carballido-Perrig N, et al. Triggering the succinate receptor GPR91 on dendritic cells enhances immunity. Nature Immunology. 2008 Nov;9(11):1261–9.

46. Rubić-Schneider T, Carballido-Perrig N, Regairaz C, Raad L, Jost S, Rauld C, et al. GPR91 deficiency exacerbates allergic contact dermatitis while reducing arthritic disease in mice. Allergy. 2017;72(3):444–52.

47. Liang H-E, Reinhardt RL, Bando JK, Sullivan BM, Ho I-C, Locksley RM. Divergent expression patterns of IL-4 and IL-13 define unique functions in allergic immunity. Nat Immunol. 2012 Jan;13(1):58–66.

48. von Moltke J, Ji M, Liang H-E, Locksley RM. Tuft-cell-derived IL-25 regulates an intestinal ILC2-epithelial response circuit. Nature. 2016 Jan 14;529(7585):221–5.

49. Fallon PG, Ballantyne SJ, Mangan NE, Barlow JL, Dasvarma A, Hewett DR, et al. Identification of an interleukin (IL)-25-dependent cell population that provides IL-4, IL-5, and IL-13 at the onset of helminth expulsion. J Exp Med. 2006 Apr 17;203(4):1105–16.

50. Mohrs M, Ledermann B, Köhler G, Dorfmüller A, Gessner A, Brombacher F. Differences between IL-4- and IL-4 receptor alpha-deficient mice in chronic leishmaniasis reveal a protective role for IL-13 receptor signaling. J Immunol. 1999 Jun 15;162(12):7302–8.

51. Paik J, Pershutkina O, Meeker S, Yi JJ, Dowling S, Hsu C, et al. Potential for using a hermetically-sealed, positive-pressured isocage system for studies involving germ-free mice outside a flexible-film isolator. Gut Microbes. 2015 Jul 4;6(4):255–65.

52. Gray EE, Winship D, Snyder JM, Child SJ, Geballe AP, Stetson DB. The AIM2-like receptors are dispensable for the interferon response to intracellular DNA. Immunity. 2016 Aug 16;45(2):255–66.

53. Huang DW, Sherman BT, Lempicki RA. Bioinformatics enrichment tools: paths toward the comprehensive functional analysis of large gene lists. Nucleic Acids Res. 2009 Jan;37(1):1–13.

54. Huang DW, Sherman BT, Lempicki RA. Systematic and integrative analysis of large gene lists using DAVID bioinformatics resources. Nat Protoc. 2009;4(1):44–57.

55. Chudnovskiy A, Mortha A, Kana V, Kennard A, Ramirez JD, Rahman A, et al. Host-Protozoan Interactions Protect from Mucosal Infections through Activation of the Inflammasome. Cell. 2016 Oct 6;167:444-456.e14.

56. Nadjsombati MS, McGinty JW, Lyons-Cohen MR, Jaffe JB, DiPeso L, Schneider C, et al. Detection of Succinate by Intestinal Tuft Cells Triggers a Type 2 Innate Immune Circuit. Immunity. 2018 Jul 17;49(1):33-41.e7.

57. Luo X-C, Chen Z-H, Xue J-B, Zhao D-X, Lu C, Li Y-H, et al. Infection by the parasitic helminth Trichinella spiralis activates a Tas2r-mediated signaling pathway in intestinal tuft cells. PNAS. 2019 Mar 19;116(12):5564–9.

58. Lund SJ, Portillo A, Cavagnero K, Baum RE, Naji LH, Badrani JH, et al. Leukotriene C4 Potentiates IL-33-Induced Group 2 Innate Lymphoid Cell Activation and Lung Inflammation. J Immunol. 2017 01;199(3):1096–104.

59. von Moltke J, O'Leary CE, Barrett NA, Kanaoka Y, Austen KF, Locksley RM. Leukotrienes provide an NFAT-dependent signal that synergizes with IL-33 to activate ILC2s. Journal of Experimental Medicine. 2017 Jan 1;214(1):27–37.

60. Haeggström JZ, Funk CD. Lipoxygenase and Leukotriene Pathways: Biochemistry, Biology, and Roles in Disease. Chem Rev. 2011 Oct 12;111(10):5866–98.

61. Peters-Golden M, Henderson WR. Leukotrienes. New England Journal of Medicine. 2007 Nov 1;357(18):1841–54.

62. Uozumi N, Kume K, Nagase T, Nakatani N, Ishii S, Tashiro F, et al. Role of cytosolic phospholipase A 2 in allergic response and parturition. Nature. 1997 Dec;390(6660):618.

63. Keppler D, Huber M, Baumert T, Guhlmann A. Metabolic inactivation of leukotrienes. Adv Enzyme Regul. 1989;28:307–19.

64. Haber AL, Biton M, Rogel N, Herbst RH, Shekhar K, Smillie C, et al. A single-cell survey of the small intestinal epithelium. Nature. 2017 16;551(7680):333–9.

65. Doherty TA, Khorram N, Lund S, Mehta AK, Croft M, Broide DH. Lung Type 2 innate lymphoid cells express CysLT1R that regulates Th2 cytokine production. J Allergy Clin Immunol. 2013 Jul;132(1):205–13.

66. Liang H-E, Reinhardt RL, Bando JK, Sullivan BM, Ho I-C, Locksley RM. Divergent expression patterns of IL-4 and IL-13 define unique functions in allergic immunity. Nat Immunol. 2011 Dec 4;13(1):58–66.

67. Wunder F, Tinel H, Kast R, Geerts A, Becker E, Kolkhof P, et al. Pharmacological characterization of the first potent and selective antagonist at the cysteinyl leukotriene 2 (CysLT2) receptor. Br J Pharmacol. 2010 May;160(2):399–409.

68. Barlow JL, Peel S, Fox J, Panova V, Hardman CS, Camelo A, et al. IL-33 is more potent than IL-25 in provoking IL-13–producing nuocytes (type 2 innate lymphoid cells) and airway contraction. Journal of Allergy and Clinical Immunology. 2013 Oct 1;132(4):933–41.

69. Lynch KR, O'Neill GP, Liu Q, Im D-S, Sawyer N, Metters KM, et al. Characterization of the human cysteinyl leukotriene CysLT 1 receptor. Nature. 1999 Jun;399(6738):789.

70. Maezawa Y, Nakajima H, Suzuki K, Tamachi T, Ikeda K, Inoue J, et al. Involvement of TNF receptor-associated factor 6 in IL-25 receptor signaling. J Immunol. 2006 Jan 15;176(2):1013–8.

71. Wong CK, Cheung PFY, Ip WK, Lam CWK. Interleukin-25-induced chemokines and interleukin-6 release from eosinophils is mediated by p38 mitogen-activated protein kinase, c-Jun N-terminal kinase, and nuclear factor-kappaB. Am J Respir Cell Mol Biol. 2005 Aug;33(2):186–94.

72. Molofsky AB, Savage AK, Locksley RM. Interleukin-33 in Tissue Homeostasis, Injury, and Inflammation. Immunity. 2015 Jun 16;42(6):1005–19.

73. Sato T, Vries RG, Snippert HJ, van de Wetering M, Barker N, Stange DE, et al. Single Lgr5 stem cells build crypt-villus structures in vitro without a mesenchymal niche. Nature. 2009 May 14;459(7244):262–5.

74. Tait Wojno ED, Monticelli LA, Tran SV, Alenghat T, Osborne LC, Thome JJ, et al. The prostaglandin D 2 receptor CRTH2 regulates accumulation of group 2 innate lymphoid cells in the inflamed lung. Mucosal Immunology. 2015 Nov;8(6):1313–23.

75. Rouzer CA, Kargman S. Translocation of 5-lipoxygenase to the membrane in human leukocytes challenged with ionophore A23187. J Biol Chem. 1988 Aug 5;263(22):10980–8.

76. Wong A, Hwang SM, Cook MN, Hogaboom GK, Crooke ST. Interactions of 5-lipoxygenase with membranes: studies on the association of soluble enzyme with membranes and alterations in enzyme activity. Biochemistry. 1988 Sep 6;27(18):6763–9.

77. McKinley ET, Sui Y, Al-Kofahi Y, Millis BA, Tyska MJ, Roland JT, et al. Optimized multiplex immunofluorescence single-cell analysis reveals tuft cell heterogeneity. JCI Insight. 2017 Jun 2;2(11).

78. Liu Y, Qi Z, Li X, Du Y, Chen Y-G. Monolayer culture of intestinal epithelium sustains Lgr5 + intestinal stem cells. Cell Discovery. 2018 Jun 12;4(1):32.

79. Thorne CA, Chen IW, Sanman LE, Cobb MH, Wu LF, Altschuler SJ. Enteroid Monolayers Reveal an Autonomous WNT and BMP Circuit Controlling Intestinal Epithelial Growth and Organization. Developmental Cell. 2018 Mar 12;44(5):624-633.e4.

80. Deckmann K, Rafiq A, Erdmann C, Illig C, Durschnabel M, Wess J, et al. Muscarinic receptors 2 and 5 regulate bitter response of urethral brush cells via negative feedback. FASEB J. 2018;32(6):2903–10.

81. Hofmann T, Chubanov V, Gudermann T, Montell C. TRPM5 is a voltage-modulated and Ca(2+)-activated monovalent selective cation channel. Curr Biol. 2003 Jul 1;13(13):1153–8.

82. Prawitt D, Monteilh-Zoller MK, Brixel L, Spangenberg C, Zabel B, Fleig A, et al. TRPM5 is a transient Ca2+-activated cation channel responding to rapid changes in [Ca2+]i. PNAS. 2003 Dec 9;100(25):15166–71.

83. Shimokawa C, Kanaya T, Hachisuka M, Ishiwata K, Hisaeda H, Kurashima Y, et al. Mast Cells Are Crucial for Induction of Group 2 Innate Lymphoid Cells and Clearance of Helminth Infections. Immunity. 2017 16;46(5):863-874.e4.

84. Ualiyeva S, Hallen N, Kanaoka Y, Ledderose C, Matsumoto I, Junger WG, et al. Airway brush cells generate cysteinyl leukotrienes through the ATP sensor P2Y2. Science Immunology [Internet]. 2020 Jan 17 [cited 2020 Feb 12];5(43). Available from: https://immunology.sciencemag.org/content/5/43/eaax7224

85. Kanaoka Y, Boyce JA. Cysteinyl Leukotrienes and Their Receptors: Cellular Distribution and Function in Immune and Inflammatory Responses. The Journal of Immunology. 2004 Aug 1;173(3):1503–10.

86. Cardoso V, Chesné J, Ribeiro H, García-Cassani B, Carvalho T, Bouchery T, et al. Neuronal regulation of type 2 innate lymphoid cells via neuromedin U. Nature. 2017 Sep;549(7671):277–81.

87. Klose CSN, Mahlakõiv T, Moeller JB, Rankin LC, Flamar A-L, Kabata H, et al. The neuropeptide neuromedin U stimulates innate lymphoid cells and type 2 inflammation. Nature. 2017 14;549(7671):282–6.

88. Wallrapp A, Riesenfeld SJ, Burkett PR, Abdulnour R-EE, Nyman J, Dionne D, et al. The neuropeptide NMU amplifies ILC2-driven allergic lung inflammation. Nature. 2017 21;549(7672):351–6.

89. Vannella KM, Ramalingam TR, Borthwick LA, Barron L, Hart KM, Thompson RW, et al. Combinatorial targeting of TSLP, IL-25, and IL-33 in type 2 cytokine–driven inflammation and fibrosis. Science Translational Medicine. 2016 May 4;8(337):337ra65-337ra65.

90. Pelly VS, Kannan Y, Coomes SM, Entwistle LJ, Rückerl D, Seddon B, et al. IL-4-producing ILC2s are required for the differentiation of T H 2 cells following Heligmosomoides polygyrus infection. Mucosal Immunol. 2016 Nov;9(6):1407–17.

91. Bäck M, Dahlén S-E, Drazen JM, Evans JF, Serhan CN, Shimizu T, et al. International Union of Basic and Clinical Pharmacology. LXXXIV: Leukotriene Receptor Nomenclature, Distribution, and Pathophysiological Functions. Pharmacol Rev. 2011 Sep 1;63(3):539–84.

92. Chudnovskiy A, Mortha A, Kana V, Kennard A, Ramirez JD, Rahman A, et al. Host-Protozoan Interactions Protect from Mucosal Infections through Activation of the Inflammasome. Cell. 2016 Oct 6;167(2):444-456.e14.

93. Escalante NK, Lemire P, Cruz Tleugabulova M, Prescott D, Mortha A, Streutker CJ, et al. The common mouse protozoa Tritrichomonas muris alters mucosal T cell homeostasis and colitis susceptibilityTritrichomonas muris alters T cell homeostasis. J Exp Med. 2016 Dec 12;213(13):2841–50.

94. Schütz B, Ruppert A-L, Strobel O, Lazarus M, Urade Y, Büchler MW, et al. Distribution pattern and molecular signature of cholinergic tuft cells in human gastro-intestinal and pancreatic-biliary tract. Sci Rep. 2019 Nov 25;9(1):1–13.

95. Reese TA, Liang H-E, Tager AM, Luster AD, Rooijen NV, Voehringer D, et al. Chitin induces accumulation in tissue of innate immune cells associated with allergy. Nature. 2007 May;447(7140):92–6.

96. Maekawa A, Austen KF, Kanaoka Y. Targeted gene disruption reveals the role of cysteinyl leukotriene 1 receptor in the enhanced vascular permeability of mice undergoing acute inflammatory responses. J Biol Chem. 2002 Jun 7;277(23):20820–4.

97. Beller TC, Maekawa A, Friend DS, Austen KF, Kanaoka Y. Targeted gene disruption reveals the role of the cysteinyl leukotriene 2 receptor in increased vascular permeability and in bleomycin-induced pulmonary fibrosis in mice. J Biol Chem. 2004 Oct 29;279(44):46129–34.

98. Johnston CJC, Robertson E, Harcus Y, Grainger JR, Coakley G, Smyth DJ, et al. Cultivation of Heligmosomoides Polygyrus: An Immunomodulatory Nematode Parasite and its Secreted Products. J Vis Exp [Internet]. 2015 Apr 6 [cited 2019 Jun 11];(98). Available from: https://www.ncbi.nlm.nih.gov/pmc/articles/PMC4401400/

99. Boekel J, Chilton JM, Cooke IR, Horvatovich PL, Jagtap PD, Käll L, et al. Multi-omic data analysis using Galaxy. Nat Biotechnol. 2015 Feb;33(2):137–9.

100. Sato T, Clevers H. Primary mouse small intestinal epithelial cell cultures. Methods Mol Biol. 2013;945:319–28.

101. McGinty JW, Ting H-A, Billipp TE, Nadjsombati MS, Khan DM, Barrett NA, et al. Tuft-Cell-Derived Leukotrienes Drive Rapid Anti-helminth Immunity in the Small Intestine but Are Dispensable for Anti-protist Immunity. Immunity. 2020 Mar 17;52(3):528-541.e7.